

# Printed Electronics Technologies for Additive Manufacturing of Hybrid Electronic Sensor Systems

Johanna Zikulnig,\* Sean Chang, Jo Bito, Lukas Rauter, Ali Roshanghias, Sandro Carrara, and Jürgen Kosel

Requirements for the miniaturization of electronics are constantly increasing as more and more functions are aimed to be integrated into a single device. At the same time, there are strong demands for low-cost manufacturing, environmental compatibility, rapid prototyping, and small-scale productions due to fierce competition, policies, rapid technical progress, and short innovation times. Altogether, those challenges cannot be sufficiently addressed by simply using either printed or silicon electronics. Instead, the synergies from combining those two technologies into so-called hybrid electronics create novel opportunities for advanced capabilities and new areas of applications. In the first part of this review, printing and patterning technologies are presented with potential compatibility with conventional electronics manufacturing techniques. They can be utilized for the fabrication of highly complex structures. Nonetheless, up-scalability, integration, and adaptation for industrial fabrication remain challenging due to technically limiting factors. Consequently, a special focus is placed on the up-scalability, availability of commercial printing, and manufacturing machines, as well as processing challenges for high-volume industrial applications. The second part of this review further provides an overview of exciting and innovative application possibilities of printed electronics, emphasizing sensor applications, as well as additively manufactured integrated circuits.

## 1. Introduction

Microelectronics comprise the study and manufacture of very small electronics components and designs in the micro- and sub-micrometer scale, which have become a prevalent driving force of innovation in modern society. The foundation for the success story of microelectronics was laid with the development of silicon transistors, which was the result of a head-to-head race between two independent groups at Bell Labs and Texas Instruments (TI) in the 1950's. Eventually, TI was one step ahead and became the first company to manufacture silicon transistors in volume.<sup>[1]</sup> Since then, the global market for electronic components and systems has been continuously growing, especially due to the rapid technical advancements regarding computing power, packaging density (Moore's law) as well as manufacturing costs.<sup>[2]</sup> In more recent history, "smart" everyday objects have emerged, equipped with sensors and chips, providing wireless read-out and connection to the cloud (typically,

the so-called Internet-of-Things (IoT) devices). Consequently, the need for miniaturization is increasing, as more and more functions have to be integrated into a single device. Particularly, in the field of wearable gadgets, such as smart glasses, hearing aids, and fitness trackers, the requirements for miniaturization, adaptable, and conforming form factors are high, to ensure the desired performance as well as comfort. Alongside this development, low-cost manufacturing is essential, and the implementation of a sustainable product life cycle becomes a priority. Furthermore, due to the fast-paced technical progress and short innovation times the demand for rapid prototyping and small-scale productions is rising. In conventional electronics manufacturing, patterning of microelectronic devices generally comprises multiple lithographic steps requiring customized masks, which makes it difficult to meet the aforementioned challenges. On the other hand, additive manufacturing is considered as bottom-up manufacturing process, where the component is constructed layer-upon-layer. In the context of electronics fabrication, applications of additive manufacturing are commonly referred to as printed electronics (PE). With a global market of \$31.7 billion in 2018 and forecast for doubling to reach \$77.3 billion in 2029,<sup>[3]</sup> printed

J. Zikulnig, L. Rauter, A. Roshanghias, J. Kosel  
 Silicon Austria Labs GmbH  
 Europastraße 12, Villach 9524, Austria  
 E-mail: johanna.zikulnig@silicon-austria.com

J. Zikulnig, S. Carrara  
 École Polytechnique Fédérale de Lausanne  
 Rue de la Maladière 71b, Neuchâtel CH-2000, Switzerland

S. Chang  
 Texas Instruments Inc.  
 13560 N Central Expy, Dallas, TX 75243, USA

J. Bito  
 Atheraxon Inc.  
 75 5th St NW Ste 2406, Atlanta, GA 30308, USA

 The ORCID identification number(s) for the author(s) of this article can be found under <https://doi.org/10.1002/adsr.202200073>

© 2023 The Authors. Advanced Sensor Research published by Wiley-VCH GmbH. This is an open access article under the terms of the Creative Commons Attribution License, which permits use, distribution and reproduction in any medium, provided the original work is properly cited.

DOI: 10.1002/adsr.202200073

and flexible electronics have developed beyond niche technology. With flexible printed organic light emitting diode (OLED) displays<sup>[4]</sup> and organic photovoltaics (PV),<sup>[5]</sup> printed electronics have already hit the commercial market. For PE manufacturing, conventional reproduction methods as known from graphic printing, such as inkjet-printing, screen-printing, or gravure-printing are employed. Furthermore, techniques commonly used in the field of molecular biology, such as laser induced forward transfer (LIFT),<sup>[6]</sup> or technologies originating from classic electronics manufacturing, such as additive nanoimprint lithography (NIL) are used.

Additively manufactured electronic components are frequently compared to silicon-based electronics in terms of, for example, manufacturing speed, dimensions, electrical performance, and environmental impact. Referring to environmental compatibility, printing technologies are considered to have lower ecological impact than silicon electronics. Although not much data is available to fully support this hypothesis, Zheng et al.<sup>[7]</sup> provide a comprehensive study on the life cycle assessment of inkjet-printed radio frequency (RF) antennas. Impressively, they found that printing can save resources by 95% with respect to fabrication using PCB technology. Similar findings are reported in the Ph.D. thesis by Qiansu Wan.<sup>[8]</sup>

Despite the massive market growth rate and potential for a large variety of applications, the performance and yield of many fully printed electrical devices, such as thin film transistors (TFTs),<sup>[9]</sup> inductors,<sup>[10]</sup> capacitors,<sup>[11]</sup> memories,<sup>[12]</sup> and batteries,<sup>[13]</sup> cannot keep up with their traditionally manufactured counterparts. Although PE manufacturing is generally considered cost-efficient, the cost per function is higher compared to the production of silicon electronics.<sup>[14]</sup> Hence, additive manufacturing of entire microcontrollers comprising data read out, analysis, and transmission will neither be feasible nor reasonable in the foreseeable future. That being said, printed and silicon electronics do not necessarily compete, instead the possibility to combine them creates novel areas of applications resulting in so-called hybrid electronics.<sup>[15–18]</sup> One particularly appealing field for combining silicon-based electronics with printing technologies is the back-end packaging. As an example, Roshanghias et al.<sup>[19]</sup> recently studied the feasibility of fan-out wafer-level packaging of capacitive micromachined ultrasound transducers using inkjet-printing. Thin and sensitive parts of MEMS are generally prone to deterioration when being processed using standard methods, such as laminating, molding, back-grinding, and dicing, that may result, for example, in a resonance frequency shift of a MEMS microphone, or even a membrane rupture. These issues can be addressed by employing additive packaging technologies.

As part of this review, several printing and patterning technologies are presented, that are (potentially) compatible with conventional electronics manufacturing techniques. Considering how long additive electronics manufacturing technologies have been around, it is noteworthy that there is still a large gap between academia, prototyping, and industry. Additive and printing methods bear the potentials for fabricating highly complex structures, as frequently reported in scientific literature, for example refs. [20, 21, 22, 23]. In certain areas, such as PV,<sup>[24]</sup> OLED,<sup>[25]</sup> and printed antennas,<sup>[26]</sup> PE has already hit the commercial market. Still, for many of those additive manufacturing technologies

up-scalability, integration, and adaptation for industrial fabrication appears to be challenging or even unfeasible due to technically limiting factors. Therefore, this work specially focuses on the potential up-scalability and, if applicable, availability of commercial printing and manufacturing machines to give the reader an overview of industrial possibilities. Furthermore, processing challenges, which are particularly relevant for high-volume industrial applications are pointed out, as well as challenges, which arise from the integration with silicon-based electronics. Where applicable, the adequacy of the manufacturing technologies for hybrid electronics integration and microelectronics fabrication is assessed, and an outlook on future and emerging technologies is provided.

In Section 2 of this paper, an overview of the working principles of selected high-resolution printing and patterning technologies is given. Amongst various methods around, inkjet printing (2.1), electrohydrodynamic printing (EHD) (2.2), aerosol jet (2.3), LIFT (2.4), reverse offset printing (2.5), and (additive) NIL (2.6), are discussed in detail. The second part of this work (chapter 3) gives an overview of applications possibilities of those technologies, with a special focus on sensor applications as well as additive integrated circuits (ICs). Finally, chapter 4 summarizes and concludes this work.

## 2. Additive Manufacturing and Printing Technologies

Printing technologies can be broadly classified as contact and contactless methods. A contactless printing process prevents any unfavorable physical impact of the printing process on the substrate which can be advantageous when working with sensitive carrier materials. To a certain extent, this even enables printing onto 3D structures, though further understanding of the interfaces and surface interactions are critical to process optimization. In contrast, contact-printing methods such as screen-printing, flexographic (short: flexo) printing or gravure printing are not only in direct physical contact with the substrate but may also apply pressure and, thus, limiting the selection of substrate materials. Furthermore, many methods require a master template, which increases the initial costs that arise from the production of a stencil as well as reduces the flexibility to implement quick changes to the design. Despite these obvious disadvantages, most contact printing methods enable true roll-to-roll (R2R) manufacturing with high throughput at low costs.<sup>[27]</sup> Contactless methods, such as inkjet- and aerosol jet, are usually digital printing technologies, which means that the printed image is transferred directly from a file or data stream from a computer to a printing press without using a static printing form (cliché). **Table 1** provides an overview of different printing and patterning technologies used for manufacturing of printed and hybrid electronics. It has to be noted that while classic nanoimprinting is not always an additive process as it can comprise etching steps, it can still be considered a printing method.

Electronic components have continuously decreased in dimensions, today transistors with gate lengths of as small as around 7 nm are integrated in commercially available GPUs.<sup>[56]</sup> While those dimensions are far from what can reasonably be realized using most additive manufacturing technologies, there are various applications ranging from simple interconnections and elec-

**Table 1.** Different printing and patterning technologies for electronics manufacturing.

Printing method	Ink viscosity cP	Line width $\mu\text{m}$	Thickness $\mu\text{m}$	Speed $\text{m min}^{-1}$	Substrate interaction	References
Aerosol jet printing	0.7–2500	10–10 <sup>3</sup>	0.01–6	6	Non-contact	[28–30]
Dispenser/Extruder printing	10–10 <sup>6</sup>	50–10 <sup>3</sup>	10–200	0.6	Non-contact	[31–33]
EHD inkjet	1–10 <sup>4</sup>	0.1–0.7	0.001–0.1	Slow	Non-contact	[21, 34–37]
Flexo printing	10–500	30–80	0.17–8	5–180	Contact	[38]
Gravure offset	500–50 000	5–20	0.8–8	1–10	Contact	[39]
Gravure printing	100–1100	50–200	0.02–12	0.5–18	Contact	[38, 40, 41]
Inkjet (CJC, DOD)	2–100	30–50	0.1–20	0.02–5	Non-contact	[38, 42]
Laser induced forward transfer (LIFT)	—	0.3–10	0.1–1	Slow	Non-contact	[43–46]
Nanoimprint	—	0.005–0.1	0.1–1	$\leq 15$	Contact	[47–49]
Offset printing	200–500	20–50	0.6–2	Fast	Contact	[38]
Reverse offset	1–5	1–10	0.05–1	0.01–3	Contact	[50–53]
Screen printing	500–5000	30–100	3–30	0.6–100	Contact	[38, 54, 55]

trodes to sensors, where additive and printing technologies stand out with manifold advantages. A special feature of these technologies is their great flexibility in the choice of materials. Over the years, however, certain materials have become more established than others and are now primarily used. Silver ink is the most widely used in printed electronics due to advantages such as high conductivity and its long-term oxidation resistance.<sup>[57]</sup> However, a common problem with silver, which is well-known from the traditional semiconductor industry, is its migration into dielectric layers in the presence of an electric field. This leads to unwanted short circuits or degradation of components. Therefore, this problem should be considered already in the design stage by employing other materials, such as copper. Another way to mitigate this problem is the application of coatings and passivation layers. Parylene coatings are standard in the semiconductor industry and well suited for this purpose.<sup>[58]</sup>

The different technologies presented in Table 1 are not equally qualified considering the requirements for fabricating microelectronic components and hybrid electronic systems in terms of resolution and printing accuracy. 1) Inkjet printing, 2) EHD inkjet printing, 3) aerosol jet printing, 4) LIFT, 5) reverse offset printing, and 6) nanoimprinting lithography, can be considered as most promising as resolutions and positioning accuracies in the  $\mu\text{m}$  and even nm range can be achieved. Consequently, this section focusses on these technologies dealing with their working principles as well as their applications in research and industry. **Figure 1** shows the achievable resolutions of the reviewed printing technologies in relation to the size of physical objects. It becomes obvious, that with all presented technologies fine line widths below the limit of visibility for the human eye can be realized. The feature sizes that are achievable using NIL even exceed the physical limits of optical microscopy, since resolutions smaller than the wavelengths of visible light can be achieved.

## 2.1. Inkjet Printing

As a digital, non-contact and additive method, inkjet printing is one of the most commonly used technologies for prototyping and research. The inkjet printing equipment market was esti-

mated to be \$356.6 M in the year 2018 and is expected to grow by 27% to reach \$454.2 M in 2024, primarily driven by the advancements in IoT, 5G applications, and wearables.<sup>[59]</sup> The prevalence of inkjet printing is due to its typically low material and energy consumption, making it both environmentally friendly and low-cost. As in graphical multi-color printing, multi-material printing can be easily implemented employing a multi-nozzle configuration, and material can be deposited on a variety of substrates and topographies. Additionally, the use of digital patterns, as opposed to a master plate, allows for a versatility that is hardly reached by other additive techniques. Patterns can be modified at any time, making inkjet printing exceptionally well suited for scientific research, fast prototyping, and productions of extremely small batch sizes. This is noticeably reflected in scientific literature, which has seen a sharp increase since the 2000s.<sup>[60]</sup> These benefits are similarly realized by industrial R&D (e.g., inkjet-printed OLED displays<sup>[25]</sup>) and potential high-volume applications as well, where re-tooling equipment can be cost-prohibitive and be a deciding factor in whether or not a product is considered for mass-production.

These virtues of inkjet printing, in particular, offer a variety of potential boons valued by the semiconductor industry. The evaluation of new designs or materials with conventional fabrication processes can be expensive, laborious, and time consuming compared to inkjet printing, where, in contrast, material chemistries, processes and designs can be prototyped and evaluated with much greater flexibility and speed.

While multiple modes of inkjet printing exist, this section focuses specifically on drop-on-demand (DOD) piezo-inkjet technologies, process, tools, and applications.

### 2.1.1. Drop-on-Demand Inkjet Printing

A DOD printer only releases droplets when its nozzles are triggered (**Figure 2**), which are either thermally or piezoelectrically actuated. Thermal inkjet (TIJ) DOD printing uses a heating element inside of the print head, which provokes the formation of a small vapor bubble forcing a pressurized drop of ink out of the nozzle. Commercially speaking, this is commonly referred to as

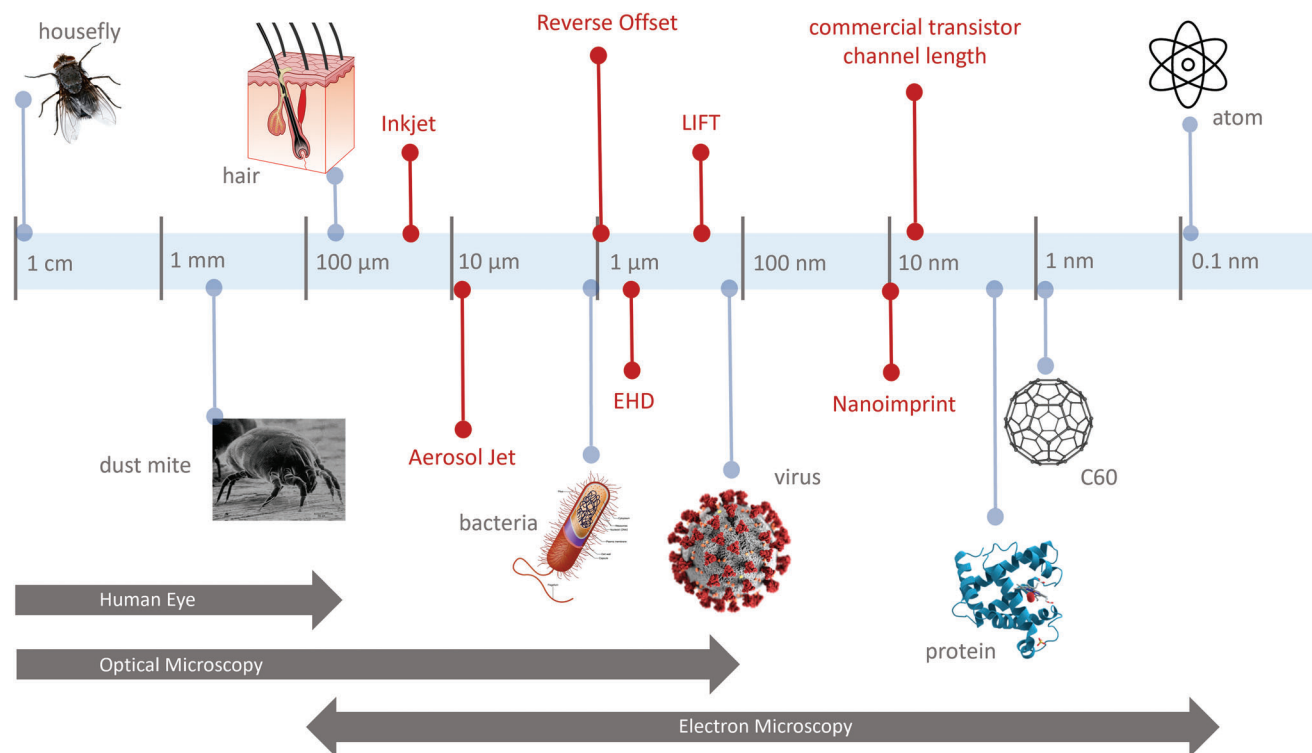


**Figure 1.** Overview of the size relationships between physical objects and the technical manufacturing possibilities that can be achieved with the presented technologies.

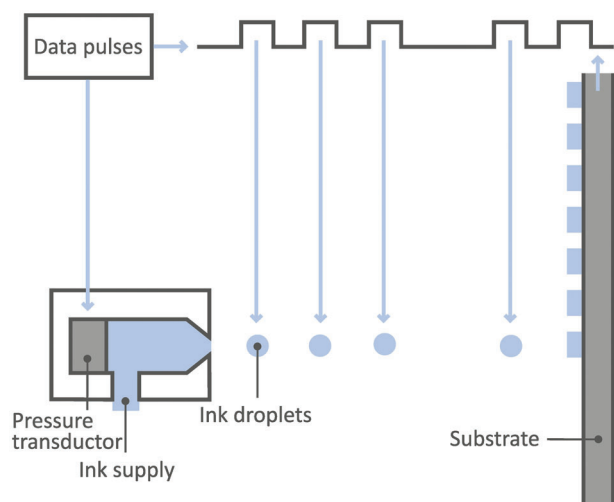


**Figure 2.** Graphical representation of drop-on-demand inkjet printing. Reproduced with permission.<sup>[61]</sup>

bubblejet. While TIJ technology has been popular in household applications, due to its low cost and ease of manufacturing, the nature of its actuation mode imposes a severe handicap on stable jetting of inkjet materials, maximum jetting frequency and printhead durability. Those issues can be overcome by using piezoelectric inkjet (PIJ) printing, where a piezoelectric actuator is deformed by applying an electrical drive voltage to facilitate drop ejection. Such PIJ DOD inkjet printers are mostly designed in

a multi-nozzle configuration. While TIJ enjoyed relatively early consumer adoption until advancements in manufacturing technology, MEMS and printhead development allowed PIJ to arise as the superior actuation mode toward the end of the 20th century. As drop ejection in a TIJ printhead is solely dependent on superheating the printhead ink and subsequent bubble collapse, PIJ offers much finer control over aspects of ink-jetting, due to precise control of the piezoelectric elements via modulation of the applied voltage and waveform.

One of the primary advantages of DOD inkjet printing over traditional subtractive manufacturing processes and even other additive techniques lie in the prospect of scalable, free-form multi-material printing. Despite various process-related challenges, small-scale demonstration of multi-material printing has been successfully demonstrated in deploying alternate routes toward bulk materials deposition<sup>[62]</sup> as well as fabricating 3D structures.<sup>[63,64]</sup>

The characterization of inkjet printing performance is focused on droplet volume, droplet velocity, drop formation, jetting straightness, and jetting stability. While these criteria are critical and well controlled in consumer and industrial printed graphics applications, printed electronics can be said to have much more stringent requirements asked of the quality of deposition and processing. Typical inks used for PIJ printing are formulated to have a surface tension in the range of 2–30 mPaS with a viscosity of 2–100 cP,<sup>[65]</sup> but otherwise may vary greatly in composition, for example, ranging from solvent-based to solvent-less inks, UV-curable monomer, or functionalized nanoparticles. The effects of droplet formation, drop velocity, jetting straightness on

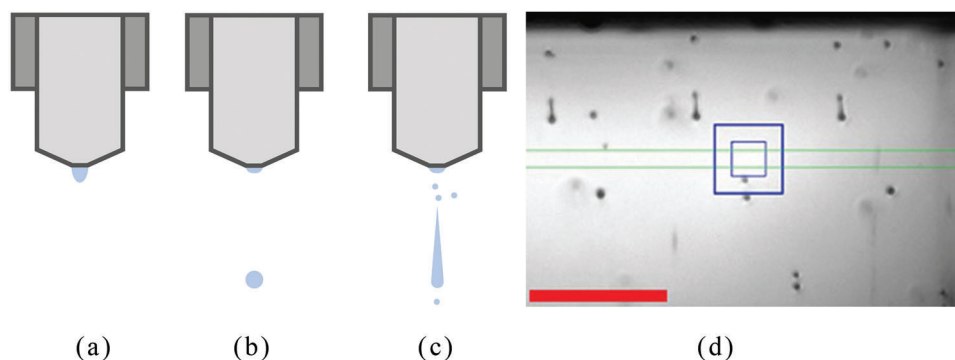


**Figure 3.** Droplet forms in inkjet printing; a) No jetting, b) ideal jetting, c) formation of satellite drop (Reproduced with permission.<sup>[61]</sup>); d) monitoring of jetting (PixDro LP50): Screenshot from the dropview camera which erratic, unstable jetting of immediately after printhead idle state. Primary droplets are present from 9 nozzles in this view, albeit with crooked jetting and accompanied with satellite droplets and undesirable misting/spraying. Scale bar represents 70  $\mu\text{m}$ .

an inkjet printing process are well understood. For a high printing quality, consistent droplets of material must arrive at their intended target location on the substrate with as much fidelity to the digital pattern as possible. If the viscosity and the surface tension of the ink together with the printing parameters do not conform clogging (Figure 3a) or the formation of so called satellite droplets (Figure 3c) can occur, which can significantly degrade the printed pattern quality. On the other hand, Figure 3b shows ideal jetting. Inkjet artifacts, which may manifest through either satellite droplets, jetting instabilities, or crooked jetting alter the quality of a printed product.<sup>[66]</sup> Jetting instabilities may arise as a result of cross-talk between the actuators of the nozzles inherent to printhead designs at certain operating points, though this has been shown to be mitigated through proper waveform tuning and optimization.<sup>[67,68]</sup>

Solvent-based inks may experience evaporation at the nozzle orifice, creating a concentration gradient between the orifice and pumping chamber and/or leaving behind solids that may clog the nozzle orifice. The practical relevance of this effect has been reported by Sowade et al.<sup>[9]</sup> As part of their investigation of electrical defects in printed structures they observed the quality of an array of inkjet-printed TFTs. They demonstrated that the first printed devices tend to be defective as the jetting had just started, which can be linked to the effects described by the “first drop problem.” The nanoparticles tend to agglomerate due to solvent evaporation when the printhead is in an idle state at the printing start position. This evaporation is causing material buildup in the printhead and particularly at the nozzle orifice negatively influencing the drop ejection.

Most commercially available inkjet printers for printed electronics prototyping provide the ability to monitor the resulting shape and speed of the droplet, as well as the stability of the jetting, typically using a high-speed camera, as illustrated in Figure 3d, or even provide software-assisted advanced drop optimization tools.<sup>[69,70]</sup> While literature on inkjet deposition of functional materials has been in abundance over the past two decades, guidance for inkjet waveform development generally remains elusive, and process development is a fine line between science and art.

Aspects of deposition such as the droplet volume, velocity, and jetting frequency are indicators of productivity and throughput,

which lend themselves to a highly tunable process suitable to laboratory development that is scalable to a high-volume manufacturing process for printed electronics.<sup>[71]</sup> However, these factors affect the overall wetting, curing, and drying kinetics of functionalized materials, and must be carefully tuned to ensure a preservation of the desired bulk material properties, morphology, and critical dimensions. Besides that, the influence of the nozzle pitch on the overall printing quality and resolution must not be neglected. As the nozzle pitch is fixed by the type of printhead, no arbitrary pitch of drop deposition can be realized either. Gan et al.<sup>[72]</sup> investigated the influence of the dot pitch on the merging effect of micrometer lines caused by ink spreading of PEDOT on a silicon substrate. As expected, a series of dots could not be merged to form a continuous line if the dot pitch is too large. On the other hand, a too small dot pitch leads to overlapping creating a larger line width than desired.

The pattern width, thickness, and quality of the print are further dependent on the inkjet drawing path, or in other words, the print direction. For commercial inkjet printing machines movement in the y- and x-direction is generally realized by either moving the printhead or the substrate table, respectively. The different positioning accuracies of the stages, consequently, lead to an orientation-dependent accuracy of the printed pattern. Apart from that, the printing pathway has an influence on the merging effect between individual droplets because of differences in the time interval between printing passes. For instance, if the ink dries before the next line printing, individual dots might not merge leading to defects in the structure. On the other hand, this effect can be beneficial for the realization of small gaps between individual lines. A recent study by Kwon et al.<sup>[73]</sup> provides more information about inkjet-printing design rules.

On fibrous substrates (e.g., cellulose-based and textiles) the porosity can lead to absorption of the ink in the direction of the fibers and consequently reduce the resulting resolution.<sup>[74,75]</sup> Non-porous, rigid substrates may facilitate pooling of deposited material and encourage bulging instabilities, reducing print resolution in a similar manner.<sup>[76]</sup> Wetting and drying behavior of inkjet inks, wetting characteristics of the bulk deposited material, jetting stability, and the print throughput are secondary to print fidelity and bulk material homogeneity/uniformity. The curing process continues to be the subject of significant research in

case of various substrates.<sup>[77–79]</sup> Hence, characterizing and tuning of an inkjet printing process must be done on a case-by-case basis for a given material, printhead, as well as for a given application.

A superb review of piezo inkjet history, nomenclature, and technology has been written by Herman Wijshoff<sup>[80]</sup> and is highly recommended by the authors for greater detail.

### 2.1.2. Inkjet Printheads

The crux of any inkjet-printing process is the printhead, which exist with a variety of actuation modes, components, and architectures that have a large influence over the stability of the jetting process and overall quality of material deposition. Commercially available state-of-the-art printheads can contain up to several hundred nozzles and enable the deposition of materials typically in the micrometer-range with a calibrated droplet volume from 1 up to 100 pL.<sup>[42]</sup> For many years, inkjet printing has been considered as too slow for the realization of large industrial throughput. However, the processing speed has been continuously increasing due to simultaneously jetting with a large number of nozzles (up to 2400 nozzles inch<sup>-1</sup>) with high drop ejection frequencies of more than 100 kHz and subsequent advances in post-processing technology.<sup>[81–83]</sup> Commercial PIJ printheads, regardless of their architecture, are optimized for high-throughput graphics printing applications and materials, and thus fall into the inconvenient position of a “one-size-fits-all” role for functional materials printing. As such, no production worthy printheads currently exist on the market that are bespoke for functional materials deposition, though numerous vendors exist to build printing tools and platforms dedicated to R&D, as well as high volume materials deposition applications. Vendor specifications for PIJ printheads, for example, droplet volume, nozzle pitch, and jetting frequency, are generally qualified using well-behaved inkjet inks with similarly optimized waveforms and printhead settings. In practice, droplet volume, droplet velocity, maximum jetting frequency, etc., are largely dependent on waveform development from the user and can deviate significantly from vendor datasheets. This holds true, especially, when considering non-standard, functional inks used for printed electronics. However, certain aspects of the printhead construction, architecture, and deformation modes bear large impacts on the performance and ease of the process development for a given application and set of materials. Yang et al.<sup>[84]</sup> demonstrated the importance of a non-wetting coating on a nozzle-plate, as well as the nozzle geometry in reducing the Rayleigh instabilities and facilitating an ideal drop formation.

As printhead development serves the graphics industry, printhead specifications have generally trended toward smaller droplet volumes, more headroom for jetting frequency, higher nozzle packing densities, and print resolutions. Within the realm of functional materials deposition, such specifications for the “latest and greatest” may be meaningless at best and detrimental at worst. Given the narrow range of surface tension and viscosity that inks must fall within for jetting, (2–100 cP), as well as consideration for loaded material that may be present in functional inkjet inks, the most sophisticated inkjet printheads may not be as well-suited to material jetting as compared to their older, more

rudimentary counterparts with larger nozzle diameters and drop volumes. Printhead heating may be an effective means to lower the viscosity and enable printing of previously un-jettable materials and is generally desirable for materials deposition. The material selection and robustness of the printhead nozzle plate have a significant impact on the drop formation and can determine whether or not an ink is suitable for sustained jetting, especially when considering high-volume deposition of functional materials. While most modern printheads can generally accommodate a broad swath of aqueous, solvent-based, or UV-curable inks, printhead maintenance, and ease of cleaning can be critical factors, which are easily overlooked when developing inkjet printing processes. The printhead architecture and actuation modes may further play a crucial role on the suitability of a printhead for a given application.

Recent development efforts within the printed electronics community have reflected this paradigm shift in rethinking the needs for a mature printed electronics ecosystem. Added Scientific, based out of Nottingham, UK, has opted to address this need with a modification to the existing PixDro LP50 platform to accommodate multi-material printing of high viscosity inks. **Figure 4** shows the printhead assembly utilizing Xaar 128 printheads.<sup>[85]</sup> The printheads utilize a bulk piezo actuator and have a nominal drop volume of 40/80 pL and are consequently low cost. Furthermore, they have been readily available and lend themselves to multi-head integration. Yet, with this setup, added scientific has demonstrated reliable jetting of high-viscosity, off the shelf SLA resins.<sup>[86]</sup> Quantica, a startup based in Berlin, has developed their own printhead and multimaterial printing system of similar capability.<sup>[87]</sup> The printhead is equipped with 84 60 μm nozzles that can produce droplets with a volume between 25–600 pL and is capable of jetting fluids between 1 and 250 cP. The printhead is described as having a bespoke actuation system utilizing volumetric displacement, as opposed to the typical acoustic modes commonly found in piezo inkjet printheads.<sup>[88]</sup> Both setups appear to be, on paper, less capable than modern printhead setups offered by traditional print industry today. However, trading off print resolution, minimum feature size and jetting frequency for a broadening window of inkjet material development and utilization may yet prove to be a worthwhile bargain for functional materials jetting development in the years to come.

### 2.1.3. Inkjet Printers in Research and Industry

In scientific research, commercially available, low-cost desktop office inkjet printers are frequently adapted for the deposition of functional materials.<sup>[89–91]</sup> Although this usually enables fast and cheap prototyping, high resolution printing can hardly be realized, and the lack of inkjet metrology tools makes it difficult to characterize and tune inkjet parameters. Specifically, the stability of the jetting process cannot be monitored and controlled, due to the absence of a drop-view camera. The jetting voltage (in case of PIJ) or temperature (in TIJ) cannot simply be adjusted without major modifications of the hardware. Therefore, in a practical approach, the functional ink must have properties similar to those originally intended for graphic printing with the corresponding printer model in terms of viscosity, boiling point, and rheology. Although the drop-volume is commonly specified by



**Figure 4.** a) Multi-printhead array modification to the PixDro LP50;<sup>[86]</sup> b) UHV print engine manufactured by Quantica<sup>[87]</sup> (Reproduced with permission from Quantica).

the manufacturer, it is impossible to observe the actual amount of ink which is transferred to the substrate. Another limiting factor is the inaccuracy of the substrate positioning system (paper feed) impeding precise multi-layer printing. For high volume manufacturing, printhead to substrate alignment, and jetting angle compensation features must be integrated to achieve reliable sub-hundred-micron patterning.

For R&D and industrial prototyping, a large variety of desktop inkjet printing systems dedicated to the deposition of functional materials are commercially supplied by different manufacturers. Amongst others, the Dimatix Materials Printer DMP-2850 (Fujifilm) and the PixDro LP50 (former: Meyer-Burger, since April 2020: SÜSS MicroTec SE) are prevalently used machines for R&D. Both are PIJ DOD printers and come with a built-in drop jetting observation system. The mechanical positioning accuracy and repeatability lie in the range of 15<sup>[92]</sup> and 25  $\mu\text{m}$ <sup>[93]</sup> for the PixDro LP50 and the DMP-2850, respectively. Low-cost, disposable inkjet cartridges make the Dimatix platform invaluable for testing ink formulations. While the LP50 has no bespoke printhead of its own, it allows to utilize a wide range of different print-head assemblies, and it is a platform that can accommodate multiple print strategies, for example, unidirectional vs. bidirectional raster printing alongside either the x or y axis of your substrate. Other vendors further differentiate themselves by adding additional process capabilities, for example, the Ceradrop F-Serie printer, which integrates inkjet and aerosol jet together on the same platform.<sup>[94]</sup> PVNanocell is known primarily for their nanometal inks, but they also offer an inkjet platform with multi-material and built-in post-processing capabilities.<sup>[95]</sup> Notion systems GmbH and Microdrop GmbH also offer printers targeting printed electronics development, and Epson has entered the fray with their own development inkjet printer that accommodates their own MEMS printhead.<sup>[96]</sup>

The growing offerings of inkjet printing systems undoubtedly reflect the potential printed electronics holds. Particularly, in the field of OLED manufacturing large, industrial-scale inkjet printing systems have recently been established. This is spurred by the 26% global market growth rate of OLED TV panels that is expected annually with the market for all types of OLED displays expected to grow to \$26bn by 2026.<sup>[97]</sup> A few examples of commercial industrial inkjet printer providers are presented in the following. For instance, the n.jet display inkjet printer provided by the German Notion Systems GmbH enables the simultaneous deposition of up to six different inks.<sup>[98]</sup> At the end of 2019, the Japanese semiconductor production equipment supplier Tokyo

Electron (TEL) launched their Elius500 Pro inkjet printing system for the manufacturing of OLED displays.<sup>[99]</sup> It allows for the deposition of up to 12 different inks within one printing pass. Additionally, large-area OLED displays can be realized with this technology as substrates with a size of up to 2.2 m  $\times$  2.5 m can be processed. Another supplier of industrial inkjet printing system for OLED manufacturing is Kateeva, located in Silicon Valley. Their YIELDjet FLEX system is the first inkjet solution specifically designed for thin film encapsulation in the mass production of OLED displays.<sup>[100]</sup>

#### 2.1.4. Self-Aligned Inkjet Printing

The limits regarding the achievable patterning resolution and deposition accuracy of inkjet printing can be reduced by surface modification techniques that enable self-aligned printing (SAP). This process comprises three major steps: i) Inkjet printing of the first ink layer, ii) altering the surface energy of this pattern without changing the wettability of the substrate, and iii) inkjet printing of the second ink layer. This second layer self-aligns due to droplet motion and the high contrast in surface energy between the first ink layer and the substrate. The second ink layer is therefore repelled by the altered low energy surface of the first layer, leaving a small gap in the sub 100 nm range, as schematically illustrated in **Figure 5a**. This technique has been successfully applied for the fabrication of sub-100 nm structures using PEDOT:PSS on a glass substrate.<sup>[101]</sup> Selective surface treatment can be employed, which includes the modification of the surface energy of the first ink layer using a CF<sub>4</sub> treatment. In this process the surface of the pattern is fluorinated, while the surface of the glass substrate remains unaltered. **Figure 5b** shows an example of an SAP TFT with top-gate electrode.<sup>[102]</sup> Zhao et al.<sup>[103]</sup> extended the method to the fabrication of functional conductive nanostructures with gold nanoparticle ink, while Cao et al.<sup>[104]</sup> reported the successful fabrication of high-performance carbon nanotube (CNT) TFTs with sub- $\mu\text{m}$  channel length.

Another option for the surface treatment is the so-called surface segregation process, in which the ink is supplemented with surfactant molecules consisting of a polar head group and a non-polar tail group. The added molecules then organize themselves at the surface, generating a repellent layer. A sufficient stability of the repellent layer needs to be achieved, as otherwise the surfactant molecules tend to reorganize, upon contact with the second printed layer.<sup>[102]</sup>

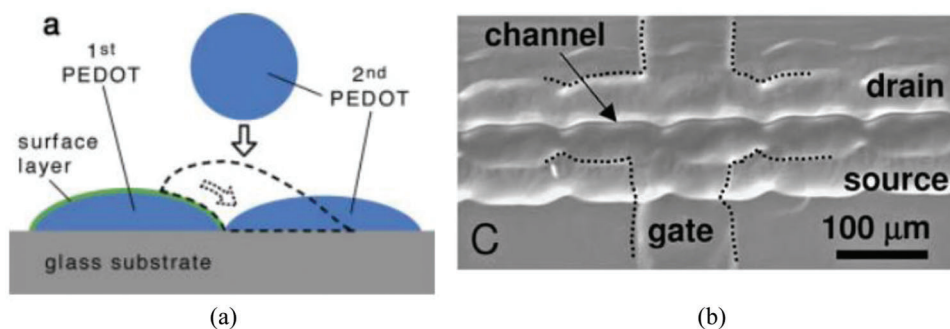


**Figure 5.** a) Schematic of the SAP printing process using PEDOT:PSS (Reproduced with permission.<sup>[101]</sup>); b) SAP printed thin film transistor with top-gate electrode (Reproduced with permission.<sup>[102]</sup>).

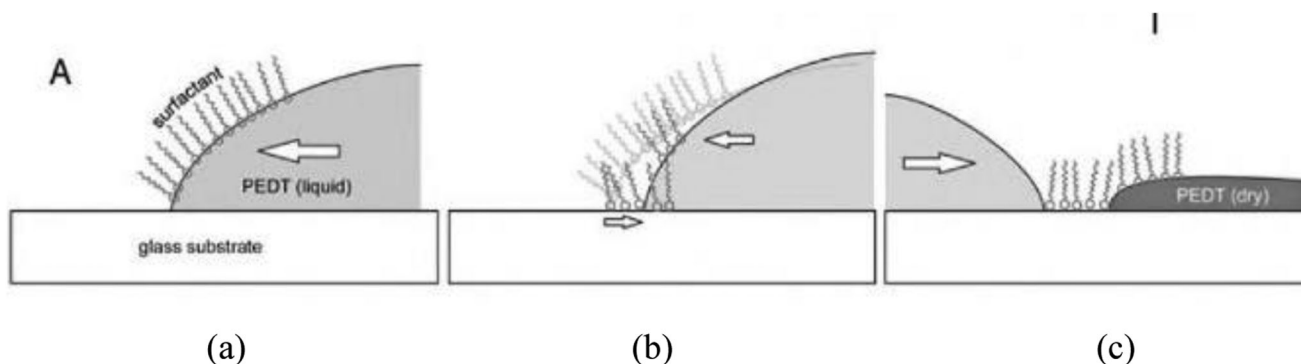


**Figure 6.** Working principle of the autophobing SAP mode on glass substrate: a) Surfactant molecules aligning around first printed droplet; b) Ink recedes due to surfactants; c) Printing of second droplet close to the first dried ink droplet resulting in a small gap due to the surfactants. Reproduced with permission.<sup>[102]</sup>

However, for lower resolution applications the usage of an autophobing surface mode may be desirable, which enables the generation of self-aligned gaps with micrometer dimensions. As part of this process the surfactants align around the ink droplet repelling it and creating a well-defined barrier between the printed droplets, as illustrated in **Figure 6a–c**.<sup>[102]</sup>

## 2.2. Electrohydrodynamic Printing

The EHD inkjet printing (sometimes referred to as electrostatic or e-jet printing) technique can be considered as an advancement of inkjet printing in terms of precision. Inkjet printing technologies quickly reach their limits when micro- and nanopatterning is required. However, further decreasing the nozzle size is neither feasible nor reasonable. A smaller nozzle orifice would adversely affect the jetting, since it becomes more difficult to push out droplets depending on the ink's viscosity and surface tension. Additionally, clogging might become an issue with inks containing solid content (e.g., nanoparticles or nanowires).<sup>[81,105]</sup>

EHD printing addresses these issues by applying an electric field between the nozzle and the substrate which pulls the ink out instead of pushing it out (**Figure 7**).

An EHD printing system basically consists of an ink supply system that generates back pressure, nozzle, substrate stage positioning systems, high voltage supply, as well as, devices for visual-

izing the ink flow to monitor the jetting behavior and imaging the printed patterns.<sup>[71]</sup> Droplets much smaller than the nozzle size can be generated when a high voltage is applied and the electric field force surpasses the surface tension force. The liquid ink is supplied to the tip of the nozzle forming a hemispherical meniscus. The ionic components migrate within the liquid depending on their charges and direction of the electric field, resulting in an accumulation of ions with identical charge at the liquid surface. Those ions, consequently, repel each other, causing tangential electric stress on the liquid surface, which is increasing with increasing voltage. At the equilibrium point, at which the electric field force equals the surface tension force the liquid ink forms a so-called Taylor's cone, which is a semi-vertical cone with an angle of  $49.3^\circ$ .<sup>[106]</sup> As soon as the electrostatic stress exceeds this equilibrium an ink jet is ejected from the Taylor's cone.<sup>[105]</sup> **Figure 8** provides a schematic illustration of how these forces act on the ink.

The speed and the shape of the generated droplets depend on the applied voltage. Very high resolutions can be achieved with a drop volume lying in the range of attoliters<sup>[107]</sup> rather than picolitres, as in conventional inkjet printing (**Figure 7**). The ratio between the inner nozzle diameter and the drop diameter is called “neck-down” ratio and ranges from about 10 in conventional systems<sup>[108]</sup> to  $10^3$  in highly optimized systems.<sup>[109]</sup> In addition, the drop size and jetting mode can be controlled by the applied voltage and the ink flow rate, as illustrated in **Figure 9**.<sup>[110]</sup> At a lower electric field strength, droplets are jetted mainly due to

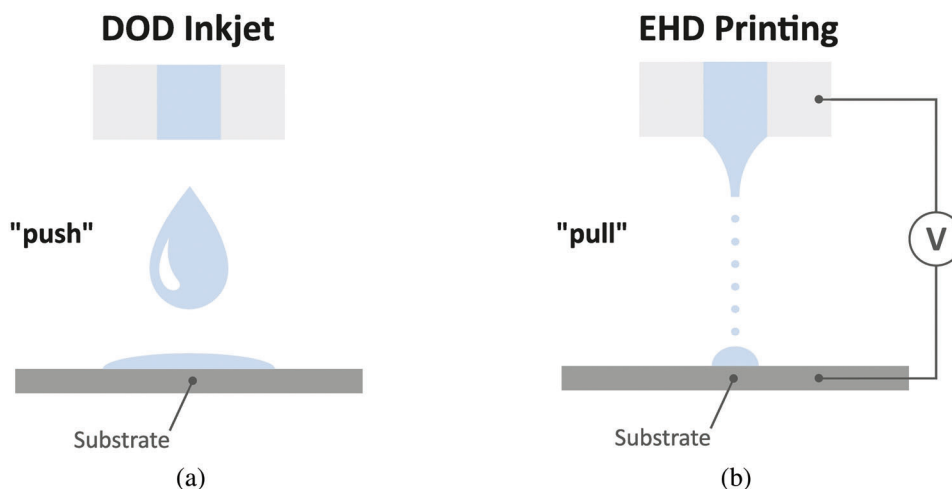


**Figure 7.** Comparison of a) DOD inkjet printing and b) EHD printing. Reproduced with permission.<sup>[61]</sup>

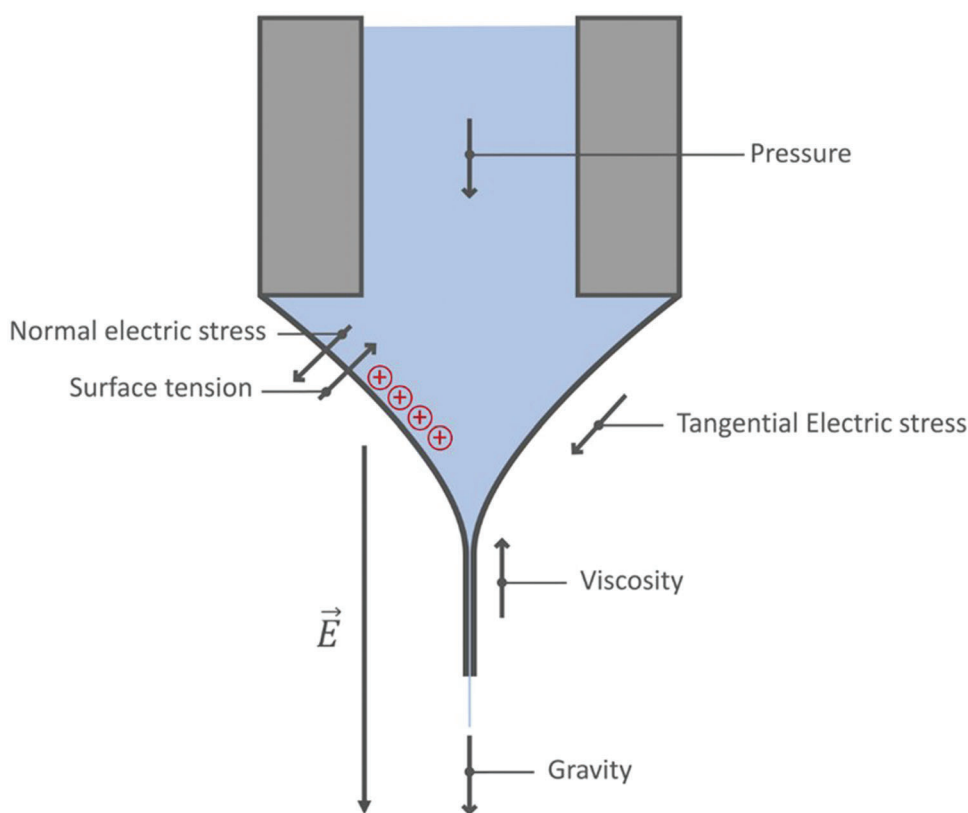


**Figure 8.** Schematic illustration of drop-formation in EHD printing and the forces that act on the ink. Reproduced with permission.<sup>[61]</sup>

gravitational forces, which is referred to as “dripping”-mode.<sup>[111]</sup> For high-resolution printing, the characteristic EHD cone-jet is desired. It is characterized by the formation of a constant Taylor cone and can be realized by increasing the electric field strength while reducing the flow rate.<sup>[71]</sup> At further increased voltages a complex jetting behavior occurs, leading to uncontrollable and multiple jets and ultimately results in an atomization or spray mode.<sup>[111]</sup>

Generally, inks with a broad range of viscosities can be printed, including liquids, nano- and microparticles,<sup>[112]</sup> as well as nanowires,<sup>[113]</sup> and even molten metal.<sup>[114]</sup> However, the viscoelastic ink properties must not be neglected when formulating a well-printable ink.<sup>[115]</sup> Furthermore, to ensure high accuracy in the placement of the drops the distance between the nozzle and the substrate surface should be as small as possible, typically in the range between 0.1 and 1 mm, and kept constant. This fact

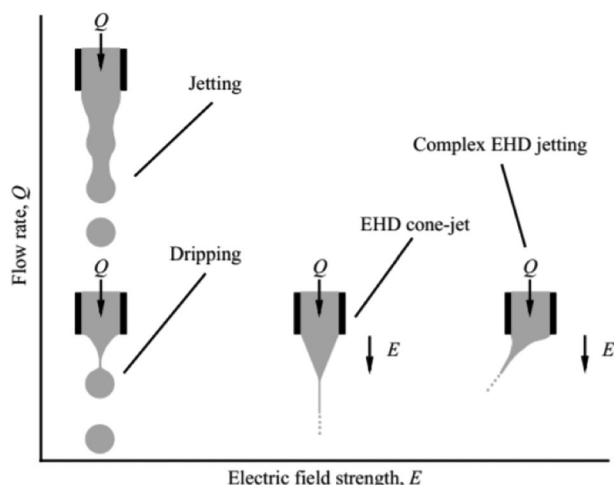


**Figure 9.** Different printing modes in EHD printing dependent on the flow rate ( $Q$ ) and electric field strength ( $E$ ). Reproduced with permission.<sup>[110]</sup>

can lead to problems in many practical applications, since already a higher substrate surface roughness might impede equidistant spatial printing.<sup>[116]</sup>

Due to the nature of EHD printing the electrical properties of the substrates need to be considered.<sup>[111]</sup> In printed electronics polymeric and hence insulating substrate materials are commonly employed. However, a cumulative buildup of charges on the surface occurs, when using dielectric substrates, which can lead to a distortion of the electric field and, consequently, to unwanted variations in drop size and drop positioning. This issue is typically addressed by employing either conductive substrates/substrate supports, or by applying an AC instead of a DC voltage.<sup>[111,117]</sup> The droplets are alternately positively or negatively charged and, consequently, electrically neutralize each other on the substrate.<sup>[111]</sup> In general, the steady jetting frequency is approximately twice the resonant oscillation frequency of the meniscus.<sup>[118]</sup> However, to increase the efficiency and speed in EHD printing, the pulsed frequency limit can be increased by utilizing high-order-mode jetting, which was recently demonstrated experimentally as well as analytically for a printing system with a rather low damping ratio by Li et al.<sup>[119]</sup>

The principle of EHD printing can either be applied to the CIJ or to the DOD inkjet printing mode. A constant voltage is applied in the CIJ-EHD printing mode, which makes the stabilization of the micron sized jet comparatively difficult. Besides that, issues have been observed regarding the placement of the drops at the beginning and the end point of the pattern. In contrast to that in the DOD-EHD printing mode the jet emission is controlled by employing a pulse generator, which leads to an increased accuracy in the placement of drops.<sup>[105]</sup>

The EHD printing technology is most commonly employed for 2D printed electronics applications, however, there are also approaches to use it for 3D printing.<sup>[120,121]</sup> As an example, Galliker et al.<sup>[21]</sup> exploit the principle of structure growth by electrostatic nanodroplet autofocusing. This means that, once the foundation of a pillar has been laid by some first few drops, the electrostatic field induced at the curved surface of the pillar tip focusses the following incoming nanodroplets, which enables the growth of

a pillar. In this way, they demonstrated the fabrication of free-standing EHD-printed gold nanopillars with a diameter of 50 nm. For a more comprehensive overview of the EHD printing principle, technical background, recent progress, and printable materials, the interested reader is referred to an excellent review by Kwon et al.<sup>[122]</sup>

### 2.2.1. Electrohydrodynamic Printers in Research and Industry

In scientific research on printed electronics, individually developed EHD printers are most commonly used.<sup>[123]</sup> These systems and components keep being improved to achieve higher resolutions and accuracies as well as to address process challenges. As an example, while the size of the nozzle plays only a secondary role for the printing quality, the influence of the nozzle geometry on the achievable resolution, droplet volume, and jetting stability can be critical.<sup>[124]</sup> In 2015, Kim et al.<sup>[34]</sup> studied the influence of the needle orifice geometries and driving voltage on the achievable printing resolution by comparing the performance of commercial flat and hypodermic needles. For the flat needle, the resulting drop-size is dependent on the shape and diameter of the needle, while for the hypodermic needle on the one hand the UV treated wall facilitates downward-slipping of the ink while the geometry contributes to the formation of a very small meniscus. In this way a line width of 0.7  $\mu\text{m}$  could be realized. Similarly, Youn et al.<sup>[35]</sup> were able to reduce the drop size by employing a tilted nozzle demonstrating the printing of fine lines of 5.8  $\mu\text{m}$  in width. A more recent approach to increase the EHD resolution was presented by Zou et al.<sup>[36]</sup> They deposited microdroplet arrays and microwires with a diameter of as small as 2.3  $\mu\text{m}$  by introducing a 20  $\mu\text{m}$  tip at the center of the nozzle orifice (diameter of 80  $\mu\text{m}$ ). In general, achieving the desired printing resolution and overall results is still a major challenge in EHD printing, due to the high complexity of the mechanism and limited process optimization techniques. To address this challenge, Jiang et al.<sup>[125]</sup> recently proposed a CFD model for the investigation of the mechanism of cone-jet printing. Their simulations showed a satisfactory agreement with experiments for the prediction of printing behavior and quality considering jetting diameter and printed droplet diameter.

Although EHD printing is generally less prone to nozzle clogging, it can still be an issue, for example, when printing colloidal inks with high concentrations. To address this challenge, Li et al.<sup>[126]</sup> proposed a circulating dual-channel nozzle system, which enables constant ink-movement during jetting and in idle state. This nozzle consists of two coaxially aligned capillaries with the ink flow passing through the inner channel and then circulating back through the outer channel by means of a syringe pump. They demonstrated this principle for rather low-resolution EHD printing (drop-sizes in the range between 130 and 230  $\mu\text{m}$ ); hence, downscaling will be required for future high-resolution applications. Besides single-nozzle EHD systems, various groups, such as Sutanto et al.,<sup>[127]</sup> have proposed and demonstrated multi-nozzle systems either to increase the throughput<sup>[128,129]</sup> or for multi-material EHD-printing.<sup>[127]</sup> Similar to conventional inkjet printing, one issue arising from multi-nozzle systems is the crosstalk between the individual jetting streams, resulting in an asymmetric electric field, which ulti-

mately has an adverse effect on the printing quality. Therefore, the distances between the nozzles as well as their position relative to each other have to be optimized by employing methods such as the triangular nozzle array.<sup>[130]</sup>

Due to the high resolutions, prominent application examples for EHD printed electronics are, for example, the fabrication of transparent metal electrode grids,<sup>[131,132]</sup> printed TFTs,<sup>[133]</sup> as well as memristors.<sup>[134]</sup>

There are only few commercial EHD systems for R&D or industrial printed electronics fabrication available yet. One example of a commercial system is offered by the Korean based company Enjet Inc., which has patented its own EHDs iEHD jet technology and commercially supplies their iEHD jet and iEHD coating platforms.<sup>[135]</sup> Their eNanojet Printer is designed to print fine lines with widths down to 1  $\mu\text{m}$ ,<sup>[136]</sup> however, the mechanical accuracy of the positioning system is limited to  $\pm 15 \mu\text{m}$  at a motion repeatability of  $\pm 1 \mu\text{m}$ . The Japanese company SIJ Technology commercially provides super fine inkjet printers capable of feature sizes smaller than 1  $\mu\text{m}$ .<sup>[137]</sup> However, the term “inkjet” is rather misleading in the context with their product, as it uses an electrostatic force for the ink ejection, making it an EHD technology. The Swiss start-up Scrona (spin-off from ETH Zürich)<sup>[107]</sup> provides a semi-commercial solution. They assist in the development of EHD printing systems at their customers’ facilities and offer technology consultancy regarding ultra-high-resolution printing solutions.

Multi-nozzle implementation of EHD printing has been proposed in scientific literature before.<sup>[138]</sup> However, crosstalk between the nozzles remains a major limiting factor for practical implementations. Therefore, a minimum nozzle pitch of 2 mm is required.<sup>[139]</sup> Yet, the principle of EHD printing has proven to be scalable for graphics printing (decoration and labelling): The Australian company Tonejet<sup>[140]</sup> offers a commercial multi-nozzle EHD inkjet printing system, which allows for the deposition of 600 dpi at a throughput of 1  $\text{m s}^{-1}$ . Even though the EHD-system is unlikely to get clogged, this machine comes with an automated ultrasonic maintenance. Since the 1990s, Tonejet has filed several patents on their EHD inkjet working principle and printhead design (e.g.,<sup>[141–143]</sup>). Those printheads have comparatively large nozzle openings which accommodate individual electrodes extending beyond the orifice. The electric field at the nozzle opening triggers the drop ejection due to repulsive forces between charged particles in the ink. The electrically conductive paths of the individual nozzle channels are isolated over their length. This helps to reduce electrophoretic effects causing a build-up of particles on the channel walls which consequently reduces the flow of material to the ejection locations. The resulting droplet size is comparable to that of conventional DOD piezo inkjet, which implies that there is no improvement of resolution compared to inkjet printing. However, the ejected droplets have a considerably larger concentration of particles compared to the bulk ink,<sup>[138]</sup> which could be beneficial for printed electronics applications due to higher solid loading.

### 2.3. Aerosol Jet Printing

Like inkjet and EHD printing, aerosol jet printing (AJP) is a digital non-contact deposition method, yet the working principle is

totally different. Instead of mechanical pushing (inkjet) or electrostatic pulling (EHD) the ink out of a nozzle, it is atomized either by an ultrasonic nebulizer or a compressor nebulizer.<sup>[28]</sup> Droplets larger than around 5  $\mu\text{m}$  get separated from the printing aerosol stream due to gravitational force. In addition, small and medium sized particles can be sorted out with the aid of an exhaust flow.<sup>[144]</sup> Afterward the aerosol carrier gas stream is collimated into a narrow beam by a sheath gas stream and deposited on the substrate at a typical ejection speed of around 100  $\text{m s}^{-1}$ .<sup>[145]</sup> In addition to the physical nozzle, the sheath gas stream acts as virtual nozzle enabling the formation of a gas stream with a much smaller diameter than the nozzle orifice. Commonly, Nitrogen is used for the gas streams. As illustrated for compressor nebulization, the AJP working principle is described in **Figure 10**.<sup>[81]</sup> For the AJP process, parameters such as the carrier gas flow rate or the flow rate of the focusing sheath gas have to be controlled to guarantee stable printing. Similarly, the speed of the stage that transports the substrate beneath the beam is adjusted to achieve consistent printing quality. It has been shown that the ratio between the sheath gas flow and the carrier gas flow, the so-called focusing ratio, can be considered as key parameter. Generally, the achievable line width decreases with increasing focusing ratio and stage speed.<sup>[146]</sup>

Nozzle clogging is generally not an issue with AJP, as the nozzle opening diameter lies in the range of more than 200  $\mu\text{m}$ . Due to the atomization process, a drop volume in the range of femtoliters can be achieved. This enables the deposition of high-resolution patterns with printed features down to 10  $\mu\text{m}$  and registration of down to 5  $\mu\text{m}$ .<sup>[147]</sup> Furthermore, the AJP process is comparatively insensitive to changes in the distance between the nozzle and the substrate surface. A nozzle-substrate distance of 1–5 mm in stream direction can typically be tolerated without any degradation of the printing quality, enabling precise printing on rough and 3D surfaces, as demonstrated by Tait et al.<sup>[148]</sup> for the fabrication of light emitting diodes. Another major advantage of the AJP principle is its compatibility with a broad range of ink viscosities if a pneumatic nebulizer is used (0.7–2500 cP).<sup>[30]</sup> The processable viscosity is typically limited to a range of 0.7–30 cP with ultrasonic nebulizers.<sup>[149]</sup> However, ultrasonic nebulizers offer the advantage of generating a spray mist that consists of droplets with more uniformly distributed sizes.<sup>[28]</sup> One drawback of the AJP principle is that during printing the jetting cannot be interrupted without wasting material, as a shutter is used.<sup>[81]</sup>

#### 2.3.1. Aerosol Jet Printers in Research and Industry

In academia, AJP has been commonly employed for electronic packaging and the fabrication of interconnects.<sup>[149–153]</sup> As an example, Khorramdel et al.<sup>[151]</sup> reported the AJP of electrical interconnects in single crystal silicon-on-insulator MEMS accelerometers on wafer-level. They deposited aluminum ink to bridge the device layer and the handle wafer over the intermediate buried oxide achieving a low resistance of around 4  $\Omega$  per via. Jabari et al.<sup>[150]</sup> studied the feasibility of printing micro-scale graphene interconnects on Si/Si<sub>2</sub> wafers. They achieved printed controllable line widths as small as 10  $\mu\text{m}$  with a resistivity of 0.018  $\Omega\text{-cm}$ .

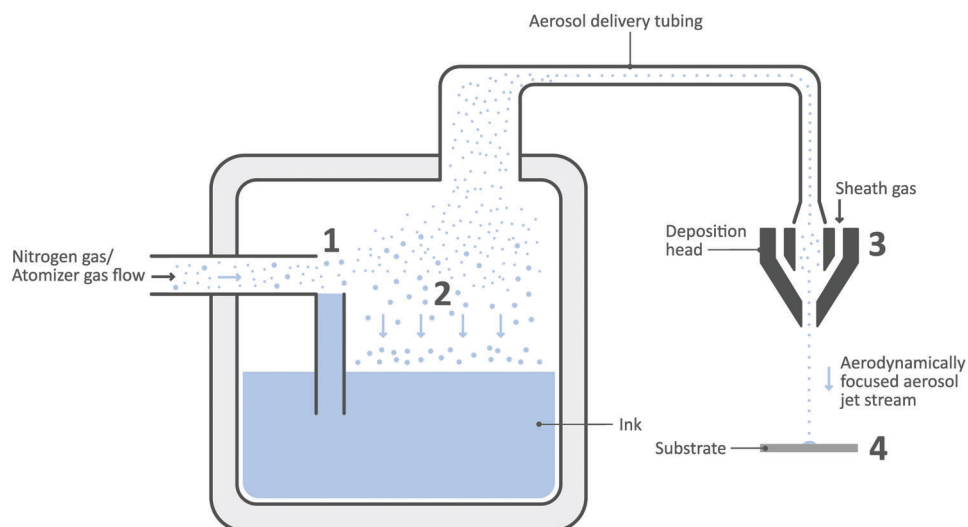


**Figure 10.** Working principle of a compressor nebulizer aerosol jet printer: 1) Atomization of the liquid content; 2) large aerosol are sorted out due to gravity; 3) focusing of aerosol jet due to sheath gas; and 4) deposition on the substrate. Reproduced with permission.<sup>[61]</sup>

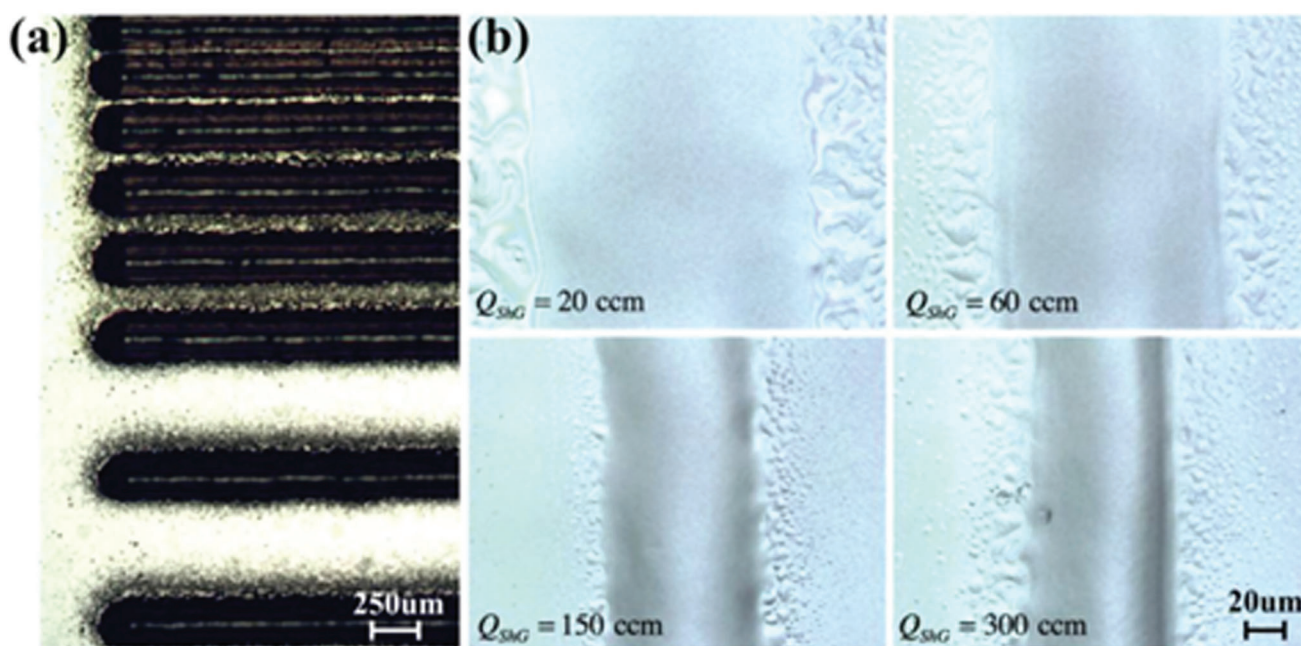


**Figure 11.** a) Example of aerosol jet printed lines with overspray artifacts on a flat glass substrate. b) Aerosol jet printed lines with a constant print speed of  $s^{-1} \frac{1}{4} \text{ mm}$  and sheath gas flow rates ranging from 20 to 300  $\text{cm}^3 \text{min}^{-1}$ . Reproduced with permission.<sup>[156]</sup>

One major advantage of AJP is the possibility to print a large variety of different inks employing only one single technology. As an example, Cao et al.<sup>[154]</sup> demonstrated the fabrication of fully printed hysteresis-free CNT thin-film transistors on a flexible polyimide substrate. The channel consisted of high-purity (>99%) semiconducting CNTs and the electrodes were made from silver nanoparticle ink, while a hydrophobic poly(vinylphenol)/ poly(methyl silsesquioxane) blend was used to fabricate the gate dielectric.

As for most printing technologies several parameters have to be controlled to avoid artifacts and guarantee high quality print-

ing. The most prominent and grievous artifact in connection with AJP is most probably the so-called overspray, as illustrated in **Figure 11**. This means that particles spread from the center of the deposition gas flow increasing the line width while impeding the formation of defined edges. In terms of resolution, this is a major limiting factor in practical applications because the line separation has to be increased in order to avoid contaminations of neighboring structures.<sup>[155]</sup>

Binder et al.<sup>[157]</sup> provided an analytical investigation of AJP and they observed that especially for small sheath gas to aerosol jet ratios the ink density is decreasing from the center to the edges of

the printed lines. It is believed that this is caused by deflection of the droplets, due to elastic collisions with substrate surface structures or by the radial flux of the aerosol jet in proximity of the substrate. In addition, dried ink residue on the inside of the nozzles can cause turbulences in the aerosol stream which again promotes the formation of overspray artifacts.<sup>[158]</sup> Chen et al.<sup>[156]</sup> studied the effect of droplet sizes on the severity of the overspray artifact. They concluded that larger drop sizes contribute to the formation of a more collimated line width, a theory that is supported by the prevalence of smaller sized droplets in the line-edge areas. Wide overspray can also be caused by the addition of surfactants, which help to reduce the particle diameter to increase the density of ultrasonic mist and to decrease the size of the droplets. This aids in the realization of more homogenous patterns, increasing the electrical conductivity.<sup>[159]</sup> While analytical approaches help to gain a deeper understanding of the overspray mechanisms, in practice minimization of overspray is currently done through empirical optimization.<sup>[28]</sup>

In comparison to, for example, inkjet and EHD printing, another challenge in AJP is the evaporation of solvents when using nanoparticle inks, which is significantly promoted by the flow of the carrier gas. The drying of the ink does not only change the physical properties of the ink (viscosity, solid content) and hence requires adaption of the printing parameters but can ultimately also lead to the formation of sludge at the bottom of the ink container.<sup>[158]</sup> Wadhwa et al.<sup>[158]</sup> proposed an ink “add-back” system to address this issue, which means that the atomizing gas stream is moistened with solvents. Especially in an industrial context this could enable longer print runs if the solvent “add-back” rate is optimized for the given system and ink.

In an approach to reduce the practical relevance of typical artifacts, Salary et al.<sup>[160]</sup> presented a comprehensive attempt for the inline monitoring of process conditions in AJP by employing multiple temporal and imaging sensors into a commercial AJP system. By employing a novel digital image processing quantification of the printed line morphology (line density, overspray, continuity, edge smoothness, etc.) the identification of incipient process drifts was enabled. In addition, computational fluid dynamics investigation of pneumatic atomization, aerosol transport, and deposition in the AJP process was presented.<sup>[160]</sup>

Even if there are still some process parameters to be optimized and a lot of research is going on in this direction, AJP has already been commercialized by Optomec Inc. and integrated deposition systems, since the late 1990s.<sup>[28]</sup> Optomec holds patents on the majority of know-how related to the AJP deposition technology itself<sup>[161]</sup> and numerous associated advancements, such as the miniaturization and usage of aerosol jet arrays<sup>[162]</sup> as well as the shuttering of aerosol jet streams.<sup>[163]</sup> Therefore, Optomec is the only commercial provider of AJP systems. As of today, they provide different printing solutions from commercial R&D AJPs (e.g., Aerosol Jet FLEX system<sup>[164]</sup>), which are reportedly used by various research groups, to an industrial R2R-capable aerosol jet print engine.<sup>[165]</sup> With a nominal feature size of down to 10  $\mu\text{m}$  and a motion repeatability accuracy of  $\pm 2 \mu\text{m}$  comparatively high-resolution printing can be realized. Employing Optomec’s aerosol jet print engine for high-volume throughput, the simultaneous deposition of two different materials is enabled when two modules are installed. An optional add-on to the FLEX-system is

the tilt-and-rotate trunnion making the system full 5-axis of coordinated motion capable for printing onto 3D structures. All Optomec AJP systems are available either with pneumatic or with ultrasonic nebulizers.

The French company Ceradrop commercially offers a hybrid printer integrating up to four inkjet heads and one Optomec aerosol jet head into one single system.<sup>[94]</sup> Besides Optomec’s AJP, several different commercially available inkjet printheads, such as Dimatix, Konika-Minolta, and many others, are compatible with this system.

On an industrial scale, AJP has already hit the commercial market for the direct spraying of antennas and other electronics onto non-planar mechanical structures.<sup>[166]</sup> Other commercial fields of applications in mass production cover the printing of RF interconnects, replacement of wire-bond in IC packaging, as well as the fabrication of multilayer and miniature circuits.<sup>[167]</sup>

#### 2.4. Laser Induced Forward Transfer

LIFT is a high-resolution, digital, non-contact, solvent-free, extremely versatile Laser-direct write technique with its origins dating back to 1970.<sup>[168]</sup> Since then, this technology has been extensively developed, inter alia for the precise deposition of DNA<sup>[169]</sup> and biomolecules.<sup>[170]</sup> However, this technology was also brought into the context of printed electronics as early as 1986, when Bohandy et al.<sup>[171]</sup> reported the laser deposition of copper onto silicon substrates inside a vacuum chamber. As illustrated by its schematic working principle in **Figure 12**, the irradiation of a high-power laser causes the ablation of the donor material (ink), which can either be liquid or solid. This way a large variety of organic and inorganic materials can be processed. In fact, nearly every material that can somehow be deposited on transparent supporting substrates (like glass, quartz, or transparent foils) could potentially be LIFT printed. Liquid donor materials are prepared employing different standard liquid coating methods, such as spin coating, blade coating,<sup>[172]</sup> and roller coating,<sup>[173]</sup> resulting in thin films with a thickness of tens of  $\mu\text{m}$ . Metallic thin films are commonly fabricated by evaporation.<sup>[44]</sup> After the LIFT process, the individual deposited drops are commonly referred to as voxels. Using LIFT printing a high lateral resolution is achievable, since it is ultimately solely limited by the laser spot-size itself, which typically lies in the range of a few  $\mu\text{m}$ . However, as demonstrated by Willis and Grosu,<sup>[174]</sup> processing conditions can be optimized in a way that only the central region of the donor film is transferred. This enhances the resolution significantly, the deposition of features with areas  $\approx 100$  times smaller than the laser spot size have been demonstrated. Therefore, the application of LIFT for high resolution printing has been widely studied and exploited. As an example, Banks et al.<sup>[44]</sup> reported the printing of structures with a resolution in the range of 300 nm from a 30 nm thick Cr source film using a femto second Ti:sapphire laser. The deposition speed is generally limited by the laser repetition rate. In the general context of printed electronics applications of LIFT, the interested reader is referred to an excellent and highly focused review article by Piqué and Kim<sup>[175]</sup> as well as a comprehensive review by Fernández-Pradas and Serra.<sup>[176]</sup>

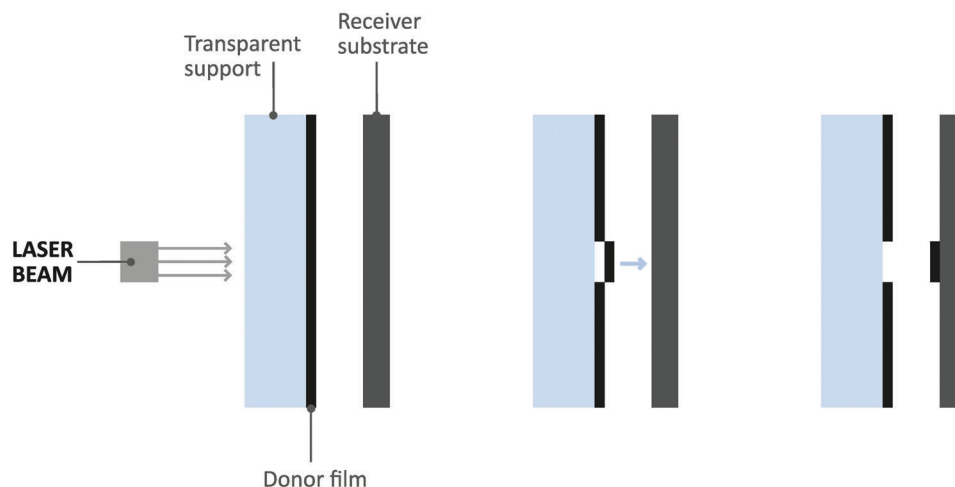


Figure 12. Working principle of LIFT. Reproduced with permission.<sup>[61]</sup>

#### 2.4.1. Laser Induced Forward Transfer in Research and Industry

LIFT has been recognized for its compatibility with a broad variety of different deposition materials and substrates. In the context of hybrid and printed electronics manufacturing, traditional materials, such as nanoparticle inks<sup>[177]</sup> and silver nanowires,<sup>[178,179]</sup> can be employed for the fabrication of conductive traces and invisible electrodes, respectively. Another approach recently presented by Neumaier et al.<sup>[180]</sup> demonstrates the feasibility of material conversion from polyimide to laser induced graphene and direct laser transfer of electrodes to virtually any substrate in one single scribing step.

Apart from the large variety of materials suitable for deposition, as a non-contact technique LIFT allows for the printing onto sensitive or 3D surfaces. In general, it has proven to be compatible with a large variety of substrates, even untreated regular paper.<sup>[181,182]</sup>

One advantage of LIFT over the most prominent digital non-contact printing technology, namely inkjet printing, is the possibility to deposit micro-sized particles. For printed electronics applications this can be highly favorable, as it enables the digital deposition of screen-printing ink to achieve highly conductive patterns.<sup>[172]</sup> Another example of printing micron sized particles was reported by Fernández-Pradas et al.,<sup>[181]</sup> who demonstrated the LIFT of a suspension of carbon nanofibers for the fabrication of a fully functional humidity sensor on paper substrate. Furthermore, LIFT also offers the possibility to directly transfer pure metal.<sup>[183]</sup> As part of the deposition process the material liquidates due to the laser irradiation and subsequently solidifies when being transferred to the substrate. However, this leads to the formation of interfaces between adjacent voxels reducing the electrical, thermal and mechanical properties of the printed patterns, which is particularly critical for printed electronics applications.<sup>[175]</sup> This issue can be addressed by introducing either a thermal, absorptive layer or a dynamic release layer, which avoids direct exposure of the donor to the incident laser, as first reported by Tolbert et al.<sup>[184]</sup> Those sacrificial layers commonly consist of either metals, such as Ti, Au, Pt, Cr, or UV-sensitive photopolymers.<sup>[177]</sup>

On the other hand, the liquidation and quick solidification of pure metal can be advantageous, as it enables the fabrication of 3D metallic micro-structures.<sup>[173]</sup> Figure 13 illustrates two examples of such 3D-printed structures using LIFT, a) a 10  $\mu\text{m}$  thick and 250  $\mu\text{m}$  high functional printed thermocouple made from platinum and gold pillars,<sup>[185]</sup> and b) a free-standing 860  $\mu\text{m}$  long copper pillar with a diameter of as small as 5  $\mu\text{m}$ .<sup>[46]</sup>

In addition, this technology enables the direct printing of multi-layers in a single step, as demonstrated by Constantinescu et al.<sup>[186]</sup> for the fabrication of TFTs.

The principle of LIFT appears to be very straight forward, yet a lot of processing challenges have arisen regarding the precise deposition of delicate materials as contamination and stress can be induced during the transfer process of thermally and mechanically sensitive materials. To address these challenges, Kattamis<sup>[187]</sup> presented the incorporation of a thick film polymer absorbing layer, which can dissipate shock energy through mechanical deformation. Using this approach, he demonstrated the contamination-free laser transfer of living mammalian embryonic stem cells. This principle could also be applied for the fabrication of printed electronics, although it was originally designed for the deposition of living biomaterial.

LIFT is commonly conducted at atmospheric conditions, yet the processing under reduced pressure or in vacuum can have significant advantages for certain applications. Claeysens et al.<sup>[188]</sup> employed LIFT for the deposition of Zn for chemical ZnO nanostructure growth. While the in-vacuum transferred Zn patterns enable the formation of dense well-aligned ZnO nanorod arrays, the rods grown from the patterns deposited in air show rather random, flower-like structures. This indicates that the LIFT of Zn pattern in vacuum resulted in a more homogeneous printed layer. In another study by Shaw-Steward et al.<sup>[189]</sup> the quality of a LIFT process employing an intermediate dynamic release layer of a triazene polymer in air and in reduced pressure at different substrate-substrate gaps was studied. They concluded that for small substrate-substrate gaps the low-pressure environment leads to a significant improvement of the printing quality due to the reduction of the reflected acoustic shock wave and the air drag.

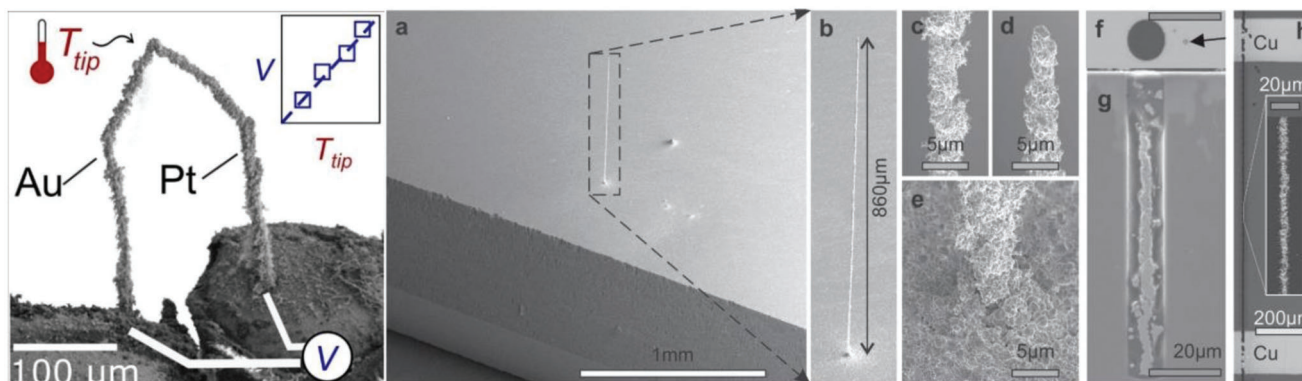


**Figure 13.** Examples of 3D-printed metallic microstructures using LIFT. a) Printed thermocouple consisting of gold and platinum pillars and b) free-standing copper pillar. Reproduced with permission.<sup>[46,185]</sup>

**Table 2.** Overview on different laser types used for LIFT.

Application/Materials	Laser type	Wavelength	Pulse width	Reference
Pure metal: Au and Ni thin films	Excimer	248 nm	30 ns	[190]
Pure metal: Au, Zn, and Cr thin film	Ti:Sapphire	800 nm	200 fs	[191]
Cr thick film	Ti:sapphire	800 nm	110 fs	[44]
High viscosity silver paste	Diode pumped solid state Nd:YVO <sub>4</sub>	532 nm	< 15 ns	[192]
High viscosity silver paste	High-power industrial ps-Laser	532 nm	< 13 ps	[192]
High viscosity Ag screen printing ink	Diode-pumped ytterbium fiber laser	1064 nm	100 ns	[172]
Low viscosity Ag nanoparticle ink	Nd:YAG	266 nm	10 ns	[177]
Ag nanowires	Nd:YAG	1064 nm	150 ns	[178]
One-step multi-material deposition (semiconductor, dielectric, Ag)	Nd:YAG	355 nm	50 ps	[86]
Biomolecules; DNA	Nd:YAG	355 nm	10 ns	[169, 170]
Living mammal cells	Nd:YVO <sub>4</sub>	355 nm	15 ns	[187]

Considering the large variety of different materials to be deposited different requirements regarding the laser source arise. **Table 2** provides some examples of laser types and parameters used for different LIFT applications reported in literature.

The speed of the LIFT printing process is ultimately defined by the laser repetition rate and the desired resolution in dpi. Although high laser repetition rates in the range of several tens of MHz can be realized, at some point the repetition rate cannot be further increased, because then the time between successive laser shots becomes shorter than the average lifetime of a single jet.<sup>[193]</sup> To further increase the processing speed multi-jet LIFT can be employed.<sup>[194]</sup> One way to realize that is to split the primary Laser beam into several quasi-identical beams using a series of beam splitters and mirrors. Those beams can then be fired either simultaneously or alternately, however, depending on the beam-to-beam distance, the firing delay, as well as the used donor material, significant crosstalk resulting in inseparable jets can occur.<sup>[193]</sup> **Figure 14** shows an example of an optimized multi-jet LIFT employing five jets with a spacing of 25  $\mu\text{m}$  and a delay of 2  $\mu\text{s}$ .

Research LIFT systems reported in literature are mostly designed and implemented for the individual topic and specific tasks. Yet, there are commercialized solutions available. As an

example, the Fraunhofer ILT provides a table-top LIFT system, which consists of a modified Nanoplotter by the company GeSiM GmbH, as well as the larger LIFTSYS machine. Their systems are primarily designed for processing high viscosity or solid materials for biomedical applications.<sup>[195]</sup>

Interprint and MDC Max Daetwyler founded the joint venture DI Projekt AG with the aim to develop a large-area LIFT printing machine, the so called LaserSonic, for graphic and labelling applications using offset printing ink. In 2011 the first LaserSonic industrial scale machine was constructed<sup>[196]</sup> which offers a 0.53 m web size and a throughput of 1.3  $\text{m}^2 \text{min}^{-1}$ .<sup>[193]</sup> In the context of electronics manufacturing, laser enabled advanced placement (LEAP) by UniQarta<sup>[197]</sup> is an industrial technology using the principle of LIFT to transfer dies from a carrier to a substrate. Employing a combination of single- and multi-beam transfer modes a high deposition speed of more than 100 million units per hour can be realized. The dies are bonded to the transparent support using a dynamic release layer material, which protects the die from the direct laser exposure while minimizing placement errors and mechanical motion when simultaneously depositing multiple chips. One unique feature is the so called known-good-die placement mode, where in a first step a single-beam mode is employed to remove unwanted dies from the support. In a sub-

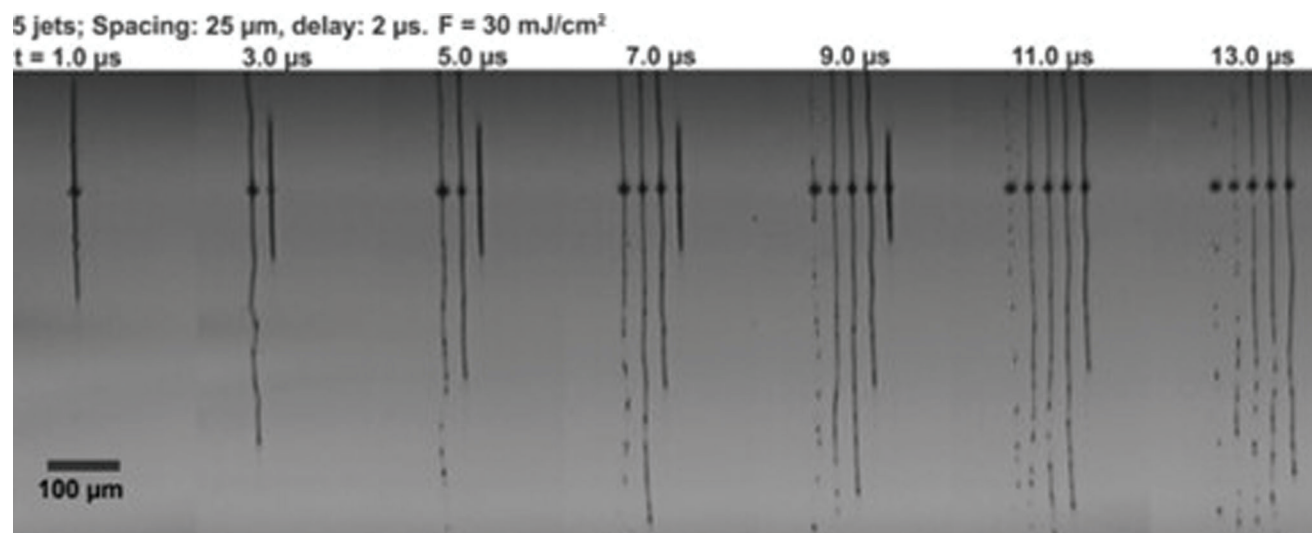


**Figure 14.** Multi-jet LIFT of silver nanoparticle ink a high repetition rate UV picosecond laser (343 nm; 30 ps; 500 kHz) with a jet-spacing of 25  $\mu\text{m}$  and a delay of 2  $\mu\text{s}$ . Reproduced with permission.<sup>[194]</sup>

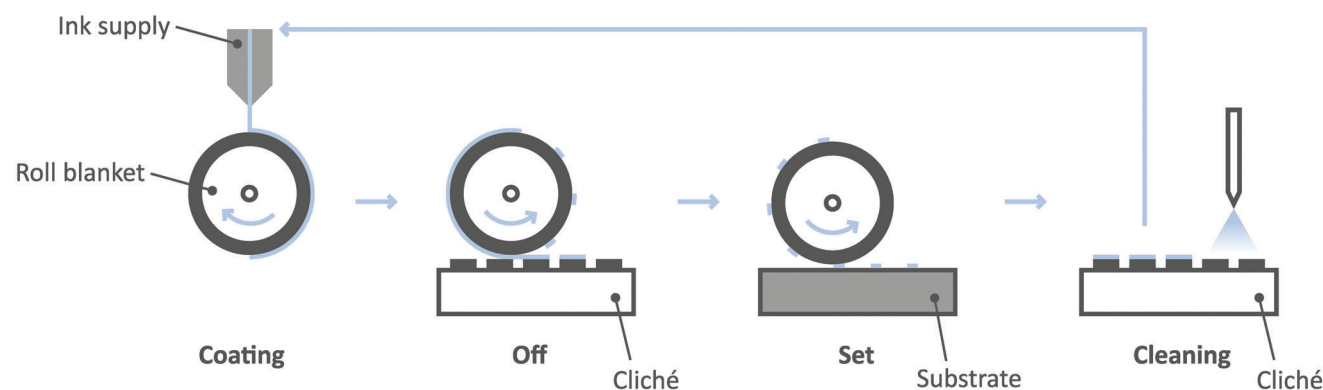


**Figure 15.** Schematic principle of roll-to-sheet reverse offset printing. Reproduced with permission.<sup>[61]</sup>

sequent step, a whole field of dies are transferred using a multi-beam mode. Finally, a single-beam mode is employed again to deposit single dies to locations that are unpopulated due to the previous removal of bad dies.

As LIFT does not require a master pattern or stencil, it is a highly appealing technology for R&D and small batch production, as changes in design can be implemented immediately at low cost. However, LIFT has as well a great potential for the in-line fabrication of hybrid and printed electronics on an industrial scale, as many production lines already have integrated lasers for marking and labelling purposes and industrial lasers can be used.<sup>[192]</sup>

## 2.5. Reverse Offset Printing

Reverse offset printing opens a new field of high-precision R2R printing.<sup>[51,198]</sup> The basic concept has first been introduced in 1980 and has been extensively developed since then, as thoroughly reviewed recently by Kusaka et al.<sup>[199]</sup> The reverse offset working flow consists of three major steps. As illustrated in **Figure 15**, first the silicon rubber (PDMS) printing cylinder is

fully coated with ink. Then the applied ink film is patterned by an engraved plate (cliché), which selectively removes the ink in the contact area. In a subsequent step the remaining ink is printed to a substrate. It is critical for the printing quality that the ink is entirely transferred, first to the engraved stamp and then to the substrate. Therefore, the adhesion forces between the ink and the stamp/substrate must be significantly higher than the adhesion forces between the ink and the surface of the printing plate. Second, the cohesion force of the ink needs to be higher than the adhesion force of the rubber printing roll and lower than the adhesion force of the stamp and the substrate.<sup>[200]</sup> In addition, there must not be any chemical bonding between the ink and the silicon of the printing plate.<sup>[201]</sup> After one printing pass the cliché has to be cleaned which leads to waste of (potentially expensive) ink as the ink that has been transferred to the cliché can hardly be recycled.<sup>[52]</sup> Reverse offset printing can be considered as semidry process and therefore enables the printing of very fine lines with resolutions down to the sub- $\mu\text{m}$  range. This means that the liquid ink starts drying out after being transferred to the offset printing cylinder as PDMS partially absorbs nonpolar solvents (e.g., hydrocarbons) and hence promotes drying of the

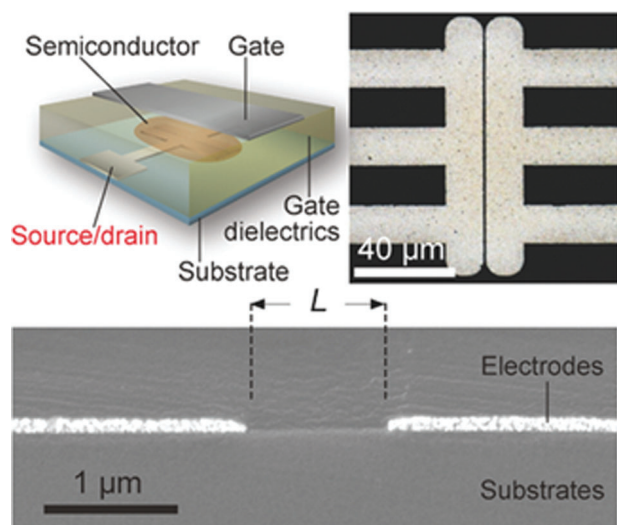


**Figure 16.** Reverse offset printed thin film transistor with a gate length of 0.6  $\mu\text{m}$ . Reproduced with permission.<sup>[204]</sup>

ink. Consequently, the printed patterns are well defined and do not experience extensive wetting on the substrate.<sup>[199]</sup> Although reverse offset printing is a contact printing method, it can be compatible with sensitive substrates as the elastic PDMS printing roll applies only low pressure to the substrate. In addition, the softness of the blanket cylinder ensures conformable contact also when printing on substrates with higher surface roughness.

### 2.5.1. Reverse Offset Printing in Research and Industry

Reverse offset printing has been considered as one particularly promising method for the R2R high resolution printed electronics manufacturing. Commonly, a fine line width of less than 5  $\mu\text{m}$  can be realized and even line widths in the range of as narrow as 1  $\mu\text{m}$  have been reported in scientific research.<sup>[51]</sup> Due to the high achievable resolutions reverse offset printing has become an interesting enabling technology for the fabrication of printed (organic) TFT<sup>[22,202]</sup> and OLEDs.<sup>[203]</sup> In 2015, Fukuda et al.<sup>[204]</sup> demonstrated the printing of TFTs with a channel length of 0.6  $\mu\text{m}$ , as illustrated in **Figure 16**.

A lot of scientific effort has been dedicated to optimizing the reverse offset printing process regarding the controlling of the ink transfer,<sup>[205]</sup> the positioning accuracy,<sup>[206]</sup> the used materials,<sup>[53]</sup> and the surface energies<sup>[207]</sup> resulting in an enhancement of the overall quality. Furthermore, the processing speed has been increased while reducing the related processing costs.<sup>[50]</sup> One area which bears the potential to save costs is the production of the cliché. It is usually manufactured utilizing photolithography or NIL and etching processes applied on a Silicon wafer or glass substrate, which makes it comparatively cost-intensive.<sup>[50]</sup> Therefore, the stamps are not immediately disposed, but cleaned and reused, which might have a degrading effect on the quality of the subsequent printing processes. However, there are endeavors to reduce the process costs, as for example Choi et al.<sup>[52]</sup> presented a novel disposable low-cost plastic cliché. They even demonstrated the printing of lines for the fabrication of visually transparent conductive electrodes consisting of metal meshes as thin as 3.6

$\mu\text{m}$ . Similarly, Cho et al.<sup>[50]</sup> presented a flexible plastic cliché and printed TFT gate lines with around 2  $\mu\text{m}$  width. Furthermore, they reported an enhancement of the printing speed to 50  $\text{mm s}^{-1}$ , due to an improved ink off-speed (transfer speed of the ink from the coated printing cylinder to the cliché).

Artifacts in reverse offset printing are commonly caused by contact-defect formations, which mean that the blanket cylinder touches the bottom-region of the cliché removing ink that should have been printed on the substrate. Reasons for that, are a too large pattern size or a shallow depth of the cliché. In an approach to address this issue, Kusaka et al.<sup>[205]</sup> proposed a so-called “push-pull” process for the ink transfer. Instead of simply pushing the blanket roller onto the cliché, negative pressure is applied as well, which improves the ink transfer. By employing a roll-to-sheet reverse offset printing machine they demonstrated the contact defect-free formations of large-area patterns with a size of up to 4.0 mm  $\times$  5.0 mm using a cliché depth of 2.6  $\mu\text{m}$  as well as of finer patterns with size of 10–50  $\mu\text{m}$  width lines using a cliché with 1.6  $\mu\text{m}$  shallow depth.

The blanket cylinder slightly deforms when contacting the cliché as well as during printing, due to its softness, which can again result in artifacts in the pattern formations (size-tolerance problem), as studied by Kusaka et al.<sup>[208]</sup> In addition, they observed the slipping of ink between the blanket cylinder and the substrate. These effects can lead to registration errors, which are a major degrading factor for high-resolution multi-layer printing, in particular, when neighboring patterns are closely located. This effect can be reduced by simulating the blanket deformations and employing corrections to cliché patterns accordingly.

Considering multilayer reverse offset printing, the well-defined edges, as realized due to the semidry nature of this process, are not necessarily beneficial. Due to those edges, when printing a second layer, the elastic blanket roller cannot deform accordingly in order to ensure continuous contact with the surface, which can lead to interruptions and defects in the printed structure. To address this issue, Kusaka et al.<sup>[209]</sup> proposed a reflow-process, where the silicone blanket roller with the semi-dried patterns was placed into a vapor saturated chamber. Due to the vapor, the ink pattern liquefies again and after transferring them to the substrate, the printing of structures with rounded edge can be achieved. In a subsequent second printing step the formation of continuous structures was demonstrated.

Recently, Izumi et al.<sup>[210]</sup> presented an extension of the conventional reverse offset printing technology, namely the “soft blanket reverse-offset printing.” As part of this process, an extremely thick and soft blanket is used as an offset roller, which enables the printing onto uneven and curved surfaces. They demonstrated this principle by printing fine lines with a width of 30  $\mu\text{m}$  on curved surfaces using commercially available silver nanoparticle inks and achieved uniform thicknesses and low resistivities, equivalent to when printing on planar substrates.

As presented in this chapter, several research groups and organizations, such as the advanced manufacturing systems research division of the Korea Institute of Machinery and Materials (KIMM) as well as scientists of the Helsinki University of Technology in Finland have demonstrated the up-scalability and great potential for R2R printed electronics manufacturing of this technology.<sup>[211,212]</sup> Although the concept has been known for a long time, a lot of research has been done in the field in re-

cent years, which indicates that reverse offset printing is considered as emerging technology with a lot of potential for different applications. While research groups around the globe employ customized systems, there are a few commercial reverse-offset printing-systems available for printed-electronics applications (e.g., Naraenanotech,<sup>[213]</sup> Jemflex by Nihon Denshi Seiki<sup>[214]</sup>).

## 2.6. Nanoimprint Lithography

Nanoimprinting techniques enable the patterning of structures with a resolution in the sub- $\mu\text{m}$  range<sup>[23]</sup> while being compatible with R2R manufacturing<sup>[215]</sup> and allowing for the patterning on flexible substrates.<sup>[216]</sup> However, in contrast to the previously presented technologies, conventional NIL is not an additive technology as it usually involves etching procedures. In principle, NIL consists of four major processing steps:<sup>[23]</sup>

Preparation of the nanostructured stamp employing either nanolithography or etching, the stamp is commonly also referred to as daughter mold;

Deposition of the resist and pre-treatment (e.g., soft-baking to remove residual solvents);

Imprinting of the designated patterns using the stamp prepared in step 1; the three most commonly employed techniques are a) hot embossing, b) ultraviolet light (UV) based NIL, and c) soft lithography.

Post-processing, typically an etching procedure to remove the residual layer.

For the deposition of the resist onto the substrate (step 2), different coating technologies are applied. Among those technologies, spin coating is frequently used. As a part of this spin coating process, a thin and uniform surface can be created. First, the resist is deposited on a flat surface, which is then rotated at a defined speed, causing even spreading of the resist due to centrifugal force. The resulting film thickness depends on the rotation speed, spinning time, as well as the viscosity of the resist. Alternatively, also inkjet printing can be used as deposition method.<sup>[217]</sup> For the imprinting step, the most prominent technologies are hot embossing, UV-NIL and soft lithography. In hot embossing (often also referred to as thermal NIL) (step 3 (a)) the resist is heated up beyond the used material's glass transition temperature, then the stamp imprints the nano-pattern into the liquefied resist. Afterward the temperature is lowered, which leads to hardening of the resist before the stamp can be removed.<sup>[47]</sup> UV-imprinting (step 3 (b)) involves a UV-curable resist requiring a stamp, which is translucent in the UV spectrum. The resist then hardens, due to exposure to UV light. In comparison to thermal NIL, UV-NIL requires a lower resist viscosity, which results in a lower imprinting pressure. Furthermore, the processing time is decreased as the low viscous ink fills the mold cavities quicker and due to the absence of a temperature cycle.<sup>[218]</sup> Thermal and UV NIL can also be combined to the so-called Simultaneous Thermal and UV (STU) technology (Obducat).<sup>[219]</sup> Soft lithography (step 3 (c)) employs an elastic mother template, the ink is deposited onto the mother template surface structure, then it is transferred to the substrate. This structure then acts as mask for subsequent etching or deposition. In soft lithography several different technologies have been presented, amongst them microcontact printing ( $\mu\text{CP}$ ) is the most prominent one, as it can

be realized utilizing rolling stamps or transfer ink-roles. Other advantages of this method are primarily the comparatively simple application, low-cost processing, and a high degree of pattern flexibility. Although  $\mu\text{CP}$  was first applied already back in 1998, this technology has not been evolved beyond the level of fundamental research for PE applications.<sup>[220]</sup>

### 2.6.1. Nanoimprint Lithography Technologies and Additive Manufacturing

The removal of the residual layer after imprinting has been one major challenge for the practical applicability of NIL. The usually employed etching step leads to an increased process complexity alongside with elevated process costs and low environmental compatibility. Furthermore, a low selectivity of the etching process can lead to subsequent degradation of the quality of the imprinted patterns. Reverse NIL addresses these issues, as it enables residual layer-free nanoimprinting. As part of this process, the stamp itself is coated instead of the substrate, then the stamp is pressed onto the substrate to transfer the deposition material (see **Figure 17**).

In contrast to standard NIL, most of the early studies on reverse NIL report the fabrication of structures with resolutions in the micrometer range. However, back in 2012 Tavakkoli et al.<sup>[222]</sup> demonstrated the reverse NIL of nanostructured pillars with 50 nm pitch employing spin-coating of a thermal UV resist onto a flexible and disposable daughter mold. Although a lower residual layer thickness than known from the standard NIL processes was achieved, it was still in the range of 20 nm. In contrast to that, Fernández et al.<sup>[221]</sup> reported the residual layer-free reverse NIL of poly(methylmethacrylate) on silicon and metallic as well as prepatterned substrates, employing a flexible PDMS stamp. The corresponding selectively coated PDMS mold is illustrated in **Figure 18a**. In this way they fabricated honeycomb like structures with a spacing of 500 nm and a height of 800 nm (see **Figure 18b**).

One major advantage of reverse NIL lies in the comparatively low imprinting pressure, as the stamp is already filled with the polymer. This is different in the case of other NIL technologies, particularly hot embossing, where a higher pressure and temperature are required to promote the resist flow into the mold's cavities. This qualifies reverse NIL for the imprinting onto flexible and rather sensitive substrates. For instance, Song et al.<sup>[223]</sup> fabricated ferroelectric polymer stripe arrays with a line spacing of 700 nm onto flexible polyethylene terephthalate (PET) coated with indium tin oxide. Furthermore, the reverse NIL technology has proven to be well suited for the fabrication of multilayer structures on already pre-patterned surfaces.<sup>[224]</sup>

In another approach toward additive manufacturing, conventional NIL is used as low-cost enhancer of the printing resolution of lower-resolution additive manufacturing technologies, such as inkjet and gravure printing. The possibilities and opportunities that arise from the combination of inkjet printing with NIL have been evaluated by the research group around Michael Mühlberger.<sup>[225]</sup> One example is the application of nanoparticle ink onto a prepatterned UV-curable polymer with microgrooves fabricated by means of UV-NIL. Due to capillary forces the nanoparticle ink is guided into the microchannels, resulting in defined conductive traces. Using this same procedure, Horváth

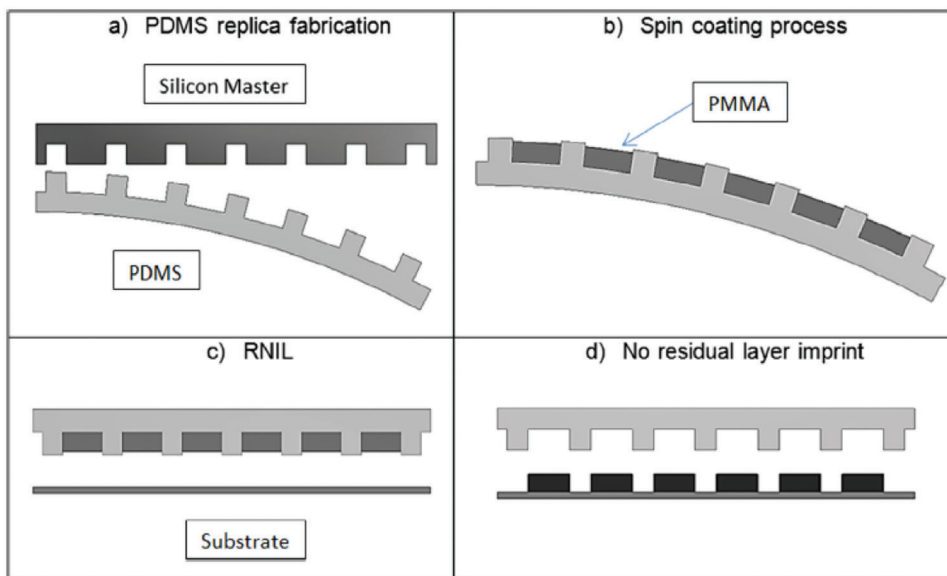


**Figure 17.** Schematic illustration of a residual-layer-free reverse NIL process: a) Fabrication of PDMS replica using a silicon master; b) spin coating of PMMA on the PDMS replica; c) imprinting; d) releasing the PDMS stamp from the substrate. Reproduced with permission.<sup>[221]</sup>

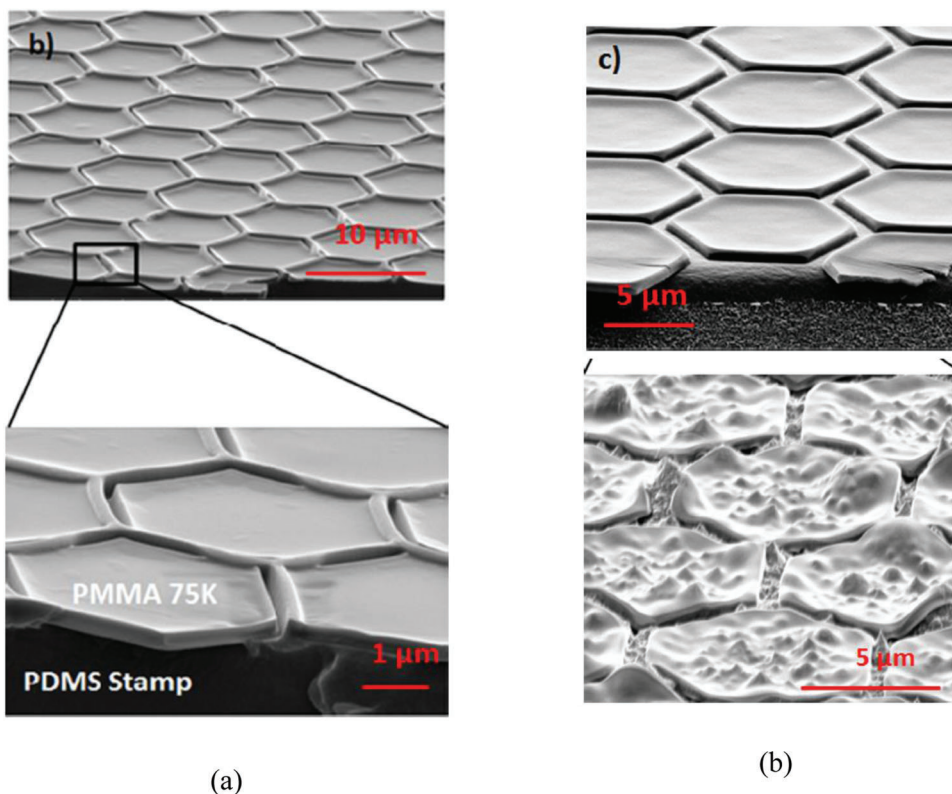


**Figure 18.** Reverse NIL: a) SEM micrograph of PMMA selectively coated onto a PDMS mold, the polymer fills the cavities; b) SEM images of imprinted honeycomb structure with no residual layer on a nickel-coated silicon substrate with low (above) and high (below) surface roughness. Reproduced with permission.<sup>[221]</sup>

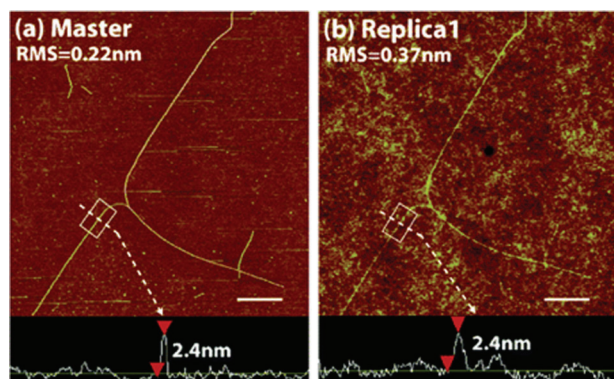


**Figure 19.** Atomic force microscopy images of a) a SWNT master and b) polymer nanostructure formed by imprinting with feature sizes as small as 2 nm; the scale bars are 1  $\mu\text{m}$ . Reproduced with permission.<sup>[230]</sup>

et al.<sup>[226]</sup> reported the realization of conductive traces with a fine line width of down to 2  $\mu\text{m}$ . Teng et al.<sup>[227]</sup> exploited the principle of nanoimprint-assisted inkjet printing for the fabrication of sub-micron channel organic field effect transistors with channel lengths down to 750 nm.

### 2.6.2. Nanoimprint Lithography in Research and Industry

NIL was first introduced back in 1995 by Chou et al.<sup>[228]</sup> They pressed a mold into a thermoplastic polymer film and demonstrated the fabrication of vias and trenches with a minimum size of 25 nm and a depth of 100 nm. In 1999 Chou founded the company Nanonex, which commercially provides tools for NIL. Since their founding, they claim to have installed nearly 100 tools in 11 countries on 4 continents.<sup>[229]</sup>

Since its introduction in 1995 this technology has been further developed in various aspects. On the one hand, the range of materials that can be processed has increased significantly, on the other hand, ever higher resolutions have been achieved in academia. For instance, about one decade after NIL has first been reported in literature, Austin et al.<sup>[48]</sup> fabricated nanogap metal contacts and nanoimprinted structures with 5 nm linewidth and 14 nm line pitch that can be employed for the trapping of single macromolecules. The potential of patterning on a molecular scale was also demonstrated by Hua et al.<sup>[230]</sup> already back in 2004. By employing single-walled CNTs as templates the imprinting of structures with feature sizes as small as 2 nm was realized (**Figure 19**).

From R&D to the industrial scale, NIL is primarily employed for the fabrication of flexible sensors, transparent conductive electrodes for example, solar cells, optoelectronic devices, flexible micro lenses, flexible energy devices, as well as bioinspired adhesive structures.<sup>[231]</sup> Furthermore, NIL is frequently used for the fabrication of biomedical instruments, such as transdermal drug delivery devices.<sup>[232]</sup> However, due to deficiencies regarding defectivity rates, overlay and throughput it is hardly employed in the fabrication of semiconductor applications. Nowadays, NIL's primary fields of application lie in areas where it does not directly compete against established lithographic techniques.<sup>[233]</sup> Although ultra-high-resolution NIL has been reported in literature, there are various process-related challenges regarding the

practically achievable resolution and imprinting quality in industrial applications. One major challenge is that the hardware of NIL system must meet certain requirements, such as nanometer motion precision of the wafer chucks and the alignment system. Furthermore, the resist materials must be applied with uniform thickness, as variations of only few nanometers can significantly affect the pattern transfer quality.

Amongst all different variations of NIL processes, UV-NIL and hot embossing can be considered as mature manufacturing technologies with various commercial equipment providers penetrating the R&D as well as the industrial market. The most prominent examples are Nanonex, EV Group (EVG), SÜSS MicroTec, and Canon Nanotechnologies. Nanonex has the longest tradition in NIL manufacturing and provides several full-wafer NIL systems with resolutions in the sub-10 nm range focusing on applications in opto-electronics, displays, biotechnologies, data storage, semiconductor ICs, chemical synthesis, and advanced materials. As an example, their NX-2000 full-wafer universal imprinter combines photo-curable, thermoplastic, and hot embossing NIL into one single system. Wafers with a size of 200 mm can be processed at a throughput of less than 60 s per wafer. Nanonex also offers NIL machines with alignment systems claiming to achieve a sub-micron overlay alignment accuracy.<sup>[234]</sup>

The Austrian EVG provides a series of UV-NIL and hot embossing systems, ranging from R&D mask alignment systems to fully integrated high-volume manufacturing UV-NIL-systems, such as the HERCULES. The HERCULES system can handle wafers up to 300 mm and is capable to manufacture structures with resolutions below 40 nm. Furthermore, the system can be considered as “one-stop-shop,” as it performs pre-processing (cleaning, coating, baking, chilling) together with imprinting without requiring operator intervention. Although the systems allow for the patterning of feature sizes below 40 nm, the overall alignment accuracy lies only in the range of  $\pm 3 \mu\text{m}$ .<sup>[49]</sup>

The commercial NIL technology provided by Canon Nanotechnologies (former Molecular Imprints, Inc.) is called jet and flash imprint lithography (J-FIL). As part of their process, low viscous UV imprint fluid is inkjet-printed onto the substrate. During the imprinting process, the mask contacts only the fluid resist, which is then driven into the mold cavities by capillary forces and is subsequently UV-cured. Canon Nanotechnologies do not provide complete off-the-shelf NIL systems, but they sell their J-FIL technology and solutions for the semiconductor industry.<sup>[235]</sup> As an example, in 2017 Toshiba Memory Corporation purchased FPA-1200NZ2C NIL manufacturing equipment from Canon for the mass production of semiconductor memories.<sup>[236,237]</sup>

Also in 2017, the American-Japanese multinational computer memory manufacturer Kioxia has started cooperating with Canon and Dainippon Printing Co., Ltd. (DNP) to develop mass production of NAND-flash memories using NIL.<sup>[238,239]</sup> Since then, Kioxia has established a 15 nm mass fabrication process technology and is conducting R&D of technologies below 15 nm.

Although not an additive process, NIL can be considered as more environmentally friendly than conventional photo lithography processes. Canon Nanotechnologies, Inc. claim, that a typical NIL module light source consumes about 83% less energy than a comparable light source for extreme ultraviolet lithography. Furthermore, as in Canon NIL systems the resist is accurately deposited by DOD inkjet printing in small volumes of pL, only 0.1–

**Table 3.** Overview of different fields of application for printed sensors.

Field of application	Example(s)	Printing technologies used	Benefit(s)	Limitation(s)	References
Biomedical and wearables	Epidermal electronic systems	Inkjet, EHD, water transfer printing	Flexibility, conformability, biocompatibility, disposability, printing directly on skin	Wired connections and bulky read-out electronics	[243–246]
Wireless sensor readout	Printed RF components	Inkjet	Seamless integration with printed sensors	Large form factor of readout circuits, low quality factors of antennas	[247–250]
Chemical sensors	Chemical sensing platform, Immuno-chemical sensors, drug screening devices, point of care diagnostics	Inkjet, EHD	Deposition of delicate and thermally sensitive materials (living cells, antibodies, DNA, and other biomolecules)	Long-term stability, durability, reliability, measurement range	[251–255]
Printed-sensor-on-chip devices	Add additional functionality to silicon-based electronics	Aerosol jet	Printing on non-planar surfaces	Non-contact printing methods required	[256, 257]
Environmental sensing	Multi-parameter sensing	Inkjet, dispenser printing,	Increase packaging density by including multiple functionalities in one sensing device	Long-term stability, durability, reliability, measurement range	[258, 259]
Touch sensors	Transparent and flexible touch sensor arrays	Inkjet, aerosol jet	Large area fabrication at low cost, flexible		[260, 261]
Accelerometers	Multifunctional devices for health monitoring	Screen printing, inkjet,	Cost-efficient manufacturing, hybrid manufacturing processes	Too bulky compared to MEMS devices	[151, 262–265]
Photo detectors	Flexible and organic phototransistors	Aerosol jet, inkjet, EHD, screen printing	Large area fabrication at low cost, flexible	Large form factors	[266–268]

1% of the resist of traditional spin-on systems is consumed resulting in lower waste. Consequently, the processing costs are reduced while the environmental compatibility is increased.<sup>[240]</sup>

Reverse NIL technologies provide the unique feature to produce residual layer free structures without requiring a post-processing etching step. However, with resolutions in the range of 700 nm, this technology cannot compete with commercialized standard NIL methods, such as UV-NIL and hot embossing, yet. As for today, there are no customary solutions for R&D or industrial reverse NIL applications available. If compared to other printed electronics manufacturing technologies though, reverse NIL can be considered as high-resolution patterning method (feature sizes in the sub- $\mu\text{m}$  range). Therefore, it bears the potential for being integrated with other printing technologies for the realization of advanced high-resolution multi-layer and multi-material hybrid and PE systems. In addition, the up-scalability and compatibility with R2R manufacturing qualify reverse NIL as promising candidate for future high-throughput fabrication, as demonstrated by Yakoob et al.<sup>[241]</sup> for the R2R integration of light-trapping nanostructures in the manufacturing of organic solar cells.<sup>[47,242]</sup>

### 3. Applications

The technologies presented above offer numerous possibilities for the manufacturing of microelectronic devices, and com-

mercial tools are also available; yet, only a few applications have hit the commercial market (e.g., OLED displays,<sup>[4]</sup> organic photovoltaics,<sup>[5]</sup> antennas<sup>[26]</sup>). In this section, some selected, exciting, and innovative applications in the areas of sensing as well as hybrid and flexible integrated circuits from academia are highlighted.

#### 3.1. Sensor Applications

Printing technologies have been extensively studied for the fabrication of sensors and sensor systems throughout the last years. This section aims to provide an overview of the capabilities of printing technologies for different sensing tasks with a special focus on applications, where high-resolution manufacturing and device miniaturization are required. The examples highlight the versatility and applicability of printing technologies and hybrid solutions for sensing requirements of our present everyday lives and sophisticated challenges of the future. **Table 3** provides an overview of different fields of applications for printed sensors as well as their benefits and limitations.

One distinct benefit of printing technologies is the possibility to fabricate physically flexible, large-area electronics at low cost.<sup>[38]</sup> Furthermore, the development and realization of environmentally non-hazardous, disposable sensors is enabled.<sup>[269]</sup> For many practical sensing applications, high-resolution print-

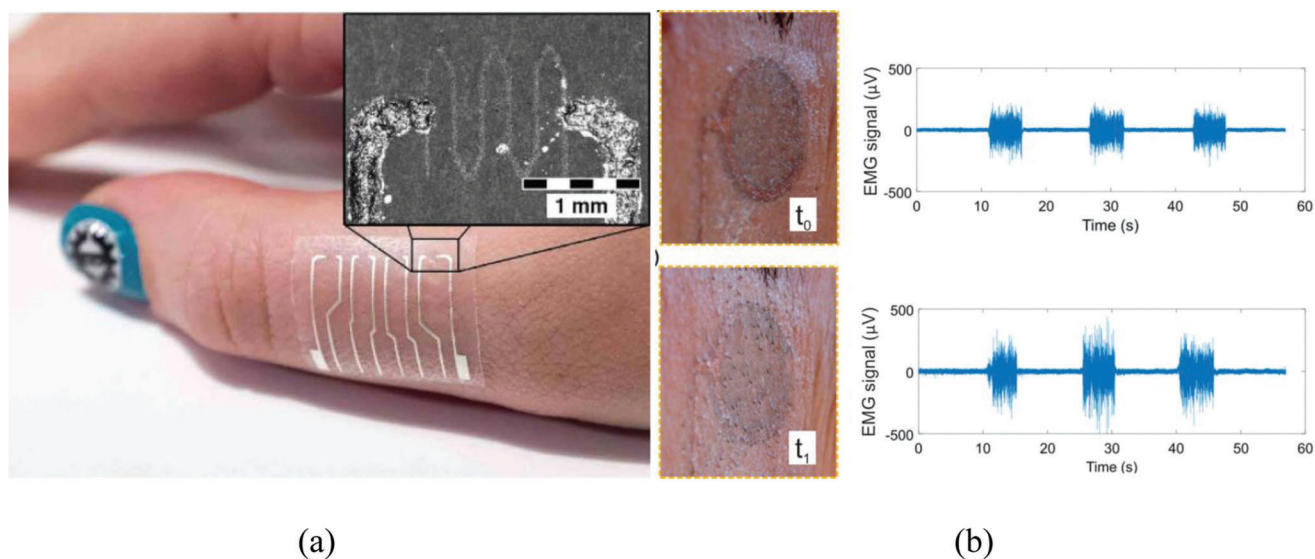


**Figure 20.** a) Inkjet-printed Graphene/PEDOT:PSS temperature sensor on skin conformable polyurethane plaster;<sup>[243]</sup> b) electromyography signal obtained with inkjet-printed PEDOT:PSS tattoo electrodes 3 h after shaving ( $t_0$ ) and 27 h after shaving ( $t_1$ ) after hair has grown through the electrode.<sup>[245]</sup>

ing is not necessarily a must, and flexible sensors are able to conform with the contours of complex geometries, a feature that has been impossible to achieve using rigid material-based electronics. Yet, for certain applications, such as biomedical sensors for, for example, monitoring of body temperature, blood flow properties, or hydration status of human skin, the device must be as comfortable as possible. In some cases, the flexibility of the sensors alone is not sufficient to achieve seamless integration of the electronics. Instead, there is also a need for miniaturization of the device dimensions. This applies in particular for the thickness of the sensing element, when the device is to be seamlessly integrated with a human body, resulting in skin-like electronics, so-called epidermal electronic systems (EESs).<sup>[243]</sup> Besides considerations regarding the comfort and biocompatibility, disposability is another important aspect for EESs, due to hygienic requirements. Hence, the sensors have to be low-cost. Vuorinen et al.<sup>[243]</sup> presented an inkjet-printed Graphene/PEDOT:PSS temperature sensor on a skin-conformable polyurethane plaster with a fine line width of 32  $\mu\text{m}$  for the purpose of monitoring human body temperature (Figure 20a). The sensor has a negative temperature coefficient of resistance, which means that the resistance decreases with rising temperature. At ambient atmosphere the functional Graphene/PEDOT:PSS layer strongly reacts to humidity, resulting in a large drift of the measurement signal over time. This effect could be reduced by employing a protective coating layer. With another approach, Vuorinen et al.<sup>[244]</sup> reported the fabrication of a resistive temperature sensors consisting of a silver nanoparticle ink on a bacterial nanocellulose substrate using EHD printing. The meander line structure has a diameter of 20  $\mu\text{m}$  with a spacing of 50  $\mu\text{m}$ . The sensor was tested in a relevant temperature range for skin and body temperature measurements (24–41  $^{\circ}\text{C}$ ) and showed good linear behavior as well as a small hysteresis. Thin, low-cost, and flexible force sensors are another technology that is of great interest for various fields, such as biomedical sensing, precision surgery, and robotics applications. In 2021, Jing et al.<sup>[20]</sup> presented such an Aerosol-jet-

printed, conformable, microfluidic force sensor, which consists of a partially filled microfluidic channel on top of a series of interdigitated electrodes. Applying force to the microfluidic channel reservoir results in a displacement of the fluid along the channel over the electrodes, leading to a capacitance change proportional to the applied force.

The use of ever thinner substrates can significantly increase conformity with the human skin. Various approaches that employ temporary tattoo paper for the manufacturing of highly conformal sensors and electrodes have been presented. As an example, Ferrari et al.<sup>[245]</sup> fabricated PEDOT:PSS electrodes using inkjet printing with a thickness of less than 1  $\mu\text{m}$ . The functionality and performance of the tattoo electrodes for electromyography and electrocardiography in comparison with standard electrodes was impressively demonstrated. The electrodes maintained functionality even after facial hair has started growing through the electrode, as illustrated in Figure 20b.

To further improve the seamless integration of electronics with human skin, approaches have been made to print EESs directly onto the human skin.<sup>[246]</sup> One possibility to transfer printed structures to non-planar surfaces without a substrate is water transfer.<sup>[270,271]</sup> Giannakou et al.<sup>[272]</sup> demonstrated the water-transfer printing of inkjet-printed nickel(II) oxide (NiO) nanoparticle-based electrodes. Therefore, they first printed the capacitive structure onto a water-soluble substrate, which was then placed on the surface of water. As soon as the substrate had been dissolved, the water level was lowered to transfer the printed structure onto the desired 3D object. The particular focus of their work was laid on wearable applications, that is, direct water transfer of electronic devices onto human skin.

Depending on the type of sensor, special functionalities of the human skin might have to be monitored. To match the receptor density in the skin, the manufacturing methods need to be able to fabricate very high-resolution sensor structures for skin-conformable electronics. Although the skin-mounted sensors themselves have become small, thin, and conformable, most

devices still require wired connections with rigid silicon-based read-out circuits as well as batteries to power those circuits. In practice, this ultimately limits the flexibility, simplification, and miniaturization of EESs. Wireless sensor systems require fundamental RF components that can maintain the operation at GHz. Cook et al. have reported the fully printed RF capacitor,<sup>[247]</sup> inductor, and transformer<sup>[248]</sup> using the combination of silver nanoparticle ink and PVP/SU-8 polymer-based ink using inkjet printing. Similarly, fully inkjet-printed antennas, which might have comparatively large dimensions depending on the read-out wavelength, to guarantee sufficient bandwidth and efficiency<sup>[249]</sup> was reported.<sup>[250]</sup>

Non-contact printing methods, such as Inkjet and EHD printing, have also been exploited for the rapid and low-cost deposition of biomolecules for different diagnostic applications, such as immunochromatographic devices<sup>[252]</sup> or drug screening devices.<sup>[273]</sup> For example, Abe et al.<sup>[251]</sup> realized an “all-inkjet-printed” chemical sensing device for the simultaneous determination of pH, total protein, and glucose in clinically relevant concentration ranges for urine analysis. In a first step they fabricated 3D hydrophilic microfluidic patterns on filter paper using inkjet printing by soaking the substrate in a solution of polystyrene in toluene and subsequently depositing toluene droplets to etch patterns on the filter paper. Then, the reagents for colorimetric analytical assays were inkjet-printed at defined areas of the patterned microfluidic paper devices. In a different work, they<sup>[252]</sup> reported the inkjet printing of antibodies on filter paper realizing a disposable paper-fluidic immuno-chemical sensing device for medical, environmental, and food analysis purposes. Similarly, fully inkjet-printed microfluidic structure for permittivity base sensing was reported by Su et al.<sup>[64]</sup> Another example of inkjet-printed antibodies was presented by Steward et al.,<sup>[253]</sup> they impressively demonstrated the deposition of a pattern of goat anti-mouse antibody and rabbit anti-horseradish peroxidase antibody for the fabrication of low-cost disposable immunoassays for biotechnology and healthcare applications. If higher resolutions are required, EHD printing can be a convenient method for biomolecular patterning, as demonstrated by Park et al.<sup>[254]</sup> They printed patterns of DNA achieving a high spatial resolution in the sub-100 nm range. For more literature on the topic of unconventional fabrication and patterning techniques for point of care diagnostics, the interested reader is referred to an excellent review by Sharma et al.<sup>[255]</sup>

The concept of printed-sensor-on-chip devices can add additional functionality to silicon-based electronics, resulting in hybrid miniaturized sensor systems, as described in a patent application by Texas Instruments.<sup>[256]</sup> Following the very same approach, Clifford et al.<sup>[257]</sup> printed thin film relative humidity sensors directly onto packages ICs using Aerosol Jet technology. The sensor design comprises a simple interdigitated structure made from silver nanoparticle ink, which is covered by a specific material acting as active sensing layer. The electrodes have a length of 2.2 mm with a 100  $\mu\text{m}$  gap in between, resulting in an overall sensing area of 2.7 mm  $\times$  2.3 mm, as illustrated in **Figure 21**.

Environmental monitoring is another application, where miniaturization of sensors is desired as various parameters have to be monitored simultaneously. In an approach to increase the packaging density, Hsiao and Liao<sup>[258]</sup> presented temperature and humidity sensors made from NiO and Nafion thin films, respec-

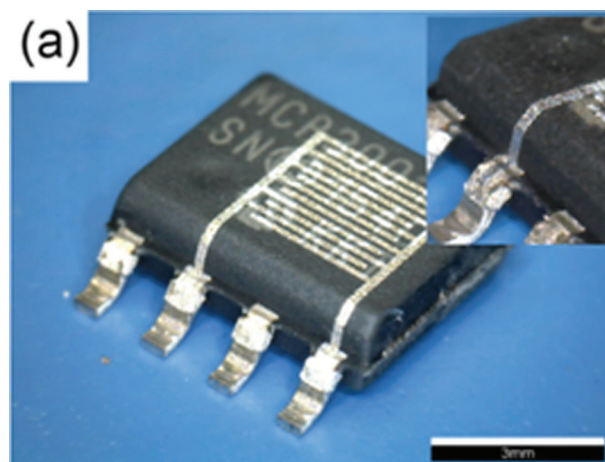


**Figure 21.** Aerosol jet printed humidity sensor on IC.<sup>[257]</sup>

tively, with dimensions less than 1  $\times$  1 mm<sup>2</sup> by employing microdispenser printing on a flexible polyimide substrate. Their results show that the sensorial circuit can detect temperature and humidity changes accurately in the range of 40–80% RH and 25–65 °C. Molina-Lopez et al.<sup>[259]</sup> utilized an inkjet-printed array of free-standing MEMS microbridges on polymeric foil for humidity sensing. The total sensing area of 2  $\times$  2 mm<sup>2</sup> contains 80 individual microbridges with a dimension of 120  $\times$  80  $\mu\text{m}^2$ . They employed a 5  $\mu\text{m}$  thick sacrificial layer to support the top electrode during printing and sintering, which was subsequently removed by dissolving it in acetone. The humidity sensing principle is based on direct utilization of the polymeric substrate as a swelling sensing layer. The substrate swelling leads to mechanical deformation of the printed microbridges, which consequently changes the capacitance. They reported a nearly linear sensor response in a range between 25% rH and 65% rH at a constant ambient temperature of 30 °C.

Touch-sensing applications are a continuously evolving field, in which the requirements for size and flexibility keep increasing. Furthermore, as with other technologies, the environmental impact of the manufacturing process has become important. Addressing those requirements, Rahman et al.<sup>[260]</sup> presented the additive manufacturing and modeling of interdigitated capacitive touch sensors. Employing AJP of silver nanoparticles on glass carrier substrates, capacitive touch sensors with feature sizes down to 50  $\mu\text{m}$  were fabricated. When the line width of structures becomes smaller than the resolution of the human eye, transparent electrodes made from non-transparent material can be realized. As an example, by exploiting particle self-assembly mechanisms, Liu et al.<sup>[261]</sup> reported the inkjet-printing of a polydopamine nanoparticle array with a spatial resolution in the sub-10  $\mu\text{m}$  range for the realization of transparent and flexible touch-sensors.

Another family of sensing elements considered here are accelerometers. They have become increasingly popular, also due to the meteoric spread of fitness trackers, as well as gaming and related consumer electronics. Consequently, there have been approaches to manufacture accelerometers in a highly cost-efficient way by employing printing technologies. In 2020, Liu et al.<sup>[262]</sup> presented a fully printed accelerometer by screen-printing a

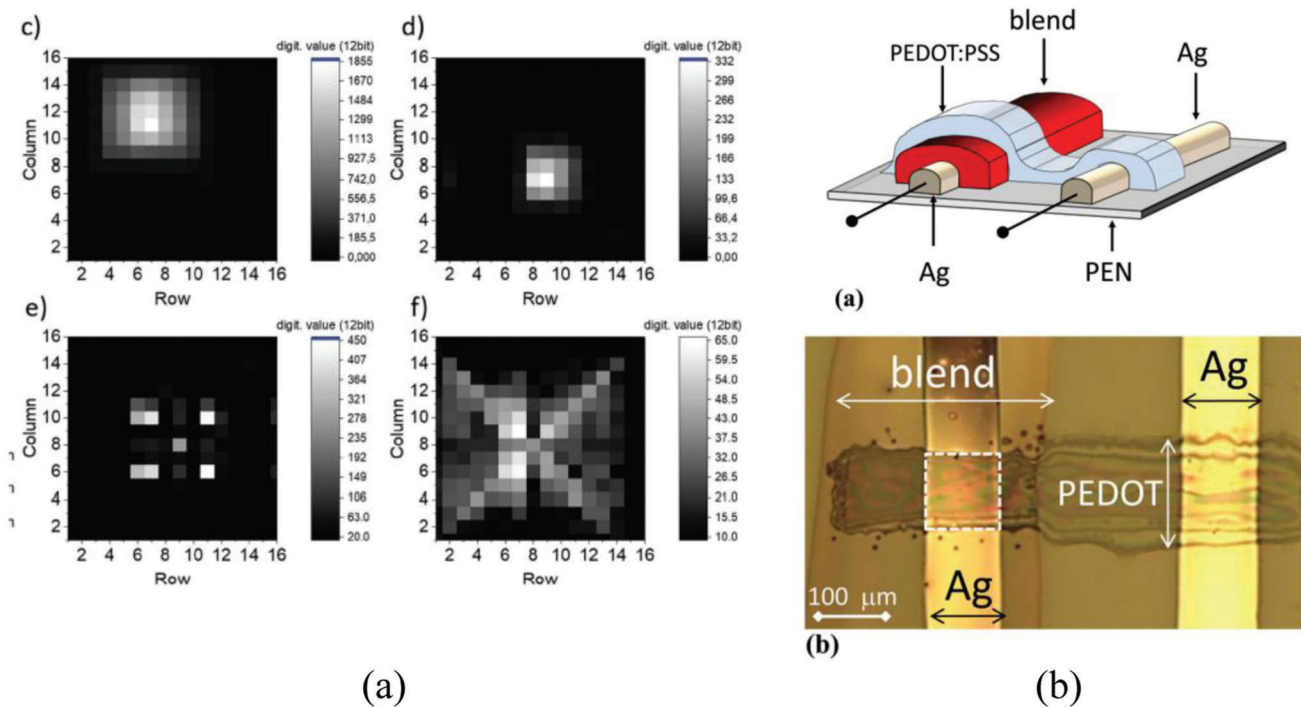


**Figure 22.** a) Sensor signal of entirely AJ-printed image detector as presented by ref. [266] (Reproduced with permission); b) fully inkjet-printed organic photodetector (Reproduced with permission.<sup>[267]</sup>).

piezoresistive carbon paste-based strain gauge on a 3D-printed carrier substrate for the purpose of measuring body motion produced in a cost-effective and highly efficient way. Another printed accelerometer for application in the low-frequency range has been presented by Andò et al.<sup>[263]</sup> The sensing principle is based on four inkjet-printed strain gauges holding the central membrane with an additional weight on a flexible PET substrate. They estimated a responsivity of  $9.4 \text{ mV G}^{-1}$  and a resolution of  $0.126 \text{ G}$  at a frequency of  $10 \text{ Hz}$ , as well as a responsivity of  $41.0 \text{ mV G}^{-1}$  and a resolution of  $0.003 \text{ G}$  at  $35 \text{ Hz}$ . A different sensing principle, namely a capacitive approach for human pulse monitoring employing cellulose paper membranes and sprayed silver nanoparticle electrodes, was presented by Zhang and Kim.<sup>[264]</sup> Yamamoto et al.<sup>[265]</sup> went one step further by fabricating a printed, multifunctional device for health monitoring comprising a three-axis acceleration sensor, as well as a temperature sensor and ECG electrodes in one single patchable device. Although the fully additive manufacturing of accelerometers can be considered as milestone in the field of printed electronics, the devices presented in refs. [262–264] cannot compete with MEMS accelerometers in terms of dimensions and are, consequently, still too bulky for the integration into a conformable wearable device. Other hybrid approaches comprise a combination of MEMS accelerometers and printing technologies. As an example, Khorramdel et al.<sup>[151]</sup> utilized AJP to electrically contact a MEMS accelerometer, more precisely, to fabricate a bridge between the device layer and the handle wafer. Hindrichsen et al.<sup>[274]</sup> integrated a screen-printed piezoelectric PZT thick film with silicon MEMS technology for the fabrication of a high bandwidth triaxial accelerometer.

Alongside the vivid development and growing maturity of organic and printed light emitting diodes,<sup>[275–277]</sup> printing technologies have found their way into the manufacturing of photodetectors and image sensors as well.<sup>[268]</sup> As an example, back in 2014 Kim et al.<sup>[278]</sup> reported the successful development and realization of a flexible organic phototransistor based on a combination of printing methods, such as roll-to-plate reverse offset printing, inkjet printing and bar coating. 4 years later, Eckstein et al.<sup>[266]</sup> presented an aerosol jet printed image sensor based on organic photodiodes employing self-alignment process of the functional layers. The detector is composed of 256 individual pixels with dimensions of  $\approx 250 \mu\text{m} \times 300 \mu\text{m}$ ; **Figure 22a** illustrates the results obtained with their fully printed image detector. An example of a fully inkjet-printed organic photodetector was presented by Azzeloni et al.<sup>[267]</sup> The sensor itself has a dimension in the range of  $100 \times 100 \mu\text{m}^2$  (**Figure 22b**) and could achieve an external quantum yield of 80% at a wavelength of  $525 \text{ nm}$ . Recently, Leng et al.<sup>[279]</sup> demonstrated the feasibility of a printed graphene/WS<sub>2</sub> battery-free wireless photosensor on paper substrate by means of screen-printing and inkjet technology. In 2021, Wang et al.<sup>[280]</sup> presented a high-resolution, flexible, and full-color Perovskite image photodetector, which was prepared using EHD printing of MAPbX<sub>3</sub> solutions with tunable absorption cut-off wavelengths on PI substrates. They were able to realize a perovskite dot array with a minimal diameter of around  $1 \mu\text{m}$  and a thickness of  $18 \text{ nm}$  with a resolution of 5080 dpi.

For more details on the functionality and examples of hybrid and fully printed photodetectors and image sensors the interested reader is referred to the review by Pace et al.<sup>[268]</sup> For image sensing applications a high packaging density is desired

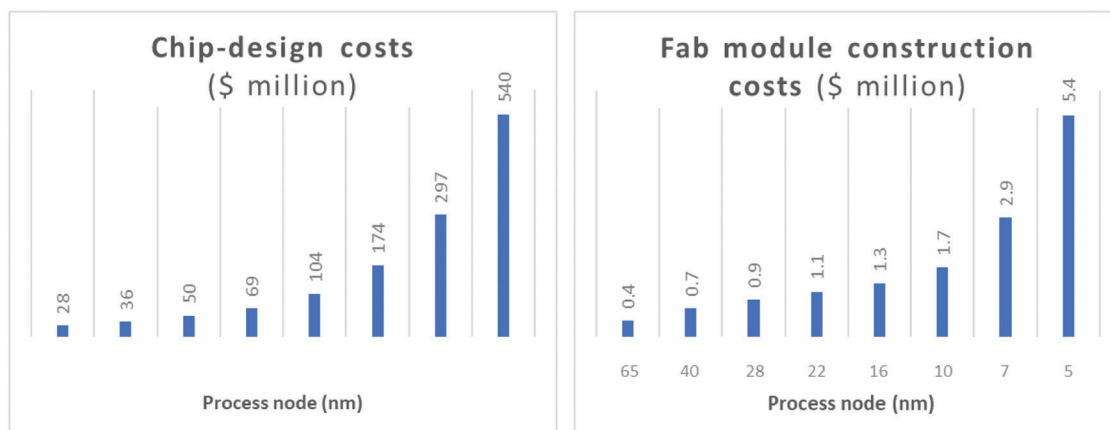


**Figure 23.** Overview of chip design and fab module construction costs depending on the process node size.<sup>[282]</sup>

to ensure a sufficient resolution. State of the art image sensors of, for example, smartphones have a typical dimension around  $6.17 \times 4.55 \text{ mm}^2$  at a resolution of 20 Megapixels. For instance, if the printed image sensor presented by Eckstein et al.<sup>[266]</sup> was up-scaled to a resolution of 20 Megapixels, then the sensor would have an area of more than  $1 \text{ m}^2$ . Hence, printing is far from being a competitive and convenient technology for high resolution imaging and photography sensors.

### 3.2. Integrated Circuits and Flexible Electronics

An overarching goal of the semiconductor industry has been the approach to improve throughput and reduce manufacturing costs, which has been typically done via statistical process control and careful fine-tuning of conventional processing techniques within a fab. Semiconductor manufacturing has traditionally been extremely intensive with respect to labor, energy, as well as, material usage, and cost reductions in any of these areas are pursued relentlessly and continuously improved. On the smaller scale this may require fine tuning of resist dispense volumes for a particular spin coater in use, or it may encompass larger industry-wide efforts to improve throughput such as the transition from 200 mm silicon wafers to 300 mm. In particular, the cost of processing chips on 300 mm wafers has been cited as being up to 40% less compared to chips processed on 200 mm wafers, representing an increase in gross margin of up to 8%.<sup>[281]</sup> However, tools and accompanying processes for wafer fabrication are extremely specialized and are generally limited to a single substrate format in manufacturing; thus, specific tools used to process 200 mm wafers and their accompanying technology nodes cannot be used to accommodate 300 mm wafers, and vice versa. Tools and recipes optimized for applications on 200mm are not necessarily interchangeable with 300mm.

Tool cost increases exponentially with increasing substrate size, and hence, represents a significant capital expenditure. As a result, the overall chip design and fab costs have increased dramatically with the shrinking size of process nodes, as illustrated in **Figure 23**.<sup>[282]</sup> Except for lithography tooling, the process technologies have remained largely unchanged, and scaling remains a significant challenge that is currently addressed through con-

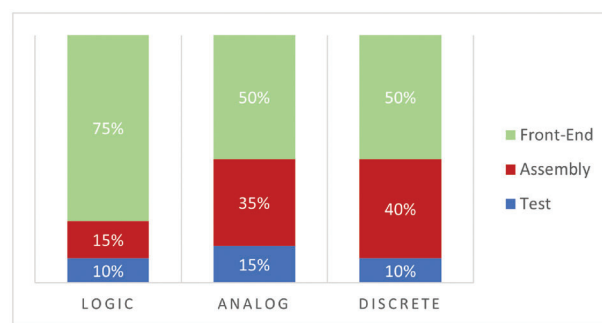


**Figure 24.** Cost breakdown for the production of logic, analog, and discrete electronics.<sup>[283]</sup>

tinuous improvement and process development, which in turn increases the cost of setting up fab infrastructure.

Additive printing technologies are currently (and still will be in the near future) not suitable for nanometer-scale feature sizes commonly found in today's most advanced digital ICs. However, many opportunities for additive technologies lie within analog integrated circuits, which bear a significant portion of production costs within the back-end-of-line and packaging. An example of the cost breakdown between analog and digital chips can be seen in **Figure 24**. Consider the notion that additive technologies are insufficient for traditional front-end wafer fabrication, analog circuits still have  $\approx 35\%$  of their cost associated with back-end assembly and packaging and represents a large opportunity for additive manufacturing to intercept.

Other applications involving MEMS, CMOS, and heterogeneous integration in package require flexible, cost-effective solutions that can be implemented at scale. Disruptive implementation of additive manufacturing, therefore, can potentially address the issues of time-to-market for analog chip R&D, as well as the scalability issues encountered through traditional fabrication methods.

Additive manufacturing and inkjet printing, in particular, offer a variety of features that can revolutionize semiconductor back-end manufacturing, as well as provide an interface between front-end and back-end processing for IC packaging. Traditional back-end processing on finished wafers generally requires planariza-

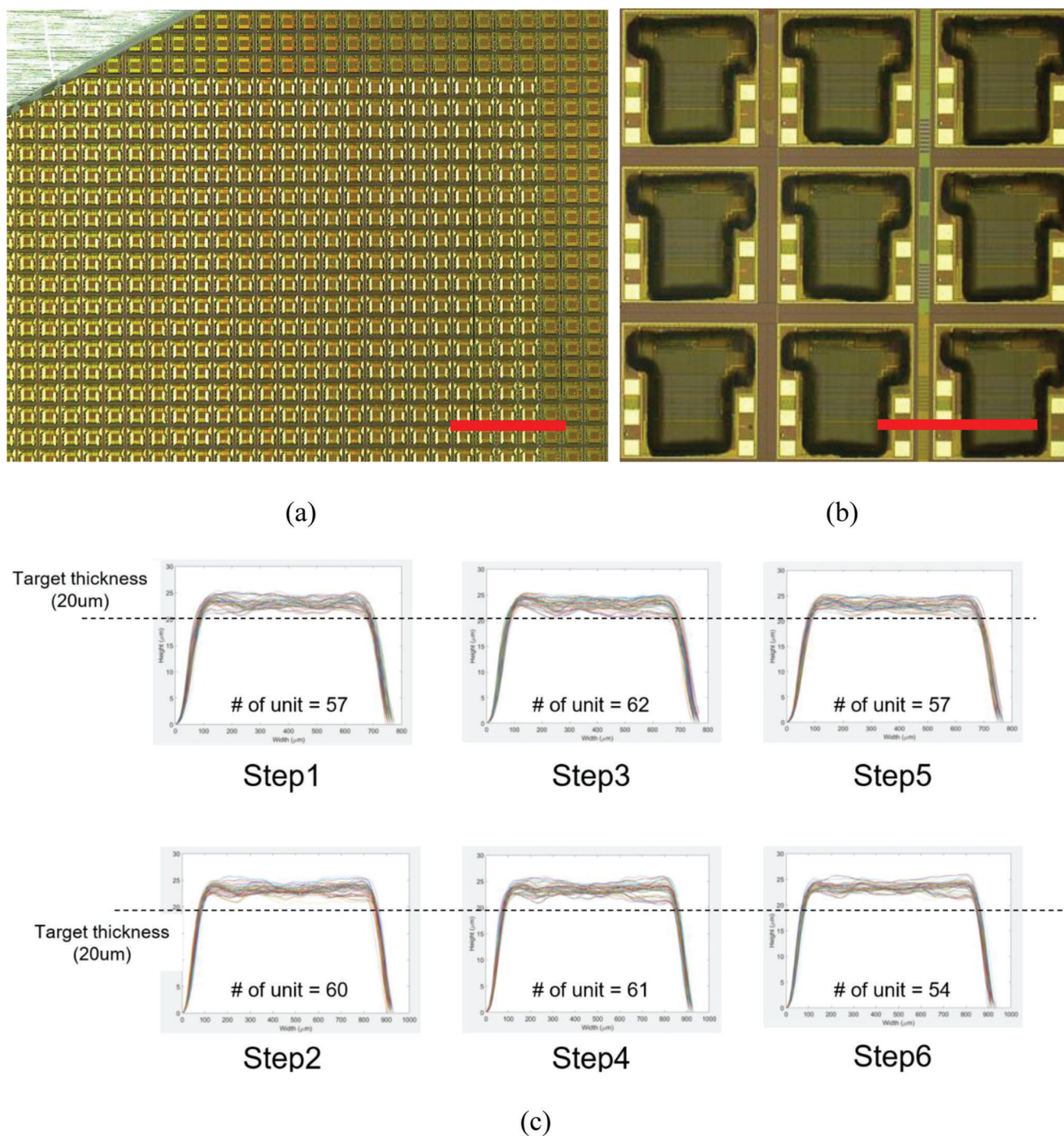


**Figure 25.** a) Inkjet-printed dielectric material on a finished production semiconductor wafer, prior to singulation and packaging. Sections of unprinted dies are clearly seen alongside the printed sections on the left, the scale bar is 5 mm. b) Close-up view of the printed dies with a 1 mm scale bar. c) Thickness measurements of inkjet-printed dielectric material taken across various sections of a silicon wafer, profiled in the cross-scan direction of the film through the center. The films were printed via a multilayer inkjet process.

tion with chemical-mechanical polishing to minimize the impact of geometries on the wafer surface with photolithography processes. In contrast to that, non-contact additive deposition techniques, while sensitive to substrate wetting effects, can deposit material on a variety of topographies. As an example, printing processes can be applied in the area of mechanical stress manage-

ment, which is done using patterned polymer film fabricated by conventional photolithography processes. This polymer stress-buffer acts as a barrier to mechanical stresses imposed sensitive die areas by mold compound filler particles in package. As IC package sizes gets smaller and performance standards get higher, ICs require low-cost, high performance stress management so-

lutions. A stress-buffer film patterned using an inkjet-printing process has been explored for this purpose.<sup>[284,285]</sup> **Figure 25a,b** shows an example of a multilayer inkjet-printed dielectric material stack on a finished production semiconductor wafer processed at Texas Instruments. As illustrated in **Figure 25c**, thickness measurements of inkjet-printed dielectric material taken across various sections of a silicon wafer reveal a high reproducibility of the inkjet printing process. Patterned deposition of such materials, which would have otherwise been created via a traditional multi-step photolithography process, can be achieved in a single step printing process. Patterned resist deposition typically utilizes spin coating, which yields a blanket-coated film of fixed thickness. The coated wafer is then put through a typical photolithography process to yield the desired pattern, but thicker films necessitate additional coat and lithography loops until the desired thickness is achieved. Inkjet printing can yield the same results simply by printing additional layers, and printed film thicknesses can be easily tailored based off number layers printed. This adds to wafer processing time but circumvents additional steps for patterned thick resist. Additionally, material usage is kept to a bare minimum while increasing throughput due to elimination of photolithography steps. Since “digital masks” are utilized, a variety of die layouts, reticle designs and wafer sizes can all be easily accommodated.

Once considered mundane, semiconductor packaging has rapidly become an area ripe for innovation. Conventional semiconductor packaging is achieved via injection molding of polymer mold compound to provide mechanical encapsulation of fragile silicon chips and interconnects. The shape of the mold chase used for molding is pre-defined, dependent on leadframe dimensions, IC chip count, chip sizes, and number IO pins. A commonly proposed answer to increase packaging throughput has been to increase leadframe area and mold chase area, though significant challenges with regard to the flow of mold compound and package uniformity across the leadframe remain. Additive manufacturing processes allow more flexible shapes and properties of molding, which could add functionality, performance improvement, and cost advantages that conventional injection and transfer molding could not offer.<sup>[286,287]</sup> Similarly, printing technologies allow more flexibility and performance improvement in interconnect such as wire-bonding and metal-bump.<sup>[288]</sup> Using inkjet-printed adhesion promoters, precise control over the die-attachment process and other aspects of leadframe performance (**Figure 26**) can potentially be other applications of the printing process to minimize the impact of package stress on the delamination.<sup>[289]</sup>

Leadframe layouts hold a fixed shape depending on the die size with IO pins on both the silicon die and the IC. Conventional ICs, which use wire-bonding, have some flexibility in die size and the number of IO pins fitted within the same leadframe. However, the flip-chip-type package format continues to increase in popularity due to its reduced footprint and production cost. The leadframes for the flip-chip-type package are often custom designed for each type of silicon die, since the leadframe also works as routing between the die and the exposed pads. Using printing technologies provides a similar flexibility in routing, even for the flip-chip-type package.<sup>[290,291]</sup> However, flexibility and stretchability of printed electronics remains a challenge in terms of long-term stability and reliability.<sup>[292]</sup>

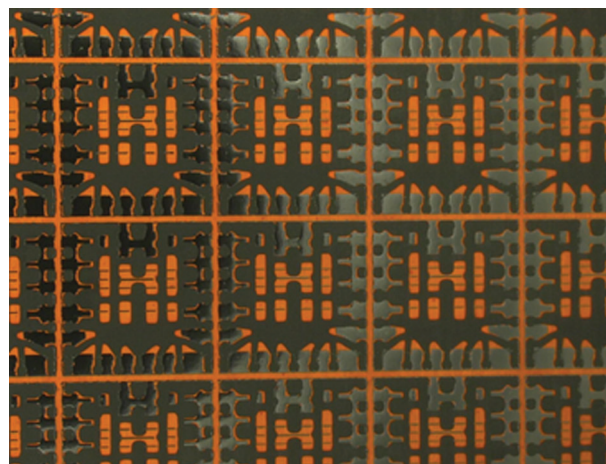


**Figure 26.** Top-down view of a pre-molded leadframe that has been modified for enhanced adhesion via inkjet material deposition.

Fan-out wafer level packaging (FOWLP) is another major trend in microelectronics packaging.<sup>[293]</sup> In FOWLP, chips are embedded inside an epoxy molding compound and the redistribution layers (RDLs), and solder balls are fabricated on the wafer surface to produce a reconstituted wafer. The RDLs are typically metal interconnection schemes that route the electrical signals from one part of the package to another. RDLs are usually fabricated by combining photolithographic processes with sputtering and plating.<sup>[294]</sup> Employing FOWLP for MEMS sensor packaging has some unique challenges, particularly if delicate devices such as capacitive micromachined ultrasound transducers are involved. The RDL must be removed above the membrane to ensure proper functionality of the sensor. In addition, there is then a need to protect these delicate structures during the RDL formation. Thus, using additive printing for the RDL formation seems to be a suitable choice, as the aforementioned challenges are eliminated by principle. As illustrated in **Figure 27a**, jet printing (inkjet, aerosol or EHD) can be used to selectively deposit metallic and dielectric interconnections.<sup>[19]</sup> By avoiding long lithography procedures, including global resist coating and high temperature sputtering, lower thermo-mechanical stresses are applied to the components, which can be ideal for sensitive MEMS devices. Preventing a mismatch of the coefficients of thermal expansion (CTE) in the production of MEMS devices is of great importance to reduce thermal stress at the material boundaries.<sup>[295]</sup> This is particularly important at high temperatures, which are which are needed in solder reflow processes. With printed electronics technologies, low temperature processible materials can be used and temperature variations can be largely avoided.<sup>[296]</sup> Besides that, due to the large variety of printable materials available, CTE mismatch can be reduced already in the design stage. As shown in **Figure 27b**, a system in package layout for FOWLP of pressure sensors, consisting of two pressure sensors and one application-specific integrated circuit, was realized by using printed interconnects. Here Ag tracks with the line width of 80  $\mu\text{m}$  were ink-jetted over the metallic pads of the components and the epoxy molding compound in a DOD manner.

As the sizes of electronic devices continue to miniaturize, the footprints of circuit boards also shrink as a result of new assem-



**Figure 27.** a) Schematic illustration of inkjet-printed redistribution layers and via filling for fan-out wafer level packaging. b) Fan-out wafer level packaging of two pressure sensors and application-specific integrated circuit with inkjet-printed redistribution layers.<sup>[19]</sup>

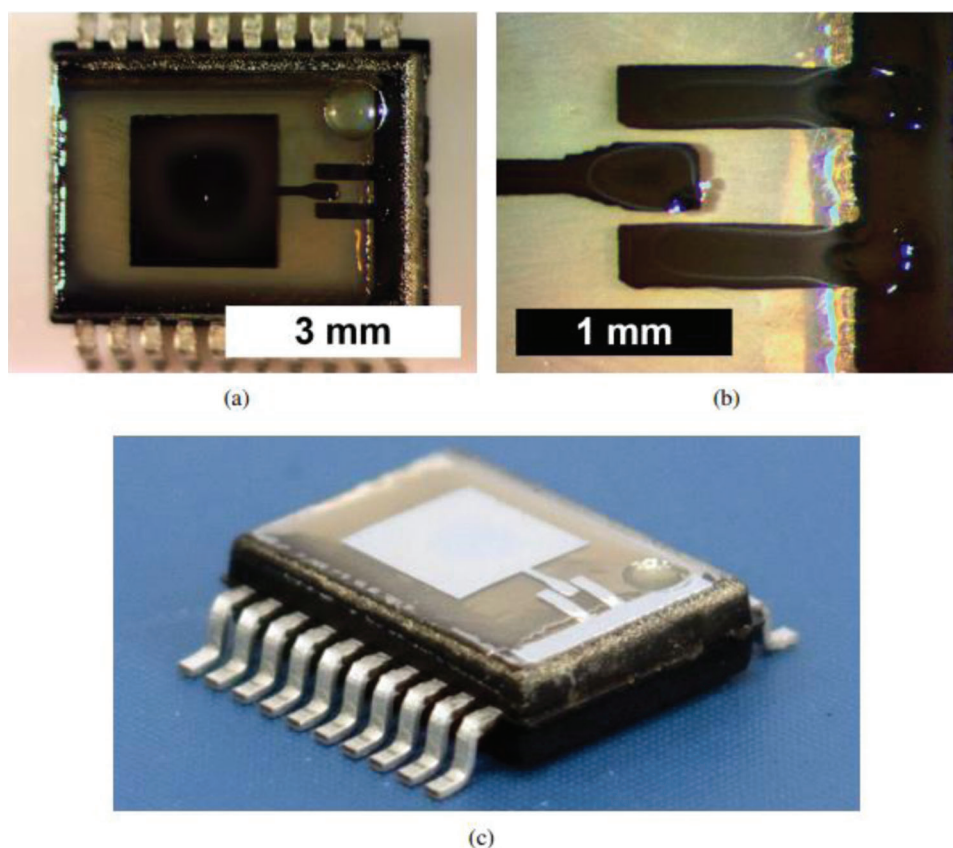


**Figure 28.** Inkjet-printed, on-package, 30 GHz, patch antenna: a) Top view, b) Co-planar waveguide feed and via detail, and c) perspective view.<sup>[285]</sup>

bly technologies, such as the double-sided surface mounted and stacked PCBs. However, the physical size of some analog circuit components, especially RF circuits, is limited by its operation frequency and extremely hard to miniaturize without sacrificing performance. One of the approaches to minimize the footprint of PCBs is to use the IC package area itself as a part of analog circuit components. One such example is the antenna-

on-package technology to significantly minimize the footprint of RF PCBs for automotive/industrial radar systems, developed by Texas Instruments.<sup>[284]</sup> However, this approach requires a custom-designed IC package and special fabrication technologies that do not allow the use of existing legacy ICs.

In contrast, a printed circuit approach potentially opens up new opportunities to utilize unused IC package surface areas for

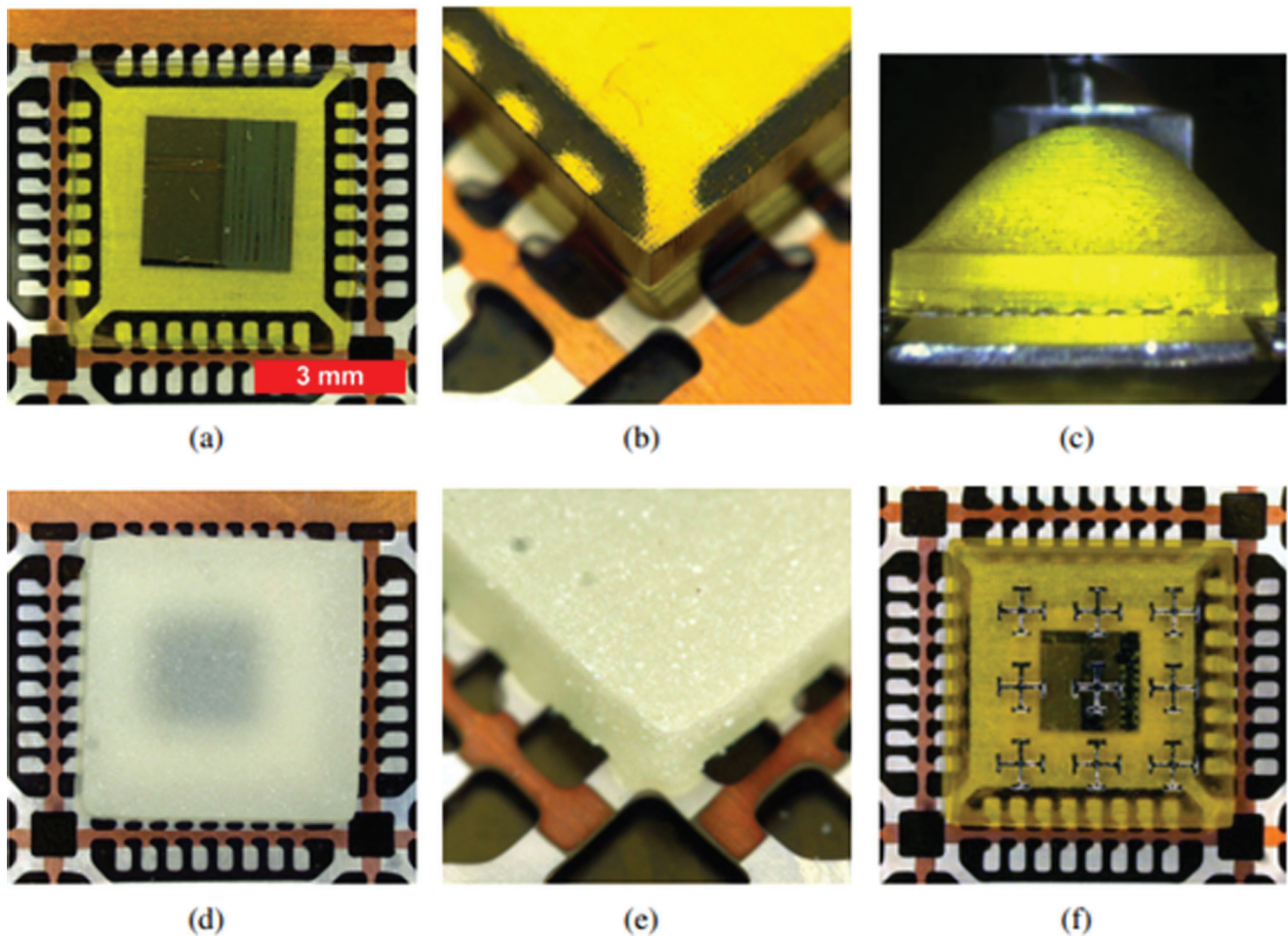


**Figure 29.** 3D-printed die encapsulation on a metallic QFN leadframe: Vorex encapsulation a) top view and b) perspective view. c) Vorex dielectric lens structure with a Porcelite encapsulation d) top view and e) perspective view. f) Vorex encapsulation with inkjet-printed metamaterial.<sup>[285]</sup>

functional circuits by depositing multi-layer 2D/3D structures. Tehrani et al.<sup>[297]</sup> reported an inkjet-printed, on-package, 30 GHz, patch antenna fabricated by inkjet printing of silver nanoparticle and dielectric inks, as illustrated in **Figure 28**. This can be extended to the interconnects between silicon die/IC package and the printed RF structures by smoothing the potential geometry gap in each circuit component.<sup>[285]</sup> With a similar approach, the combination of 3D printing and inkjet printing will provide more flexibility in terms of design. It can also offer possibilities for “add-on” features, such as an RF dielectric lens or EMI shielding, using printed metamaterial patterns on existing IC chips (**Figure 29**).

**Table 4** provides a selection of patented, printed electronics packaging applications explored by Texas Instruments.

#### 4. Conclusion

The benefits of additive technologies in semiconductor manufacturing are quite clear. The evaluation of new designs and materials with conventional fabrication processes is expensive, laborious, and time consuming compared to printing technologies. In contrast, material chemistries, processes and designs

are prototyped and evaluated with much greater flexibility and speed. In high volume applications, printed materials represent a significant cost reduction in material consumption. The ease of multi-material jetting and processing within a single tool lends to a unique flexibility with the potential to fulfill different roles/processes as needed at scale. Despite these benefits, use of such additive technologies has generally been scarce so far within the semiconductor industry, due to high costs and effort of replacing existing systems.

Anyhow, one quantitative indicator to assess the current industrial relevance of the fabrication methods are market reports and forecasts. Amongst the technologies presented in this paper, the inkjet printing equipment market is valued the highest with \$356.6 M in the year 2018 and is expected to grow with a continuous annual growth rate (CAGR) of 4.1% to reach \$454.2 M in 2024.<sup>[59]</sup> As shown in **Table 5**, the LIFT is the second largest in terms of economic interest, with a market size of \$250 M in 2019 and an estimated growth rate of 4.09% during 2020–2025.<sup>[298]</sup> Although LIFT is heavily employed in other fields, such as molecular biology, electronics is a major driving factor as it is the fastest growing application with an estimated CAGR of 4.88% during a forecast period from 2020 to 2025. NIL has an estimated market

**Table 4.** Curated selection of patented, printed electronics packaging applications explored by Texas Instruments.

USPTO#	Title	Illustration
US10516381B2	3D-printed protective shell structures for stress sensitive circuits	
US10622270B2	Integrated circuit package with stress directing material	
US10727085B2	Printed adhesion deposition to mitigate integrated circuit package delamination	
US20210151551A1	3D printed semiconductor package	
US11031311B2	Packaged semiconductor device with multilayer stress buffer	

(Continued)

Table 4. (Continued).

USPTO#	Title	Illustration
WO2020247585A1	Repassivation application for wafer-level chip-scale package	
US20200043878A1	Printed repassivation for wafer chip scale packaging	
US20200083147A1	Custom leadframe from standard plus printed leadframe portion	
US10763230B2	Integrated circuit backside metallization	

Table 5. Overview of economic factors including an assessment of the degree of commercialization of the presented printing technologies.<sup>[298,299,59]</sup>

Technology	Market size	CAGR	Driving fields of application	Degree of commercialization
Inkjet printing	\$356.6 M	4.1%	OLEDs	High
EHD	n.a.	n.a.	TFTs	Low
Aerosol jet	\$12.5 M	14%	Antennas, IC packaging	High
LIFT	\$250 M	4.1%	Biotechnology	Medium
Reverse offset printing	n.a.	n.a.	TFTs	Low
NIL	\$61 M	9.9%	Optoelectronics, wafer level processing	High

value of \$61 M with a larger CAGR of 9.9%.<sup>[299]</sup> In contrast to that, aerosol jet was rated with a market value of only \$12.5 M in 2018.<sup>[59]</sup> However, its huge potential is highlighted by a vast CAGR of 14% until 2024. On the other hand, EHD and reverse offset printing still lack global economic relevance and can be considered as rather immature, yet, emerging technologies with their main fields in applications in science and academia. Table 5 also provides an overview of the prevalent fields of applications of these different technologies. Furthermore, an assessment of the degree of commercialization is presented, which is based on the number of commercial systems available on the market as well as the overall utilization on an industrial level.

Numerous vendors exist to supply tools that leverage most of the printing technologies outlined, and chipmakers and producers of semiconductor fabrication capital expenditures continue to rise dramatically year over year, with sales of production tools up from \$59.75 billion in 2019 to \$71.19 billion in 2020<sup>[300]</sup> accompanied with increased spending in R&D. This development highlights the rising demand and economic relevance of innovative and alternative fabrication strategies, such as printing, in the semiconductor and electronics industry.

However, regardless of the current economic impact and predicted potential of the individual technologies, the primary barrier to adaptation is integration into existing fab process flows. Besides the development per se of novel fabrication technologies, the integration of a new fabrication process can be extremely challenging, unless the entire device is fully fabricated using one process. For example, some stereolithography 3D printed mechanical structures are fabricated in mass production scale, since one process can create the entire device. However, microelectronics mostly requires multiple processes with different tools to achieve the desired performance, and the transition to additive processing will likely proceed in incremental steps. Assuming that an additive process has been successfully qualified for replacing legacy tools in a fab, it is hard to justify the costs and the effort of replacing the existing system, unless the new process is highly compatible with current setups. This is especially relevant in the area of micro-fabrication, where existing processes are in tightly controlled environments and flawlessly integrated. Some of the common challenges that need to be faced during the development and qualification of a new process are: i) Material and process compatibility with the existing fab infrastructure and cleanliness specifications; ii) Optimization of material deposition and curing processes to deposit the printed material with the necessary critical dimensions without damaging any micro-fabricated devices; iii) Handling of the material between existing process tool modules (cleaning, alignment, curing, and transferring device between equipment); iv) Testing of printed material in large-scale manufacturing, process yield, throughput, and optimization of process capability index; v) Short-term and long-term maintenance and management of tools and accompanying materials and solvents, without introducing any contaminants.

The integration of any new technology into existing fab flows consumes significant engineering resources, with qualification toward production taking months or even years. For some semiconductor manufacturing processes the ratio of usable products to theoretically manufacturable products is very high. According to the American Productivity & Quality Center the median yield is around 94%, while top performers achieve higher yields of up

to 97%.<sup>[301]</sup> Although yield data for printed devices are scarce, in literature rates between 75% and 79% have been reported for printed transistors and photovoltaics, respectively.<sup>[302]</sup> This may seem comparatively low, but a high yield can only be achieved through intensive process optimization, regardless of whether semiconductor or printing processes are involved. For comparison: In 2021, Samsung's yield rate on 4 nm chips was reportedly as low as 35% before optimization of the new processes.<sup>[303]</sup>

It is perhaps inaccurate to say that additive technologies alone are the future of manufacturing. On the other hand, tandem manufacturing and coexistence of additive and traditional tools provide a viable path forward.

## Conflict of Interest

The authors declare no conflict of interest.

## Keywords

high-resolution printing, industrial printed electronics, printed integrated circuits, printed sensors

Received: November 18, 2022

Revised: January 25, 2023

Published online:

- [1] M. Riordan, *IEEE Spectrum* **2004**, 41, 44.
- [2] S. Zhang, X. Xu, T. Lin, *J. Mater. Sci.: Mater. Electron.* **2019**, 30, 13855.
- [3] IDTechEx, <https://www.idtechex.com/en/research-report/flexible-printed-and-organic-electronics-2019-2029-forecasts-players-and-opportunities/639> (accessed: June 2020).
- [4] D. Zhao, H. Wei, L. Dong, Q. Jin, Y. Tian, G. Yuan, J. Ryu, L. Wang, *Soc. Inf. Disp.* **2019**, 50, 945.
- [5] G. Bardizza, E. Salis, C. Toledo, E. D. Dunlop, *Prog. Photovoltaics* **2020**, 28, 593.
- [6] A. Narazaki, A. Oyane, S. Komuro, R. Kurosaki, T. Kameyama, I. Sakamaki, H. Araki, H. Miyaji, *Opt. Mater. Express* **2019**, 9, 2807.
- [7] L.-R. Zhang, H. Tenhunen, Z. Zou, *Smart Electronic Systems: Heterogeneous Integration of Silicon and Printed Electronics*, Wiley, Weinheim, Germany **2018**, pp. 243–267.
- [8] Q. Wan, Ph.D. Thesis, KTH Royal Institute of Technology Stockholm, Sweden, **2017**.
- [9] E. Sowade, E. Ramon, K. Y. Mitra, C. Martínez-Domingo, M. Pedró, J. Pallarès, F. Loffredo, F. Villani, H. L. Gomes, L. Terés, R. R. Baumann, *Sci. Rep.* **2016**, 6, 33490.
- [10] Y. Gu, D. Park, S. Gonya, J. Jendrisak, S. Das, D. R. Hines, *Addit. Manuf.* **2019**, 30, 100843.
- [11] V. Correia, K. Y. Mitra, J. G. Rocha, E. Sowade, R. R. Baumann, S. Lanceros-Mendez, *J. Manuf. Processes* **2017**, 31, 364.
- [12] B. A. Huber, P. Popp, M. Kaiser, A. Ruediger, C. Schindler, *Appl. Phys. Lett.* **2017**, 110, 143503.
- [13] Y. Pang, Y. Cao, Y. Chu, M. Liu, K. Snyder, D. MacKenzie, C. Cao, *Adv. Funct. Mater.* **2019**, 30, 1906244.
- [14] V. Subramanian, J. B. Chang, A. de la Fuente Vornbrock, D. C. Huang, L. Jagannathan, F. Liao, B. Mattis, S. Molesa, D. R. Redinger, D. Soltman, S. K. Volkman, Q. Zhang, in *ESSCIRC 2008-34th European Solid-State Circuits Conference*, IEEE, **2008**, pp. 17–24).
- [15] Y. Khan, A. Thielens, S. Muin, J. Ting, C. Baumbauer, A. C. Arias, *Adv. Mater.* **2019**, 32, 1905279.

- [16] M. M. Muhaisin, R. A. Khan, J. Telfort, W. Heger, G. W. Roberts, in *2019 IEEE 62nd International Midwest Symposium on Circuits and Systems (MWSCAS)*, IEEE, **2019**, pp. 746–749.
- [17] H.-E. Nilsson, T. Unander, J. Sidén, H. Andersson, A. Manuilskiy, M. Hummelgård, M. Gulliksson, *IEEE Trans. Compon., Packag., Manuf. Technol.* **2012**, *2*, 1723.
- [18] F. Roscher, R. Thalheim, T. Seifert, S. D. Paul, R. Zichner, M. Wiemer, T. Otto, in *Smart Systems Integration; 13th International Conference and Exhibition on Integration Issues of Miniaturized Systems*, VDE, **2019**, pp. 1–8.
- [19] A. Roshanghias, M. Dreissigacker, C. Scherf, C. Bretthausen, L. Rauter, J. Zikulnig, T. Braun, K. F. Becker, S. Rzepka, M. Schneider-Ramelow, *Micromachines* **2020**, *11*, 564.
- [20] Q. Jing, A. Pace, L. Ives, A. Husmann, N. Catic, V. Khanduja, J. Cama, S. Kar-Narayan, *Cell Rep. Phys. Sci.* **2021**, *2*, 100386.
- [21] P. Galliker, J. Schneider, H. Eghlidi, S. Kress, V. Sandoghdar, D. Poulidakos, *Nat. Commun.* **2012**, *3*, 890.
- [22] K. Fukuda, S. Takado, *Adv. Mater.* **2017**, *29*, 1602736.
- [23] W. Zhou, *Nanoimprint Lithography: An Enabling Process for Nanofabrication*, Springer Science & Business Media, Shanghai **2013**.
- [24] infinityPV A.pS., <https://www.infinitypv.com/home> (accessed: July 2022).
- [25] JOLED Inc., <https://www.j-oled.com/eng/> (accessed: July 2022).
- [26] R. Zichner, R. R. Baumann, *Adv. Radio Sci.* **2013**, *11*, 271.
- [27] V. Beedasy, P. J. Smith, *Materials* **2020**, *13*, 704.
- [28] N. J. Wilkinson, M. A. A. Smith, R. W. Kay, R. A. Harris, *Int. J. Adv. Manuf. Technol.* **2019**, *105*, 4599.
- [29] Aerosol Jet Print Engine, <https://www.optomec.com/printed-electronics/aerosol-jet-printers/aerosol-jet-marathon-print-engine/> (accessed: April 2021).
- [30] H. Abdolmaleki, P. Kidmose, S. Agarwala, *Adv. Mater.* **2021**, *33*, 2006792.
- [31] Y. Wei, R. Torah, Y. Li, J. Tudor, *Sens. Actuators, A* **2016**, *247*, 239.
- [32] P. K. Wright, D. A. Dornfeld, A. Chen, C. C. Ho, J. W. Evans, *Trans. NAMRI/SME* **2010**, *38*.
- [33] M. de Vos, R. Torah, J. Tudor, *Smart Mater. Struct.* **2016**, *25*, 045016.
- [34] Y. Kim, S. Jang, *Appl. Phys. Lett.* **2015**, *106*, 014103.
- [35] D.-H. Youn, S.-H. Kim, Y.-S. Yang, S.-C. Lim, S.-J. Kim, S.-H. Ahn, H.-S. Sim, S.-M. Ryu, D.-W. Shin, J.-B. Yoo, *Appl. Phys. A* **2009**, *96*, 933.
- [36] W. Zou, H. Yo, P. Zhou, L. Liu, *Mater. Des.* **2019**, *166*, 107609.
- [37] G. Miskovic, R. Kaufhold, *IEEE Open J. Nanotechnol.* **2022**, *3*, 191.
- [38] S. Khan, L. Lorenzelli, R. S. Dahiya, *IEEE Sens. J.* **2014**, *15*, 3164.
- [39] M. Pudas, J. Hagberg, S. Leppävuori, *J. Eur. Ceram. Soc.* **2004**, *24*, 2943.
- [40] K.-H. Shin, H. A. D. Nguyen, J. Park, D. Shin, D. Lee, *J. Coat. Technol. Res.* **2017**, *14*, 95.
- [41] Y. Y. Kim, T.-Y. Yang, R. Suhonen, M. Välimäki, T. Maaninen, A. Kempainen, N. J. Jeon, J. Seon, *Adv. Sci.* **2016**, *6*, 1802094.
- [42] D. Lupo, W. Clemens, S. Breitung, K. Hecker, in *Applications of Organic and Printed Electronics* (Ed: E. Cantatore), Springer Science+Business Media, New York **2013**, pp. 1–26.
- [43] Laser-Induced Forward Transfer (LIFT), <https://www.psi.ch/lmx-interfaces/laser-induced-forward-transfer#top> (accessed: February 2018).
- [44] D. P. Banks, C. Grivas, J. D. Mills, R. W. Eason, *Appl. Phys. Lett.* **2016**, *89*, 193107.
- [45] M. Kandyła, S. Chatzandroulis, I. Zergiot, *Opto-Electronics Rev.* **2010**, *18*, 345.
- [46] C. W. Visser, R. Pohl, C. Sun, G.-W. Römer, B. H. in't Veld, D. Lohse, *Adv. Mater.* **2015**, *27*, 4087.
- [47] N. Kooy, K. Mohamed, L. T. Pin, O. S. Guan, *Nanoscale Res. Lett.* **2014**, *9*, 320.
- [48] M. D. Austin, H. Ge, W. Wu, M. Li, Z. Yu, D. Wassermann, S. A. Lyon, S. Y. Chou, *Appl. Phys. Lett.* **2004**, *84*, 5299.
- [49] HERCULES NIL, <https://www.evgroup.com/de/produkte/nanopraege-lithographie/uv-nil-smartnil/hercules-nil/> (accessed: August 2020).
- [50] Y. T. Cho, Y. Jeong, Y. J. Kim, S. Kwon, S.-H. Lee, K. Y. Kim, D. Kang, T.-M. Lee, *Appl. Sci.* **2017**, *7*, 1302.
- [51] A. Sneck, T. Mäkelä, A. Alastalo, *Flexible Printed Electron.* **2018**, *2015*, 3.
- [52] Y.-M. Choi, J. Jo, E. Lee, Y. Jang, I. Kim, J. H. Park, C.-M. Yang, W. C. Kim, T.-M. Lee, S. Kwon, *Int. J. Precis. Eng. Manuf.* **2015**, *16*, 2347.
- [53] A. Sneck, H. Ailas, F. Gao, J. Leppänen, *ACS Appl. Mater. Interfaces* **2021**, *13*, 41782.
- [54] W. J. Hyun, E. B. Secor, M. C. Hersam, C. D. Frisbie, L. F. Francis, *Adv. Mater.* **2015**, *27*, 109.
- [55] M. Hösel, R. R. Sondergaard, D. Angmo, F. C. Krebs, *Adv. Eng. Mater.* **2013**, *15*, 1068.
- [56] Advanced Micro Devices, Inc, AMD "Vega" 7 nm Technology, <https://www.amd.com/en/technologies/vega7nm> (accessed: August 2020).
- [57] J. Wiklund, A. Karakoc, T. Palko, H. Yigitler, K. Ruttik, R. Jäntti, J. Paltakari, *J. Manuf. Mater. Process.* **2021**, *5*, 89.
- [58] R. Riva, C. Buttay, R. Allard, P. Bevilacqua, *Microelectron. Reliab.* **2013**, *53*, 1592.
- [59] Emerging printing fills the gap for rising electronics applications, [https://www.yole.fr/Emerging\\_Printing\\_Technologies\\_Overview.aspx#.Xvra5O5xdaT](https://www.yole.fr/Emerging_Printing_Technologies_Overview.aspx#.Xvra5O5xdaT) (accessed: June 2020).
- [60] Dimensions, <https://www.app.dimensions.ai/discover/publication> (accessed: February 2022).
- [61] J. Zikulnig, J. Kosel, *Reference Module in Biomedical Sciences*, **2021**.
- [62] C. Sturgess, C. Tuck, I. Ashcroft, R. Wildman, *J. Mater. Chem. C* **2017**, *5*, 9733.
- [63] A. Foerster, R. Wildman, R. Hague, C. Tuck, *Solid Freeform Fabr. Symp.* **2017**.
- [64] W. Su, B. Cook, Y. Fang, M. Tentzeris, *Sci. Rep.* **2016**, *6*, 35111.
- [65] Silver nanoparticles ink for inkjet printing, <https://www.sigmaaldrich.com/catalog/product/aldrich/901083?lang=de&region=AT> (accessed: April 2021).
- [66] S. Fathi, P. Dickens, R. Hague, *Rapid Prototyping J.* **2013**, *19*.
- [67] O. Oktavianty, Y. Ishii, S. Haruyama, T. Kyoutani, Z. Darmawan, S. E. Swara, *IOP Conf. Ser.: Mater. Sci. Eng.* **2021**.
- [68] O. Oktavianty, S. Haruyama, Y. Ishii, Z. Darmawan, *Univers. J. Mech. Eng.* **2019**, *7*, 12.
- [69] S. Logothetidis, *Handbook of Flexible Organic Electronics: Materials, Manufacturing and Applications*, Elsevier, Cambridge **2014**.
- [70] M. I. Baek, M. Hong, *Inkjet-Based Micromanufacturing*, **2012**.
- [71] D. Gao, J. G. Zhou, *Int. J. Bioprint.* **2019**, *5*, 172.
- [72] H. Y. Gan, X. Shan, T. Eriksson, B. K. Lok, Y. C. Lam, *J. Micromech. Microeng.* **2008**, *19*, 055010.
- [73] J. Kwon, S. Baek, Y. Lee, S. Tokito, S. Jung, *Langmuir* **2021**, *37*, 10692.
- [74] J. Zikulnig, A. Roshanghias, L. Rauter, C. Hirschl, *Sensors* **2020**, *20*, 2398.
- [75] T. Öhlund, J. Örtengren, S. Forsberg, H.-E. Nilsson, *Appl. Surf. Sci.* **2012**, *259*, 731.
- [76] B. Derby, *Annu. Rev. Mater. Res.* **2010**, *40*, 395.
- [77] M. Tavakoli, M. H. Malakooti, H. Paisana, Y. Ohm, D. Green Marques, P. A. Lopes, A. P. Piedade, *Adv. Mater.* **2018**, *30*, 1801852.
- [78] E. Saleh, J. Vaithilingham, C. Tuck, R. Wildman, I. Ashcroft, R. Hague, P. Dickens, in *Proceedings of the 26th Annual International Solid Freeform Fabrication Symposium*, University of Texas, **2015**, pp. 1554-1559.
- [79] A. Roshanghias, M. Krivec, M. Baumgart, *Flexible Printed Electron.* **2017**, *2*, 045002.
- [80] H. Wijshoff, *Phys. Rep.* **2010**, *491*, 77.
- [81] Z. Cui, *Printed Electronics: Materials, Technologies and Applications*, John Wiley & Sons, China **2016**.

- [82] M. Kriss, *Handbook of Digital Imaging*, John Wiley & Sons, West Sussex, UK **2015**, pp. 876–877.
- [83] A. Albrecht, A. Rivadeneyra, A. Abdellah, P. Lugli, J. F. Salmerón, *J. Mater. Chem. C* **2016**, *4*, 3546.
- [84] Q. Yang, H. Li, M. Li, Y. Li, S. Chen, B. Bao, Y. Song, *ACS Appl. Mater. Interfaces* **2017**, *9*, 41521.
- [85] Xaar Group, <https://www.xaar.com/en/products/xaar-printheads/xaar-128/> (accessed: November 2022).
- [86] C. Sturgess, in *Solid Freeform Fabrication 2022*, Austin, Texas **2022**.
- [87] B. Hartkopp, M. Strobel, R. Borrell, in *NIP & Digital Fabrication Conference*, Vol. 37, Society for Imaging Science and Technology, **2021**, pp. 1–4.
- [88] L. Färber, B. Hartkopp, *European Patent EP3825100A1*, **2019**.
- [89] A. Moya, G. Gabriel, R. Villa, F. J. del Campo, *Curr. Opin. Electrochem.* **2017**, *3*, 29.
- [90] J. D. Retief, P. R. Fourie, W. J. Perold, in *3rd Biennial South African Biomedical Engineering Conference (SAIBMEC)*, IEEE, **2018**, pp. 1–4.
- [91] A. Gbaguidi, F. Madiyar, D. Kim, S. Namilae, *Smart Mater. Struct.* **2020**, *29*, 085052.
- [92] SÜSS MICROTEC SE, LP50 – Datasheet, [https://www.suss.com/brochures-datasheets/SUSS\\_MicroTec\\_Inkjet\\_Printer\\_PiXDRO\\_LP50.pdf](https://www.suss.com/brochures-datasheets/SUSS_MicroTec_Inkjet_Printer_PiXDRO_LP50.pdf) (accessed: May 2020).
- [93] FUJIFILM Holdings America Corporation, Dimatix Materials Printer DMP-2850 – Data&Specs Sheet, [https://www.fujifilmusa.com/shared/bin/dimatix\\_materials\\_printer\\_dmp-2850.pdf](https://www.fujifilmusa.com/shared/bin/dimatix_materials_printer_dmp-2850.pdf) (accessed: May 2020).
- [94] Ceradrop, C. P. F.-S., <https://www.ceradrop.com/en/products/f-serie/> (accessed: June 2020).
- [95] P. V. Nanocell, Printers for Prototyping & Manufacturing of Printed Electronics, <https://www.pvnanocell.com/printers.html> (accessed: April 2021).
- [96] Seiko Epson Corporation, Micro Piezo Inkjet Technology, [https://www.global.epson.com/technology/printer\\_inkjet/micro\\_piezo.html](https://www.global.epson.com/technology/printer_inkjet/micro_piezo.html) (accessed: January 2022).
- [97] IDTechEx, OLED Display Forecasts 2016–2026: The Rise of Plastic and Flexible Displays, <https://www.idtechex.com/en/research-report/oled-display-forecasts-2016-2026-the-rise-of-plastic-and-flexible-displays/477> (accessed: June 2020).
- [98] Notion Systems GmbH, n.jet display, <https://www.notion-systems.com/n-jet-display.html> (accessed: June 2020).
- [99] TEL Announces the Launch of Elius™500 Pro, an Inkjet Printing System for OLED Display Production, [https://www.tel.com/news/topics/2019/20191017\\_001.html](https://www.tel.com/news/topics/2019/20191017_001.html) (accessed: June 2020).
- [100] Inkjet for OLED thin film encapsulation deposition, <https://www.kateeva.com/products/inkjetjet-flex/> (accessed: June 2020).
- [101] C. W. Sele, T. von Werne, R. H. Friend, H. Sirringhaus, *Adv. Mater.* **2005**, *17*, 997.
- [102] H. Sirringhaus, C. W. Sele, T. von Werne, C. Ramsdale, in *Organic Electronics: Materials, Manufacturing, and Applications*, WILEY-VCH Verlag GmbH & Co. KGaA, Weinheim, Germany **2006**, pp. 294–321.
- [103] N. Zhao, M. Chiesa, H. Sirringhaus, *J. Appl. Phys.* **2017**, *101*, 064513.
- [104] X. Cao, F. Wu, C. Lau, Y. Liu, Q. Liu, C. Zhou, *ACS Nano* **2017**, *11*, 2008.
- [105] P. V. Rajee, N. C. Murmu, *Int. J. Emerging Technol. Adv. Eng.* **2014**, *4*, 174.
- [106] J. F. de la Mora, *Annu. Rev. Fluid Mech.* **2007**, *39*, 217.
- [107] Scrona, <https://www.scrona.ch/> (accessed: May 2020).
- [108] C.-H. Chen, D. A. Saville, I. A. Aksay, *Appl. Phys. Lett.* **2006**, *89*, 124103.
- [109] H. F. Foon, D. A. Saville, I. A. Aksay, *Appl. Phys. Lett.* **2008**, *93*, 133114.
- [110] R. T. Collins, M. T. Harris, O. A. Basaran, *J. Fluid Mech.* **2007**, *588*, 75.
- [111] M. S. Onses, E. Sutanto, P. M. Ferreira, A. G. Alleyne, J. A. Rogers, *Small* **2015**, *11*, 4237.
- [112] Y. Guan, Electrohydrodynamic (EHD) printing of microparticle streams for additive manufacturing, Doctoral dissertation, Massachusetts Institute of Technology, **2016**.
- [113] Z. Cui, Y. Han, O. Huang, J. Dong, Y. Zhu, *Nanoscale* **2018**, *10*, 6806.
- [114] Y. Han, J. Dong, *Procedia Manuf.* **2017**, *10*, 845.
- [115] M. Yu, K. H. Ahn, S. J. Lee, *Mater. Des.* **2016**, *89*, 109.
- [116] Z. Yin, Y. Huang, Y. Duan, H. Zhang, *Electrohydrodynamic Direct-Writing for Flexible Electronic Manufacturing*, Springer, Singapore **2018**.
- [117] C. Wei, H. Qin, N. A. Ramírez-Iglesias, C.-P. Chiu, Y.-S. Lee, J. Dong, *J. Micromech. Microeng.* **2014**, *24*, 045010.
- [118] U. Stachewicz, C. U. Yurteri, J. C. M. Marijnissen, J. F. Dijkman, *Appl. Phys. Lett.* **2009**, *95*, 224105.
- [119] H. Li, W. Yang, Y. Duan, Q. Nie, Z. Shao, Z. Yin, Y. Huang, *Phys. Fluid* **2021**, *33*, 081704.
- [120] A. Reiser, M. Lindén, P. Rohner, A. Marchand, H. Galinski, A. S. Sologubenko, J. M. Wheeler, R. Zenobi, D. Poulikakos, R. Spolenak, *Nat. Commun.* **2019**, *10*, 1853.
- [121] Y. Han, C. Wei, J. Dong, *J. Manuf. Processes* **2015**, *20*, 485.
- [122] H.-j. Kwon, J. Hong, S. Y. Nam, H. H. Choi, X. Li, Y. Y. Jeong, S. H. Kim, *Mater. Adv.* **2021**, *2*, 5593.
- [123] K. Barton, S. Mishra, K. A. Shorter, A. Alleyne, P. Ferreira, J. Rogers, *Mechatronics* **2010**, *20*, 611.
- [124] J.-Y. Kim, V. Nguyen, D.-Y. Byun, *J. Korean Soc. Visualization* **2011**, *9*, 48.
- [125] L. Jiang, L. Yu, P. Premeratne, Z. Zhang, H. Qin, *J. Manuf. Processes* **2021**, *66*, 125.
- [126] Z. Li, K. N. Al-Milaji, H. Zhao, D.-R. Chen, *J. Micromech. Microeng.* **2019**, *29*, 035013.
- [127] E. Sutanto, K. Shigetani, Y. K. Kim, P. G. Graf, D. J. Hoelzle, K. L. Barton, A. G. Alleyne, P. M. Ferreira, J. A. Rogers, *J. Micromech. Microeng.* **2012**, *22*, 045008.
- [128] A. Khan, K. Rahman, M.-T. Hyun, D.-S. Kim, K.-H. Choi, *Appl. Phys. A* **2011**, *104*, 1113.
- [129] Y. Pan, Y. Huang, L. Guo, Y. Ding, Z. Yin, *AIP Adv.* **2015**, *5*, 047108.
- [130] K.-H. Choi, A. Khan, K. Rahman, Y.-H. Doh, D.-S. Kim, K.-R. Kwan, *Journal of Electrostat.* **2011**, *69*, 380.
- [131] Y. Jang, J. Kim, D. Byun, *J. Phys. D: Appl. Phys.* **2013**, *46*, 155103.
- [132] S. M. Yang, Y. S. Lee, Y. Jang, D. Byun, S.-H. Choa, *Microelectron. Reliab.* **2016**, *65*, 151.
- [133] S. Khan, Y. H. Doh, A. Khan, A. Rahman, K. H. Choi, D. S. Sim, *Curr. Appl. Phys.* **2011**, *11*, S271.
- [134] M. N. Awais, H. C. Kim, Y. H. Doh, K. H. Choi, *Thin Solid Films* **2013**, *536*, 308.
- [135] High-Resolution Super-Fine Innovative Coating & Printing Solution for Manufacturing, <https://www.en.enjet.co.kr/ceo/> (accessed: June 2020).
- [136] Enjet Inc., eNanojet Printer, <https://www.en.enjet.co.kr/p/iehd-jet-printer/1> (accessed: June 2020).
- [137] S. I. J. Technology, Super Inkjet Printer, <https://www.sijtechnology.com/en/products/#pro1> (accessed: December 2020).
- [138] K.-S. Kwon, M. K. Rahman, T. H. Phung, S. D. Hoath, S. Jeong, J. S. Kim, *Flexible Printed Electron.* **2020**, *5*, 043003.
- [139] A. Khan, K. Rahman, M.-T. Hyun, D.-S. Kim, K.-H. Choi, *Appl. Phys. A* **2011**, *104*, 1113.
- [140] Tonejet – Digital Printing Solutions for Packaging, KISS, <https://www.tonejet.com/> (accessed: May 2020).
- [141] L. Lima-Marques, *Worldwide Application Patent WO1994018011A1*, **1994**, <https://patents.google.com/patent/CA2155942A1/en>
- [142] G. C. F. Newcombe, *Worldwide Applications Patent WO1998042515A1*, 24 March **1998**, <https://patents.google.com/patent/US6409313>
- [143] J. W. Teape, G. C. F. Newcombe, D. R. Mace, P. J. Atkin, **2001**, [https://patents.google.com/patent/WO2001030576A1/RED\\_FLAGS-Oct.2007\\_.pdf](https://patents.google.com/patent/WO2001030576A1/RED_FLAGS-Oct.2007_.pdf)

- [144] R. Salary, J. P. Lombardi, M. S. Tootooni, R. Donovan, P. K. Rao, P. Borgesen, M. D. Poliks, *J. Manuf. Sci. Eng.* **2017**, *139*, 021015.
- [145] Aerosol Jet HD System, <https://www.optomec.com/printed-electronics/aerosol-jet-printers/aerosol-jet-high-density-printed-electronics/> (accessed: October 2020).
- [146] A. Mahajan, C. D. Frisbie, L. F. Francis, *ACS Appl. Mater. Interfaces* **2013**, *5*, 4856.
- [147] D. Jahn, R. Eckstein, L. M. Schneider, N. Born, G. Hernandez-Sosa, J. C. Balzer, I. Al-Naib, U. Lemmer, M. Koch, *Adv. Mater. Technol.* **2018**, *3*, 1700236.
- [148] J. G. Tait, E. Witkowska, M. Hirade, T.-H. Ke, P. E. Malinowski, S. Steudel, C. Adachi, P. Heremans, *Org. Electron.* **2015**, *22*, 40.
- [149] W. Verheecke, M. Van Dyck, F. Vogeler, A. Voet, H. Valkernaers, in 8th International DAAAM Baltic Conference Industrial Engineering, **2012**, pp. 373-379.
- [150] E. Jabari, E. Toyserkani, *Carbon* **2015**, *91*, 321.
- [151] B. Khorramdel, A. Torkkeli, M. Mäntysalo, *IEEE J. Electron Devices Soc.* **2017**, *6*, 34.
- [152] T. Seifert, M. Baum, F. Roscher, M. Wiemer, T. Gessner, *Mater. Today: Proc.* **2015**, *2*, 4262.
- [153] S. Stoukatch, P. Laurent, S. Dricot, F. Axisa, L. Seronveaux, D. Vandormael, E. Beeckman, B. Heusdens, J. Destiné, in 2012 4th Electronic System-Integration Technology Conference, IEEE, **2012**, pp. 1–5).
- [154] C. Cao, J. B. Andrews, A. D. Franklin, *Adv. Electron. Mater.* **2017**, *3*, 1700057.
- [155] M. Smith, Y. S. Choi, C. Boughey, S. Kar-Narayan, *Flexible Printed Electron.* **2017**, *2*, 015004.
- [156] G. Chen, Y. Gu, H. Tsang, D. R. Hines, S. Das, *Adv. Eng. Mater.* **2018**, *20*, 1701084.
- [157] S. Binder, M. Glatthaar, E. Rädlein, *Aerosol Sci. Technol.* **2014**, *48*, 924.
- [158] A. Wadhwa, Degree of Masters in Science, Rochester Institute of Technology, xx xx **2015**.
- [159] K. Skarżyński, J. Krzemiński, M. Jakubowska, M. Słoma, *Sci. Rep.* **2021**, *11*, 18141.
- [160] R. Salary, J. P. Lombardi, D. L. Weerawarne, P. Rao, M. D. Poliks, *J. Micro Nano Manuf.* **2021**, *9*, 010903.
- [161] M. J. Renn, B. H. King, M. Essien, L. J. Hunter, U.S. Patent No. 7,045,015, **2006**.
- [162] B. H. King, M. J. Renn, J. A. Paulsen, U.S. Patent No. 8,132,744, **2012**.
- [163] K. K. Christenson, M. J. Renn, J. A. Paulson, J. D. Hamre, C. Conroy, J. Q. Feng, U.S. Patent No. 10,632,746, **2020**.
- [164] Optomec Inc, Aerosol Jet FLEX Systems, <https://www.optomec.com/printed-electronics/aerosol-jet-printers/aerosol-jet-flex-system/> (accessed: June 2020).
- [165] Aerosol Jet Print Engine, <https://www.optomec.com/printed-electronics/aerosol-jet-printers/aerosol-jet-marathon-print-engine/> (accessed: June 2020).
- [166] Lite-on Uses Electronics 3D Printing for Mass Production, 3D Printing Industry, <https://www.3dprintingindustry.com/news/lite-on-uses-electronics-3d-printing-for-mass-production-75297/> (accessed: October 2020).
- [167] Samsung Electronics Selects Optomec's Aerosol Jet for Next-Generation Electronics Production, DE 247 Digital Engineering, <https://www.digitalengineering247.com/article/samsung-electronics-selects-optomecs-aerosol-jet-for-next-generation-electronics-production/electronic-cad> (accessed: October 2020).
- [168] M. L. Levene, R. D. Scott, B. W. Siry, *Appl. Opt.* **1970**, *9*, 2260.
- [169] P. Serra, M. Colina, J. M. Fernández-Pradas, L. Sevilla, J. L. Morenza, *Appl. Phys. Lett.* **2004**, *85*, 1639.
- [170] J. M. Fernández-Pradas, M. Colina, P. Serra, J. Domínguez, J. L. Morenza, *Thin Solid Films* **2004**, *453*, 27.
- [171] J. Bohandy, B. F. Kim, F. J. Adrian, *J. Appl. Phys.* **1986**, *60*, 1538.
- [172] M. Sopena, J. M. Fernández-Pradas, P. Serra, *Appl. Surf. Sci.* **2020**, *507*, 145047.
- [173] M. Zenou, Z. Kotler, *Opt. Express* **2016**, *24*, 1431.
- [174] D. H. Willis, V. Grosu, *Appl. Phys. Lett.* **2005**, *86*, 244103.
- [175] A. Piqué, H. Kim, *J. Laser Micro /Nanoeng.* **2014**, *9*, 192.
- [176] J. M. Fernández-Pradas, P. Serra, *Crystals* **2020**, *10*, 651.
- [177] M. Makrygianni, I. Kalpyris, C. Boutopoulos, I. Zergioti, *Appl. Surf. Sci.* **2014**, *297*, 40.
- [178] P. Sopena, P. Serra, J. M. Fernández-Pradas, *Appl. Surf. Sci.* **2019**, *476*, 828.
- [179] T. Araki, R. Mandamparambil, D. M. van Bragt, J. Jiu, H. Koga, J. van den Brand, T. Sekitani, J. M. J. den Toonder, K. Suganuma, *Nanotechnology* **2016**, *27*, 45LT02.
- [180] L. Neumaier, L. Rauter, S. Lengger, S. Khan, J. Kosel, in 2022 IEEE International Conference on Flexible and Printable Sensors and Systems (FLEPS), IEEE, **2022**, pp. 1–3.
- [181] J. M. Fernández-Pradas, P. Sopena, S. González-Torres, J. Arrese, A. Cirera, P. Serra, *Appl. Phys. A* **2018**, *124*, 214.
- [182] P. Sopena, J. Siero, J. M. Fernández-Pradas, J. M. López-Villegas, P. Serra, *Adv. Mater. Technol.* **2020**, *5*, 2000080.
- [183] F. J. Adrian, J. Bohandy, B. F. Kim, A. N. Jette, *J. Vac. Sci. Technol., B: Microelectron. Process. Phenom.* **1987**, *5*, 1490.
- [184] W. A. Tolbert, I. Y. S. Lee, M. M. M. Doxtader, E. W. Ellis, D. D. Dlott, *J. Imaging Sci.* **1993**, *37*, 411.
- [185] Y. Luo, R. Pohl, L. Qi, G.-W. Römer, C. Sun, D. Lohse, C. W. Visser, *Small* **2016**, *13*, 1602553.
- [186] C. Constantinescu, A. K. Diallo, L. Rapp, P. Cremillieu, R. Mazurcyk, F. Serein-Spirau, J. P. Lère-Porte, P. Delaporte, A. P. Alloncle, C. Vidélot-Ackermann, *Appl. Surf. Sci.* **2015**, *336*, 11.
- [187] N. T. Kattamis, *Appl. Phys. Lett.* **2007**, *91*, 171120.
- [188] F. Claeysens, A. Klini, A. Mourka, C. Fotakis, *Thin Solid Films* **2007**, *515*, 8529.
- [189] J. Shaw-Steward, B. Chu, T. Lippert, Y. Maniglio, M. Nagel, F. Nüesch, A. Wokaun, *Appl. Phys. A* **2011**, *105*, 713.
- [190] T. Sano, H. Yamada, T. Nakayama, I. Miyamoto, *Appl. Surf. Sci.* **2002**, *186*, 221.
- [191] A. Klini, P. A. Loukakos, D. Gray, A. Manousaki, C. Fotakis, *Opt. Express* **2008**, *16*, 11300.
- [192] Y. Chen, D. Munoz-Martin, M. Morales, C. Molpeceres, E. Sánchez-Cortzon, J. Murillo-Gutierrez, *Phys. Procedia* **2016**, *83*, 204.
- [193] A. Patrascioiu, C. Florian, J. M. Fernández-Pradas, J. L. Morenza, G. Hennig, P. Delaporte, P. Serra, *Appl. Phys. Lett.* **2014**, *105*, 014101.
- [194] E. Biver, L. Rapp, A.-P. Alloncle, P. Delaporte, *Appl. Surf. Sci.* **2014**, *302*, 153.
- [195] Biofabrication, <https://www.ilt.fraunhofer.de/en/technology-focus/medical-technology-and-biophotonics/biofabrication.html> (accessed: November 2020).
- [196] History, <https://www.daetwyler-usa.com/pressroom/en/information/History> (accessed: November 2020).
- [197] Uniqarta, <https://www.uniqarta.com/> (accessed: December 2020).
- [198] N. Choi, H. Wee, S. Nam, J. Lavelle, M. Hatalis, *Microelectron. Eng.* **2012**, *91*, 93.
- [199] Y. Kusaka, N. Fukuda, H. Ushijima, *Jpn. J. Appl. Phys.* **2020**, *59*, 112005.
- [200] Y.-M. Choi, E. Lee, T.-M. Lee, *J. Micromech. Microeng.* **2015**, *25*, 075019.
- [201] S. M. Garner, *Flexible Glass: Enabling Thin, Lightweight, and Flexible Electronics*, John Wiley & Sons, **2017**.
- [202] M. Kim, I.-K. You, H. Han, S.-W. Jung, T.-Y. Kim, B.-K. Ju, J. B. Koo, *Electrochem. Solid-State Lett.* **2011**, *14*, H333.
- [203] S. M. Kim, S. Won, J. Seo, S. K. Jeong, C. Kim, K.-S. Kim, S. H. Kim, S. S. Cho, J.-H. Kim, *ACS Appl. Mater. Interfaces* **2021**, *13*, 26601.

- [204] K. Fukuda, Y. Yoshimura, T. Okamoto, Y. Takeda, D. Kumaki, Y. Katayama, S. Tokito, *Adv. Electron. Mater.* **2015**, *1*, 1500145.
- [205] Y. Kusaka, K. Sugihara, H. Ushijima, *Flexible Printed Electron.* **2016**, *1*, 1500145.
- [206] H. Kim, E. Lee, Y.-M. Choi, S. Kwon, S. Lee, J. Jo, T.-M. Lee, D. Kang, *Rev. Sci. Instrum.* **2016**, *87*, 015102.
- [207] J. Leppäniemi, A. Sneck, Y. Kusaka, N. Fukuda, A. Alastalo, *Adv. Electron. Mater.* **2019**, *5*, 1900272.
- [208] Y. Kusaka, S. Kanazawa, M. Koutake, H. Ushijima, *J. Micromech. Microeng.* **2017**, *27*, 015003.
- [209] Y. Kusaka, K. Sugihara, M. Koutake, H. Ushijima, *J. Micromech. Microeng.* **2016**, *27*, 017002.
- [210] K. Izumi, H. Saito, Y. Yoshida, S. Tokito, H. Ushijima, *Jpn. J. Appl. Phys.* **2020**, *59*, 031003.
- [211] Z. Zhong, P. Ko, J. Y. Seok, H. Kim, S. Kwon, H. Youn, K. Woo, *Adv. Eng. Mater.* **2020**, *22*, 2000463.
- [212] J. Zheng, J. Ala-Laurinaho, A. Sneck, T. Makela, A. Alastalo, A. V. Raisanen, *Roll-to-roll reverse offset printing of millimeter-wave transmission lines and antennas on flexible substrates*, **2018**.
- [213] Naraenanotech, <https://www.en.naraenano.co.kr/> (accessed: September 2020).
- [214] Adhesion Contrast Planography Printing System, <https://www.en.jemflex.co.jp/images/products/1-acpp-catalog.pdf> (accessed: January 2023).
- [215] M. Lohse, M. W. Thesen, A. Haase, M. Smolka, N. B. Iceta, A. A. Izquierdo, I. Ramos, C. Salado, A. Schleunitz, *Nanomaterials* **2021**, *11*, 902.
- [216] S. H. Ahn, L. J. Guo, *Adv. Mater.* **2008**, *20*, 2044.
- [217] C.Inc., Canon Technology – Nanoimprint Lithography, <https://www.global.canon/en/technology/frontier07.html> (accessed: August 2020).
- [218] M. Vogler, S. Wiedenberger, M. Mühlberger, I. Bergmair, T. Glinser, H. Schmidt, E.-B. Kley, G. Grützner, *Microelectron. Eng.* **2007**, *84*, 984.
- [219] Obducat A. B., Technologies and Market, <https://www.obducat.com/about-obducat/technologies-markets/> (accessed: August 2020).
- [220] Y. Xia, G. M. Whitesides, *Angew. Chem., Int. Ed.* **1998**, *37*, 550.
- [221] A. Fernández, J. Medina, C. Benkel, M. Guttman, B. Bilenberg, L. H. Thamdrupe, T. Nielsen, C. M. S. Torres, N. Kehagias, *Microelectron. Eng.* **2015**, *141*, 56.
- [222] A. Tavakkoli KG, M. Ranjbar, S. M. Piramanayagam, S. K. Wong, W. C. Poh, R. Sbiaa, T. C. Chong, *Nanosci. Nanotechnol. Lett.* **2012**, *4*, 835.
- [223] J. Song, H. Lu, S. Li, L. Tan, A. Gruverman, S. Ducharme, *Nanotechnology* **2016**, *27*, 015302.
- [224] A. R. Moharana, H. M. Außerhuber, T. Mitteramskogler, M. J. Haslinger, M. M. Mühlberger, *Coatings* **2020**, *10*, 301.
- [225] M. Mühlberger, M. J. Haslinger, J. Kurzmann, M. Ikeda, A. Fuchsbaauer, T. Faury, T. Koepplmayr, H. Ausserhuber, J. Kastner, C. Woegerer, D. Fechtig, in *33rd European Mask and Lithography Conference*, Vol. 10446, SPIE, **2017**, pp. 201–210.
- [226] B. Horváth, B. Krivora, H. Schiff, *Micro Nanoeng.* **2019**, *3*, 22.
- [227] L. Teng, M. Plötner, A. Türke, B. Adolphi, A. Finn, R. Kirchner, W.-J. Fischer, *Microelectron. Eng.* **2013**, *110*, 292.
- [228] S. Y. Chou, P. R. Krauss, P. J. Renstrom, *Appl. Phys. Lett.* **1995**, *67*, 3114.
- [229] Nanoimprint Tools & Solutions, <https://www.nanonex.com/> (accessed: August 2020).
- [230] F. Hua, Y. Sun, A. Gaur, M. A. Meitl, L. Bilhaut, L. Rotkina, J. Wang, P. Geil, M. Shim, J. A. Rogers, A. Shim, *Nano Lett.* **2004**, *4*, 2467.
- [231] J. Shao, X. Chen, X. Li, H. Tian, C. Wang, B. Lu, *Sci. China: Technol. Sci.* **2018**, *62*, 175.
- [232] R. Jiawook, B. Heidari, *Emerging Applications of Nanoparticles and Architecture Nanostructures*, pp. 141–175.
- [233] What Happened to Nanoimprint Litho?, <https://www.semiengineering.com/what-happened-to-nanoimprint-litho/> (accessed: August 2020).
- [234] Nanonex Nanoimprintor Family, <https://www.nanonex.com/machines.htm> (accessed: August 2020).
- [235] C. Nanotechnologies, Inc., C. Nanotechnologies, Inc, <https://www.cnt.canon.com/> (accessed: August 2020).
- [236] S. V. Sreenivasan, *Microsyst. Nanoeng.* **2017**, *3*, 17075.
- [237] Canon provides nanoimprint lithography manufacturing equipment to Toshiba Memory's Yokkaichi Operations plant, <https://www.global.canon/en/news/2017/20170720.html> (accessed: August 2020).
- [238] Kioxia joins hands with NDP and Jiali to push NIL technology, <https://www.12chip.com/article/Electronic%20Components%20News/can-5nm-chips-be-made-without-euv-lithography-machine-kioxia-joins-hands-with-ndp-and-jiali-to-push-nil-technology.html> (accessed: January 2023).
- [239] iMedia, DNP/Kioxia/Canon jointly develop nanoimprint lithography technology! Power consumption is only 1/10 of EUV process, <https://www.min.news/en/digital/74234bcb123a8b1ed70e0932b556e023.html> (accessed: January 2023).
- [240] C. Nanotechnologies, Inc., N. I. L., and, t. Environment, <https://www.cnt.canon.com/352-2/> (accessed: August 2020).
- [241] M. A. Yakoob, J. Lamminaho, K. Petersons, A. Prajapati, E. Destouesse, B. R. Patil, H.-G. Rubahn, G. Shalev, J. Stensborg, M. Madsen, *ChemSusChem* **2021**, *15*, e202101611.
- [242] H. Lan, in *Micro/Nanolithography – A Heuristic Aspect on the Enduring Technology*, **2017**, pp. 43–68.
- [243] T. Vuorinen, J. Niittyneen, T. Kankkunen, T. M. Kraft, M. Mäntysalo, *Sci. Rep.* **2016**, *6*, 35289.
- [244] T. Vuorinen, M.-M. Laurila, R. Mangayil, M. Karp, M. Mäntysalo, *EM-BEC* **2017**, *65*, 839.
- [245] L. M. Ferrari, S. Sudha, S. Tarantino, R. Esposti, F. Bolzoni, P. Cavallari, C. Cipriani, V. Mattoli, F. Greco, *Adv. Sci.* **2018**, *5*, 1700771.
- [246] W.-H. Yeo, Y.-S. Kim, J. Lee, A. Ameen, L. Shi, M. Li, S. Wang, R. Ma, S. H. Jin, Z. Kang, Y. Huang, J. A. Rogers, *Adv. Mater.* **2013**, *25*, 2773.
- [247] B. S. Cook, J. R. Cooper, M. M. Tentzeris, *IEEE Microwave Wireless Compon. Lett.* **2013**, *23*, 353.
- [248] B. S. Cook, C. Mariotti, J. R. Cooper, D. Revier, B. K. Tehrani, L. Aluigi, M. M. Tentzeris, in *2014 IEEE MTT-S International Microwave Symposium (IMS2014)*, IEEE, **2014**, pp. 1–4.
- [249] M. Fallahpour, R. Zoughi, *IEEE Antennas Propag. Mag.* **2018**, *60*, 38.
- [250] J. Bito, B. Tehrani, B. Cook, M. Tentzeris, in *2014 IEEE Antennas and Propagation Society International Symposium (APSURSI)*, IEEE, **2014**, pp. 854–855.
- [251] K. Abe, K. Suzuki, D. Citterio, *Anal. Chem.* **2008**, *80*, 6928.
- [252] K. Abe, K. Kotera, K. Suzuki, D. Citterio, *Anal. Bioanal. Chem.* **2010**, *398*, 885.
- [253] T. N. Steward, B. E. Pierson, R. Aggarwal, R. J. Narayan, *Biotechnol. J.* **2009**, *4*, 206.
- [254] J.-U. Park, J. H. Lee, U. Paik, Y. Lu, J. A. Rogers, *Nano Lett.* **2008**, *8*, 4210.
- [255] H. Sharma, D. Nguyen, A. Chen, V. Lew, M. Khine, *Ann. Biomed. Eng.* **2011**, *39*, 1313.
- [256] B. S. Cook, J. A. Herbsommer, D. Trombley, S. A. Kummerl, P. Emerson, U.S. Patent No. 9,646,906, **2017**.
- [257] B. Clifford, D. Beynon, C. Phillips, D. Deganello, *Sens. Actuators, B* **2018**, *255*, 1031.
- [258] F.-R. Hsiao, Y.-C. Liao, *IEEE Sens. J.* **2018**, *18*, 6788.
- [259] F. Molina-Lopez, D. Briand, N. F. de Rooij, in *2014 IEEE 27th International Conference on Micro Electro Mechanical Systems (MEMS)*, IEEE, **2014**, pp. 506–509.

- [260] M. T. Rahman, A. Rahimi, S. Gupta, R. Panat, *Sens. Actuators, A* **2016**, 248, 94.
- [261] L. Liu, Y. Pei, S. Ma, X. Sun, T. J. Singler, *Adv. Eng. Mater.* **2020**, 22, 1901351.
- [262] M. Liu, Q. Zhang, Y. Zhao, Y. Shao, D. Zhang, *Sensors* **2020**, 20, 3395.
- [263] B. Andò, S. Baglio, C. O. Lombardo, V. Marletta, A. Pistorio, *IEEE Trans. Instrum. Meas.* **2016**, 65, 1242.
- [264] Y. Zhang, W. S. Kim, *MRS Online Proc. Libr.* **2014**, 1690, 1.
- [265] Y. Yamamoto, S. Harada, D. Yamamoto, W. Honda, T. Arie, S. Akita, K. Takei, *Appl. Sci. Eng.* **2016**, 2, e1601473.
- [266] R. Eckstein, N. Strobel, T. Rödlmeier, K. Glaser, U. Lemmer, G. Hernandez-Sosa, *Adv. Opt. Mater.* **2018**, 6, 1701108.
- [267] G. Azzeloni, A. Grimoldi, M. Binda, M. Caironi, M. Natali, M. Sampietro, *Adv. Mater.* **2013**, 25, 6829.
- [268] G. Pace, A. Grimoldi, M. Sampietro, D. Natali, M. Caironi, *Semicond. Sci. Technol.* **2015**, 30, 104006.
- [269] J. Zikulnig, C. Hirschl, L. Rauter, M. Krivec, H. Lammer, F. Riemelmoser, A. Roshanghias, *Flexible Printed Electron.* **2019**, 4, 015008.
- [270] M. Knoll, C. Offensteller, B. Jakoby, W. Hilber, *Microelectron. Eng.* **2019**, 209, 49.
- [271] B. Le Borgne, O. De Sagazan, S. Crand, E. Jacques, M. Harnois, *ACS Appl. Mater. Interfaces* **2017**, 9, 29424.
- [272] P. Giannakou, M. O. Tas, B. L. Borgne, M. Shkunov, *ACS Appl. Mater. Interfaces* **2020**, 12, 8456.
- [273] G. Arrabito, B. Pignataro, *Anal. Chem.* **2010**, 82, 3104.
- [274] C. C. Hindrichsen, N. S. Almind, S. H. Brodersen, R. Lou-Moller, K. Hansen, E. V. Thomsen, *J. Electroceram.* **2010**, 25, 108.
- [275] J. Hast, M. Tuomikoski, R. Suhonen, K.-L. Väisänen, M. Välimäki, T. Maaninen, P. Apilo, A. Alastalo, A. Maanineny, *Soc. Inf. Disp.* **2013**, 44, 192.
- [276] J. Claypole, A. Holder, C. McCall, A. Winters, W. Ray, T. Claypole, *Proceedings* **2019**, 32, 24.
- [277] S. G. R. Bade, J. Li, X. Shan, Y. Ling, Y. Tian, T. Dilbeck, T. Besara, T. Geske, H. Gao, B. ma, K. Hanson, T. Siegrist, C. Xu, Z. Yu, *ACS Nano* **2016**, 10, 1795.
- [278] M. Kim, H.-J. Ha, H.-J. Yun, I.-K. You, K.-H. Baeg, Y.-H. Kim, B.-K. Ju, *Org. Electron.* **2014**, 15, 2677.
- [279] T. Leng, K. Parvez, K. Pan, J. Ali, D. McManus, K. S. Novoselov, C. Casiraghi, Z. Hu, *2D Mater.* **2020**, 7, 024004.
- [280] Q. Wang, G. Zhang, H. Zhang, Y. Duan, Z. Yin, Y. Huang, *Adv. Funct. Mater.* **2021**, 31, 2100857.
- [281] Texas Instruments & RFAB, <https://www.tialumni.org/sites/tialumni.org/files/file-ct/rfab-external-presentation-slides.pdf> (accessed: November 2022).
- [282] McKinsey & Company, Semiconductor design and manufacturing: Achieving leading-edge capabilities, <https://www.mckinsey.com/industries/advanced-electronics/our-insights/semiconductor-design-and-manufacturing-achieving-leading-edge-capabilities> (accessed: January 2022).
- [283] A. Mahindroo, D. Rosensweig, B. Wiseman, *Will analog be as good tomorrow as it was yesterday?*, McKinsey & Company, New York **2011**.
- [284] Antenna-on-package technology simplifies automotive in-cabin radar sensor design, <https://www.edn.com/antenna-on-package-technology-simplifies-automotive-in-cabin-radar-sensor-design/> (accessed: January 2022).
- [285] B. K. Tehrani, Doctoral dissertation, Georgia Institute of Technology, **2021**.
- [286] B. S. Cook, D. L. Revier, U.S. Patent No. 10,910,465, **2021**.
- [287] B. Tehrani, R. Bahr, D. Revier, B. Cook, M. Tentzeris, in *2018 IEEE 68th Electronic Components and Technology Conference (ECTC)*, IEEE, **2018**, pp. 111–117.
- [288] D. P. Parekh, B. S. Cook, D. L. Revier, J. Bito, U.S. Patent No. 10,879,151, **2020**.
- [289] H. Sada, S. Iriguchi, G. Yano, L. T. Nguyen, A. Prabhu, A. Poddar, Y. Yan, H. Nguyen, U.S. Patent No. 11,367,699, **2022**.
- [290] J. Bito, B. S. Cook, S. Kummerl, U.S. Patent Application No. 16/123,100, **2020**.
- [291] M. H. Malik, G. Grosso, H. Zangl, A. Binder, A. Roshanghias, *Microelectron. Reliab.* **2021**, 123, 114204.
- [292] M. H. Behfar, B. Khorramdel, A. Korhonen, E. Jansson, A. Leinonen, M. Tuomikoski, M. Mäntysalo, *Adv. Eng. Mater.* **2021**, 23, 2100264.
- [293] J. H. Lau, M. Li, M. L. Qingqian, T. Chen, I. Xu, Q. X. Yong, Z. Cheng, N. Fan, E. Kuah, Z. Li, K. H. Tan, Y. M. Cheung, E. Ng, P. Lo, W. Kai, J. Hao, S. W. Koh, J. Ran, C. Xi, R. Beica, S.-P. Lim, N. C. Lee, C.-T. Ko, H. Yang, Y.-H. Chen, M. Tao, J. Lo, S.-W. R. Lee, *IEEE Trans. Compon., Packag., Manuf. Technol.* **2018**, 8, 1544.
- [294] J. Lau, P. Tzeng, C. Lee, C. Zhan, M. Li, J. Cline, K. Saito, Y. Hsin, P. Chang, Y. Chang, J. Chen, S. Chen, C. Wu, H. Chang, C. Chien, C. Lin, T. Ku, R. Lo, M. Kao, *Int. Symp. Microelectron.* **2013**, 2013, 000434.
- [295] Z. Chen, M. Guo, R. Zhang, B. Zhou, Q. Wei, *Sensors* **2018**, 18, 2603.
- [296] V. Scenev, J. Szalapak, L. Werft, O. Hoelck, M. Jakubowska, M. Krshiwoblozki, C. Kallmayer, M. Schneider-Ramelow, *Adv. Eng. Mater.* **2022**, 24, 2101752.
- [297] B. K. Tehrani, B. S. Cook, M. M. Tentzeris, in *2016 IEEE MTT-S International Microwave Symposium (IMS)*, IEEE, **2016**, pp. 1–4.
- [298] IndustryARC, L. I. F. T., (LIFT) Market – Forecast(2020–2025), <https://www.industryarc.com/Report/19311/laser-induced-forward-transfer-market.html> (accessed: April 2021).
- [299] Global Nanoimprint Lithography System Market Research Report 2022 Professional Edition, <https://www.xcellentsights.com/reports/nanoimprint-lithography-system-market-15031> (accessed: January 2023).
- [300] Sales of Fab Tools Surge to Over \$71 Billion in 2020, <https://www.anandtech.com/show/16620/sales-of-fab-tools-surge-to-over-71-billion-in-2020> (accessed: January 2022).
- [301] APQC, <https://www.apqc.org/resource-library/resource-listing/how-improve-first-pass-quality-yield-manufacturing> (accessed: January 2023).
- [302] J. Willmann, D. Stocker, E. Dörsam, *Org. Electron.* **2014**, 15, 1631.
- [303] Low yield on Samsung's 4 nm process node prompts Qualcomm to go with TSMC for future chips, <https://www.techspot.com/news/93520-low-yield-samsung-4nm-process-node-prompts-qualcomm.html> (accessed: January 2023).



**Johanna Zikulnig** obtained a Master's degree in Biomedical Engineering from the Graz University of Technology in 2017. After working as a Junior Researcher in the Smart Systems Group at Carinthian Tech Research, she joined the Sensor Applications Group at Silicon Austria Labs, where she is currently working as a Scientist. Since 2022, she has been enrolled in the doctoral program in electrical engineering at EPFL in Switzerland. Her scientific interests are in the development of sustainable sensors focusing on printing and hybrid technologies.



**Sean Chang** is a Process Engineer in Kilby Labs at Texas Instruments with over 7 years of experience in the inkjet and semiconductor industry. His current interests include inkjet materials and process development, applications of printed electronics for the semiconductor industry, as well as, piezoelectric MEMS development. Sean performed his undergraduate studies at the University of Washington, Seattle, and his graduate studies at the University of Oregon.



**Jo Bito** received a B.S. degree in Electrical and Electronic Engineering from Okayama University in Japan in 2013. Later, he earned M.S. and Ph.D. degrees in Electrical and Computer Engineering from the Georgia Institute of Technology in the US in 2016 and 2017, respectively. He has worked as an IC Package Engineer at Texas Instruments, Inc., researching additive manufacturing technologies and mmWave Radar ICs from 2017 to 2021. Currently, he is the Head of Perception at Atheraxon, Inc developing mmWave Radar asset tracking solutions. Dr. Bito was awarded the Japan Student Services Organization Long Term Scholarship in 2013.



**Lukas Rauter** received his Master's degree in Physical Energy and Measurement Engineering at the Technical University of Vienna. Already during his studies there, he focused on the topics of sensor technology and material sciences. After completing his Master's degree, he started to work mainly on printed and flexible sensor technology. He is currently finalizing his Ph.D. in the field of printed sustainable sensors at the Alpen-Adria University Klagenfurt.



**Ali Roshanghias** is currently a Staff Scientist in the department of heterogeneous integration technologies at Silicon Austria Labs (SAL). He received his Ph.D. in Materials Science and Technology from the Sharif University of Technology (Iran) in 2012. He pursued his career as a post-doc researcher at Nagaoka University of Technology (Japan) and Vienna University (Austria) in the fields of electronic materials and advanced microelectronics packaging. In 2015 he joined Silicon Austria Labs (formerly known as CTR Carinthian Tech Research AG). His research interests include heterogeneous integration technologies, hybrid flexible electronics, and 3D integration.



**Sandro Carrara** (F'15) is an IEEE Fellow and also the recipient of the IEEE Sensors Council Technical Achievement Award. He is faculty at the EPFL (Switzerland), a former Professor at the Universities of Genoa and Bologna (Italy). He published 7 books, with publishers like Springer/NATURE and Cambridge University Press. He is author of more than 360 publications and 17 patents. He is Editor-in-Chief of the IEEE Sensors Journal, and Associate Editor of IEEE Transactions on Biomedical Circuits and Systems. He is a member of the IEEE Sensors Council, and was member of the Board-of-Governors of the Circuits and Systems IEEE Society.



**Jürgen Kosel** is the PI of the research unit Printed Flexible Electronics and Sensor Applications at Silicon Austria Labs. He is an Adjunct Professor of Electrical Engineering at KAUST. He has been founder and CSO of Solutions for Nanotechnology in 2015 and 2016. In 2008 and 2009, he was a Postdoctoral Fellow at the University of Stellenbosch working in the automotive industry at MAGNA Powertrain in Austria for two years. He completed his Habilitation at the Vienna University of Technology in 2022 and received a Ph.D. and MSc with honors from the same university in 2006 and 2002, respectively.